Control and Power Management of Hybrid Energy Storage Systems

Zur Erlangung des akademischen Grades einer

DOKTORIN DER INGENIEURWISSENSCHAFTEN (Dr.-Ing.)

von der KIT-Fakultät für Elektrotechnik und Informationstechnik des
Karlsruher Instituts für Technologie (KIT)

angenommene

DISSERTATION

von

M.Sc. Seyede Masoome Maroufi
geb. in Kerman

Tag der mündlichen Prüfung:	27.01.2026
Hauptreferent:	Prof. Dr.-Ing. Giovanni De Carne
Korreferent:	Prof. Dr.-rer.nat. Thomas Ebel

Acknowledgments

First and foremost, I would like to express my sincere gratitude to my supervisor, Prof. Giovanni De Carne, for his continuous support, encouragement, and invaluable guidance throughout my PhD journey. His ability to create a professional yet enjoyable working atmosphere has been a source of motivation and inspiration for me.

I am also grateful to Prof. Thomas Ebel for his insightful input and support, as well as to Dr. Shahab Karrari, Dr. Davide Fusco, and Dr. Dario Pelosi for their valuable collaboration, which greatly enriched this work. I would also like to acknowledge Prof. Mathias Noe for his guidance.

The experimental work at KIT's EnergyLab was made possible through the generous support of Mr. Christian Lange, Mr. Frank Gröner, and Mr. Dieter Riegel. I am particularly thankful to Christian for his sense of humour, exceptional problem-solving skills, and his insightful understanding of the technical devices, which greatly contributed to the success of the experiments.

I would like to extend my heartfelt thanks to my colleagues and friends, Fargah, Qiucen, Maëva, Ali, Gabriele, Mahshid, Nima, Karthik, Nils, Felix, Sarah, Michael, Honeymol, Danilo, Malik, Moein, Evangelos, and Jonghung. Working alongside such competent, supportive, and fun people made this journey not only productive but also truly enjoyable.

My deepest gratitude goes to my parents and my brothers, who first introduced me to electrical engineering and whose constant support and guidance have shaped who I am today. Without their influence and encouragement, this achievement would not have been possible.

Finally, I wish to thank Louis, whose love, patience, and unwavering support carried me through the most challenging times. This thesis is dedicated to him.

Kurzfassung

Die zunehmende Integration erneuerbarer Energiequellen und die Elektrifizierung des Verkehrs haben die Nachfrage nach effizienten und zuverlässigen Energiespeichersystemen deutlich erhöht. Unter den verfügbaren Technologien haben sich Lithium-Ionen Batteriespeichersysteme (BESS) aufgrund ihrer hohen Energiedichte und ausgereiften Technologie als die am weitesten verbreitete Lösung etabliert. Allerdings stoßen BESS in Anwendungen, die schnelle Leistungsfluktuationen, hochfrequentes Laden/Entladen und häufige Ladezyklen erfordern, an ihre Grenzen. Diese Betriebsbedingungen beschleunigen die Alterung der Batterien, verkürzen die Lebensdauer und erhöhen die über die Zeit gemittelten Speicherkosten. Diese Einschränkungen haben die Entwicklung alternativer Systemarchitekturen motiviert, die darauf abzielen, die hochfrequenten und transienten Leistungsanforderungen vom Akku auf ein ergänzendes Speicherelement zu verlagern.

Ein vielversprechender Ansatz zur Überwindung dieser Einschränkungen ist der Einsatz von Hybriden Energiespeichersystemen (HESS), die komplementäre Speichertechnologien kombinieren, typischerweise einen Energiereich-Batteriespeicher (BESS) mit einem leistungsstarken Speicherelement wie einem Superkondensator Energiespeichersystem (SCES) oder einem Schwungrad Energiespeichersystem (FESS). Die HESS-Konfiguration ermöglicht eine Aufteilung der Leistungsanforderungen: Langsam verlaufende, energieintensive Komponenten werden dem Akku zugeordnet, während das Hilfsspeicherelement schnelle Transienten und hohe Rampenanforderungen übernimmt. Diese Entkopplung verbessert nicht nur die Leistungsfähigkeit und Reaktionsgeschwindigkeit des Speichersystems, sondern verringert auch die Alterungsmechanismen der Batterie, indem die Belastung durch schnelle Leistungsänderungen reduziert wird.

Obwohl die HESS-Architektur klare Vorteile gegenüber eigenständigen Batteriesystemen bietet, erfordert ihr effektiver Betrieb ausgeklügelte Steuerungsstrategien. Die grundlegende Herausforderung besteht darin, zwei oder mehr Speicherkomponenten mit stark unterschiedlichen Eigenschaften wie Reaktionszeit, Energiekapazität, Wirkungsgrad und Alterungsverhalten unter hochvariablen Leistungsanforderungen dynamisch zu koordinieren. Dabei muss sichergestellt

werden, dass jede Komponente innerhalb ihrer sicheren Betriebsgrenzen arbeitet, während gleichzeitig systemweite Leistungsziele (z.B. Minimierung von Verlusten, Verlängerung der Lebensdauer und Aufrechterhaltung der Leistungsqualität) erfüllt werden was Echtzeit-Kontrolle und intelligente Managementsysteme erfordert.

Insbesondere muss die Leistungsaufteilung zwischen BESS und Hilfsspeicher nicht nur auf das aktuelle Leistungsprofil reagieren, sondern auch langfristige Zustandsgrößen berücksichtigen, wie den Ladezustand (SoC) jeder Einheit und die Rampenbegrenzungen der Batterie. Traditionelle regelbasierte Methoden oder Tiefpassfilter stoßen unter dynamischen Bedingungen oft an ihre Grenzen. Die Steuerung von HESS ist daher nicht nur technisch anspruchsvoll, sondern entscheidend, um das volle Potenzial hybrider Speichersysteme auszuschöpfen.

Diese Arbeit widmet sich diesen Herausforderungen und entwickelt fortschrittliche Steuerungs- und Schätzmethoden für hybride Energiespeichersysteme. Im Besonderen werden Ansätze für eine effektive Leistungsaufteilung, eine präzise SoC-Schätzung und die Reduzierung der Batterielast unter dynamischen Betriebsbedingungen untersucht. Die Arbeit zeigt, dass durch eine gezielte Steuerung der verschiedenen Speicherkomponenten die Effizienz und Lebensdauer des Gesamtsystems verbessert werden kann. Die Ergebnisse tragen zu einem besseren Verständnis des praktischen Verhaltens von HESS bei und liefern nützliche Hinweise für die Gestaltung hybrider Speichersysteme, die in der Praxis zuverlässig und leistungsfähig arbeiten.

Abstract

The increasing integration of renewable energy sources and the electrification of transportation have significantly raised the demand for efficient and reliable energy storage systems. Among the various technologies available, Lithium-ion Battery Energy Storage Systems (BESS) have become the most widely adopted solution due to their high energy density and maturity. However, BESS alone faces several challenges when subjected to applications that involve rapid power fluctuations, high-frequency cycling, and frequent charge/discharge events. These operational conditions accelerate battery aging, reduce cycle life, and increase the levelized cost of storage over time. This limitation has motivated the development of alternative system architectures, which aim to offload the high-frequency and transient power demands from the battery to a complementary storage device.

A promising approach to overcome these limitations is the use of Hybrid Energy Storage Systems (HESS), which combine complementary storage technologies, typically a high-energy BESS with a high-power storage element such as a Supercapacitor Energy Storage System (SCES) or a Flywheel Energy Storage System (FESS). The HESS configuration enables the power demand to be split: slow, energy-intensive components are allocated to the battery, while the auxiliary storage handles fast transients and high ramp-rate events. This decoupling not only enhances the performance and responsiveness of the storage system but also mitigates the aging mechanisms of the battery by reducing the stress caused by rapid power variations.

While the HESS architecture offers clear advantages over standalone battery systems, its effective operation requires sophisticated control and power management strategies. The fundamental challenge lies in dynamically coordinating two or more storage components with vastly different characteristics, such as response time, energy capacity, efficiency, and degradation behavior, under highly variable power demands. Ensuring that each component operates within its safe limits, while jointly fulfilling system-level performance objectives (e.g., minimizing losses, extending lifespan, and maintaining power quality), requires real-time, intelligent control and management systems.

In particular, the power-splitting strategy between the BESS and the auxiliary storage must not only respond to the instantaneous power profile but also consider long-term state variables, such as the State of Charge (SoC) of each unit and the battery's ramp rate limitations. Traditional

rule-based or low-pass filter methods often fail to provide adequate flexibility or adaptability under dynamic conditions. Therefore, control of HESS is not just technically challenging; it is essential for unlocking the full potential of hybrid storage systems.

This thesis addresses these challenges by proposing advanced control and estimation strategies for hybrid energy storage systems. In particular, it explores methods for effective power management, accurate SoC estimation, and mitigation of battery aging under dynamic operating conditions. The work examines how HESSs can be controlled more effectively and demonstrates that carefully managing the various storage components can enhance the system's efficiency and longevity. The findings help to better understand how HESS behaves in practice and provide useful guidance for designing hybrid storage systems that perform effectively in real-world applications.

Contents

Acknowledgment i

Kurzfassung iii

Abstract v

Acronyms and symbols xi
Acronyms xi
Variables and Symbols xiii

1 Introduction, Motivation and Scope of Work 1
1.1 Motivation 1
1.2 PhD Research Questions 1
1.3 Scope of Work and Thesis Structure 2

2 Energy Storage Technologies and the Role of Hybrid Energy Storage Systems 5
2.1 Energy Storage System Technologies 5
2.1.1 Battery Energy Storage Systems (BESS) 6
2.1.2 Supercapacitor Energy Storage Systems (SCES) 9
2.1.3 Flywheel Energy Storage Systems (FESS) 11
2.1.4 Hydrogen-Based Energy Storage System 16
2.1.5 Superconducting Magnetic Energy Storage (SMES) 19
2.1.6 Pumped Hydro Energy Storage (PHES) 21
2.2 Comparison between energy storage technologies 22
2.3 Hybrid Energy Storage Systems (HESS) 24
2.3.1 Hybrid Energy Storage System Connections 27
2.3.2 Services and Application of Hybrid Energy Storage Systems: 30
2.4 Summary 34

3 Experimental Setup 35
3.1 Power Hardware-in-the-Loop (PHIL) Concept and Architecture 35
3.1.1 PHIL Test Case Development 37

3.2 KIT 1-MW Power Hardware in the Loop Setup with Egston Amplifier 38
3.2.1 DUT Example Installation: FESS at KIT EnergyLab 40
3.3 KIT 15-kW Power Hardware in the Loop with Spitzenberger Amplifier 43
3.3.1 DUT Example Installation: SCES at KIT EnergyLab 44
3.4 Summary 46

4 Power Management and Control of Hybrid Energy Storage Systems (HESS) 49
4.1 Challenges in HESS Control 49
4.2 Control Strategies 51
4.2.1 Rule-Based Control 51
4.2.2 Optimization-Based Control 54
4.3 Key Control Parameters 59
4.4 Summary 62

5 Control and Power Management of Hybrid Energy Storage Systems Using Moving Average and Fuzzy Logic 65
5.1 Proposed Control Strategy 65
5.2 Control Components 66
5.2.1 Moving Average (MA) 66
5.2.2 Fuzzy Logic Controller 68
5.3 Experimental Validation 71
5.3.1 Input Power Profile 72
5.3.2 Experimental Results 72
5.4 Parameter Variation Analysis 77
5.4.1 Moving Average Window Width 78
5.4.2 Low-pass Filter Cut-Off Frequency 80
5.5 Summary 82

6 Supercapacitor SoC Estimation in Hybrid Energy Storage Systems 83
6.1 Overview of Estimation Methods 83
6.1.1 Conventional Methods 83
6.1.2 Kalman Filtering (KF) Method 85
6.2 Supercapacitor Model 89
6.2.1 Three-Branch Equivalent Circuit Model 89
6.2.2 First-Order Dynamic Equivalent Circuit Model 91
6.2.3 Model Parameters Extraction 93
6.3 Results and Validation 95
6.3.1 Numerical Results 95
6.3.2 Experimental Results 98
6.3.3 Validation under Realistic Grid Power Profiles 100

6.4 Summary . . . 101

7 BESS Lifetime Extension using Hybrid Energy Storage Systems . . . 105
7.1 PHIL-Based Battery Aging Assessment . . . 105
7.2 Power management strategy . . . 106
7.2.1 Simultaneous Perturbation Stochastic Approximation (SPSA) Power Management . . . 109
7.3 Energy Storage Modeling and Device . . . 111
7.3.1 Battery Energy Storage Modeling . . . 111
7.3.2 Battery Energy Storage Experimental Setup . . . 112
7.3.3 Flywheel Energy Storage Modeling . . . 114
7.4 Experimental Data Acquisition . . . 114
7.4.1 Rainflow Cycle Counting (RFC) . . . 115
7.4.2 Design of Experiment (DoE) . . . 116
7.5 Results: State of Health Evaluation . . . 119
7.5.1 PHIL-Based Aging Results . . . 119
7.5.2 Simulation Results . . . 120
7.5.3 Results of experimental aging . . . 122
7.6 Economic Analysis . . . 124
7.6.1 Levelized Cost of Storage (LCOS) Framework . . . 125
7.6.2 Battery Replacement Frequency Estimation . . . 125
7.6.3 Long-Term Economic Evaluation over 20 Years . . . 127
7.7 Summary . . . 129

8 Summary, Conclusion, and Future Work . . . 133
8.1 Summary and Conclusion . . . 133
8.2 Outlook . . . 134

A Appendix . . . 137
A.1 Kalman Filter (KF) . . . 137
A.2 Extended Kalman Filter (EKF) . . . 137
A.3 Unscented Kalman Filter (UKF) . . . 138
A.4 Square Root UKF (SR-UKF) . . . 139
A.5 Kalman Filter Particle Filter (KF-PF) . . . 139
A.6 Adaptive Square Root UKF (ASR-UKF) . . . 139

List of Figures . . . 141

List of Tables . . . 145

List of Publications . . . 147
Journal articles . . . 147

Conference contributions 147
Book contributions 148

Bibliography 149

Acronyms and symbols

Acronyms

AC	Alternating Current
AEC	Alkaline Electrolysis Cell
AFC	Alkaline Fuel Cell
ANN	Artificial Neural Networks
ASR-UKF	Adaptive Square-Root Unscented Kalman Filter
BESS	Battery Energy Storage System
BMS	Battery Management System
CC	Constant Current
CCCV	Constant Current-Constant Voltage
CDA	COMPISO Digital Amplifiers
CDF	Cumulative Density Function
CSU	COMPISO System Unit
CV	Constant Voltage
DC	Direct Current
DER	Distributed Energy Resource
DoD	Depth of Discharge
DoE	Design of Experiment
DUT	Device Under Test
ECM	Equivalent Circuit Model
EDLC	Electrochemical Double-Layer Capacitors
EKF	Extended Kalman Filter
EMT	Electromagnetic Transient
EoL	End of Life
ESD	Energy Storage Device
ESR	Equivalent Series Resistance
ESS	Energy Storage System

EV	Electric Vehicle
FESS	Flywheel Energy Storage System
FLC	Fuzzy Logic Control
GA	Genetic Algorithm
GSC	Grid-Side Converter
HESS	Hybrid Energy Storage System
HPPC	Hybrid Pulse Power Characterization
HTS	High Temperature Superconductor
KF	Kalman Filter
KF-PF	Kalman Filter-Particle Filter
LCOS	Levelized Cost of Storage
Li-ion	Lithium-ion
LPF	Low-Pass Filter
LTS	Low-Temperature Superconductors
MA	Moving Average
MCFC	Molten Carbonate Fuel Cell
MMC	Modular Multi-level Converter
MPC	Model Predictive Control
MSC	Machine-Side Converter
MUSE	Multi-System Expansion
NOx	Nitrogen Oxides
OCV	Open-Circuit voltage
PAFC	Phosphoric Acid Fuel Cell
PEMEC	Proton Exchange Membrane Electrolyzer Cell
PEMFC	Proton Exchange Membrane Fuel Cell
PHES	Pumped Hydro Energy Storage
PHIL	Power Hardware-in-the-Loop
PMSM	Permanent Magnet Synchronous Machine
PPC	Positive Pulsed Current
PSO	Particle Swarm Optimization
RES	Renewable Energy Source
RFC	Rainflow Cycle Counting
RMS	Root-Means-Square
RoHS	Restriction of Hazardous Substances
RPM	Revolutions Per Minute
RR	Ramp Rate

RTDS	Real-Time Digital Simulator
RUL	Remaining Useful Life
SCES	Supercapacitor Energy Storage System
SFP	Small Form factor Pluggable
SMA	Simple Moving Average
SMES	Superconducting Magnetic Energy Storage
SMR	Steam Methane Reforming
SoA	State of the Art
SoC	State of Charge
SOEC	Solid Oxide Electrolysis Cell
SOFC	Solid Oxide Fuel Cell
SoH	State of Health
SOX	Sulfur Oxides
SPSA	Simultaneous perturbation stochastic approximation
SR-UKF	Square-Root Unscented Kalman Filter
UKF	Unscented Kalman Filter
UL	Underwriters Laboratories
USD	United States Dollar
VSC	Voltage-Source Converter

Variables and Symbols

C	Capacity
C_{BESS}	Battery Capacity
C_n	Rated capacitance
E	Energy
E_{BESS}	Battery Energy
E_{FESS}	Flywheel energy
E_{SCES}	Supercapacitor energy
e_m	Specific energy
e_v	Volumetric energy density
η	Efficiency
$f_{cut-off}$	Cut-off frequency
I	Current
I_{BESS}	Battery current
I_{SCES}	Supercapacitor current

$I(\tau)$	Current as a function of time
J	rotational inertia
$\dot{\omega}$	Angular Acceleration
ω	Angular velocity
ω_m	Rotational speed
P	Active power
Q	Electric charge [C or Ah]
R	Resistance
$R_{\text{BESS}}^{\text{int}}$	Battery internal resistance
ρ	Material density
s	Laplace operator
σ	Tensile strength
T	Time constant
t	Time
t_0	Initial time
V	Voltage
V_{BESS}	Battery terminal voltage
V_{ocv}	Open circuit voltage
V_{SCES}	Supercapacitor terminal voltage
V_n	Nominal voltage

1 Introduction, Motivation and Scope of Work

1.1 Motivation

The accelerating integration of Renewable Energy Sources (RES) into modern power systems is a key element of the global energy transition. However, their variability and intermittency introduce significant challenges to grid stability, power quality, and reliability. Energy storage systems (ESSs) are increasingly recognized as essential enablers for addressing these issues. Among the various technologies, Battery Energy Storage Systems (BESSs) are the most widely deployed due to their high energy density and flexibility. Nevertheless, BESS alone cannot fully meet the demands of future grids, as they suffer from limited lifetime, high degradation under frequent cycling, and significant replacement costs.

Hybrid Energy Storage Systems (HESSs), which combine complementary storage technologies, have emerged as a promising solution. By coupling high-energy devices (such as batteries) with high-power devices, such as Flywheel Energy Storage System (FESS) and Supercapacitor Energy Storage System (SCES), HESS leverages the strengths of both technologies while mitigating their weaknesses. This approach enables more efficient power management, an extended lifetime for the battery subsystem, and an overall reduction in storage costs over long operational horizons. Despite these advantages, HESS also presents new challenges, particularly regarding control, optimal sizing, and system-level justification of its added investment.

1.2 PhD Research Questions

The work presented in this thesis is guided by three central research questions:

1. **The HESS concept as a solution to high RES integration:** How can hybridization of storage technologies contribute to the reliable integration of renewable energy sources, particularly in mitigating intermittency and reducing stress on batteries?

2. **Control and power management of HESS:** What are the main technical challenges of operating a HESS, and how can control strategies be designed and validated to ensure efficient power sharing, state-of-charge (SoC) management, and improved system performance?

3. **Techno-economic assessment and lifetime evaluation of HESS:** Can the benefits of HESS be quantitatively demonstrated by extending battery lifetime, reducing degradation, and lowering the overall Levelized Cost of Storage (LCOS) compared to standalone BESS?

1.3 Scope of Work and Thesis Structure

To address these questions, this thesis combines theoretical modeling, control development, experimental validation, and techno-economic assessment. The scope covers both the fundamental principles of HESS and their application in realistic operating conditions. The main contributions are organized into the following chapters, illustrated in Figure 1.1.

- **Chapter 2** provides an overview of energy storage technologies, their characteristics, and limitations, with a focus on the motivation for hybridization. The chapter positions HESS in the context of RES integration.
- **Chapter 3** introduces the Power Hardware-in-the-Loop (PHIL) methodology used in this thesis. It describes the experimental setup, including the integration of commercial FESS and SCES, and explains how PHIL enables realistic emulation of grid conditions for HESS validation.
- **Chapter 4** reviews existing approaches to control and power management of HESS found in the literature. It discusses the main strategies developed so far, highlights their advantages and limitations, and identifies the key control parameters, such as SoC and ramp rate (RR), that must be addressed for effective hybrid operation. This chapter provides the conceptual foundation for the control methods developed later in the thesis.
- **Chapter 5** develops and experimentally validates a control strategy for HESS, including moving average and fuzzy logic approaches. This strategy is designed to optimize power sharing, preserve SoC balance of FESS, and reduce RR imposed on the BESS.
- **Chapter 6** presents a SoC estimation approach for supercapacitors using the Adaptive Square-Root Unscented Kalman Filter (ASR-UKF). The method is tailored to the nonlinear dynamics of supercapacitors and validated experimentally.
- **Chapter 7** reports on accelerated aging experiments that quantify the impact of hybridization on battery degradation. Results demonstrate slower capacity fade and extended lifetime

for BESS when operated in hybrid configurations. This chapter also provides a techno-economic analysis, comparing standalone BESS and HESS configurations. The LCOS is evaluated over a 20-year horizon, showing the economic viability of HESS despite higher initial costs.

- **Chapter 8** concludes the thesis by summarizing the key findings, highlighting their implications for future power systems, and providing an outlook on future research directions.

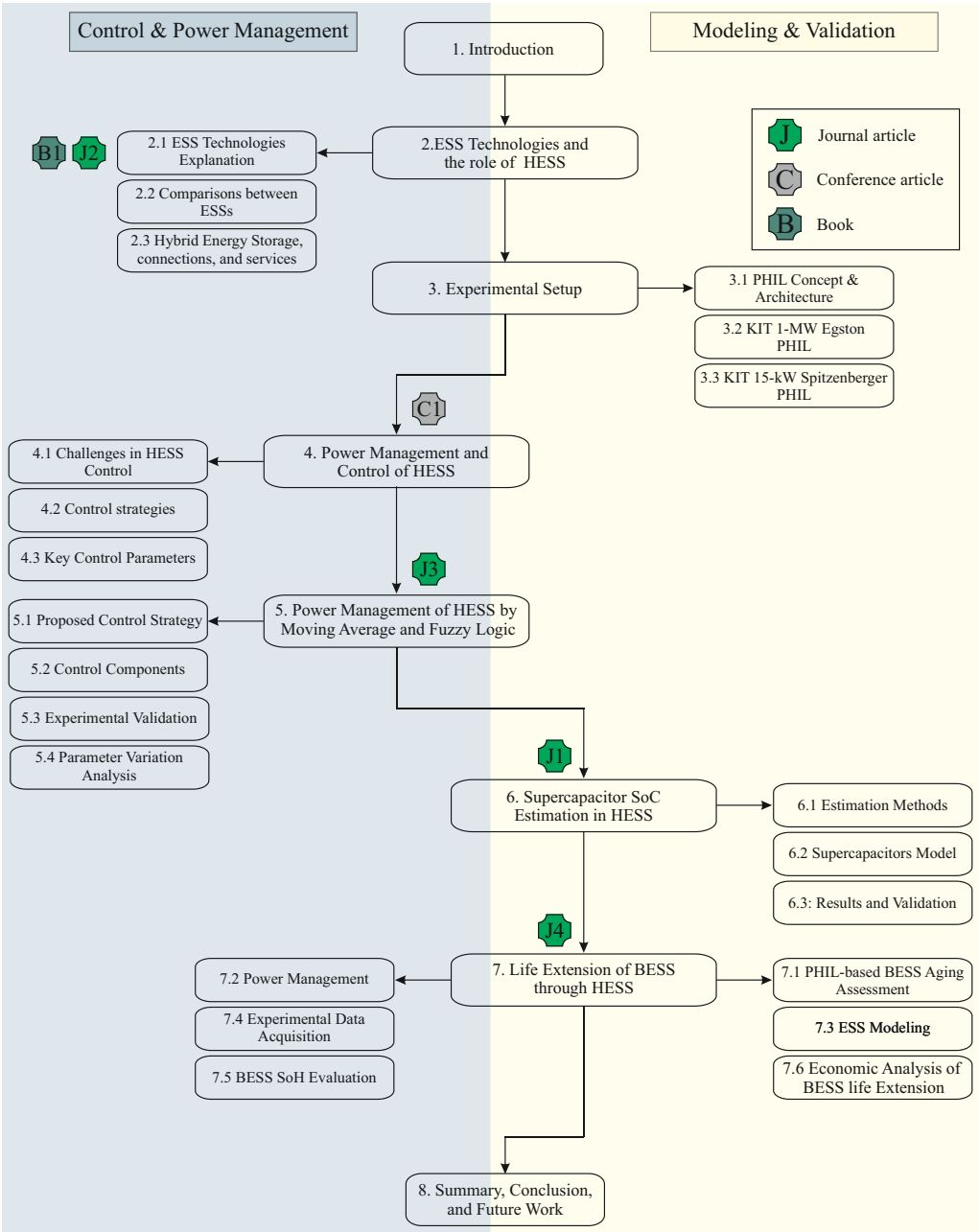

Figure 1.1: The table of contents at a glance.

2 Energy Storage Technologies and the Role of Hybrid Energy Storage Systems

To address the challenges associated with the variability of renewable energy sources, Energy Storage Systems (ESSs) have emerged as essential components of resilient, flexible, and sustainable power systems. This chapter provides a comprehensive overview of key ESS technologies, outlining their operational principles, advantages, and limitations. Particular attention is given to aspects such as energy density, cycle life, cost, and suitability for various grid applications.

Furthermore, the chapter introduces the concept of Hybrid Energy Storage Systems (HESS) as a promising solution to overcome the individual shortcomings of standalone storage technologies. It also explores different HESS topologies, real-world applications, and notable projects that demonstrate their practical relevance.

2.1 Energy Storage System Technologies

A wide range of ESS technologies have been developed to meet the diverse demands of power systems operation, especially under high integration of renewable generation. Each technology offers unique characteristics in terms of performance metrics such as energy and power density, response time, efficiency, and lifecycle, which determine their suitability for specific use cases.

The following subsections provide an overview of selected ESS technologies, including battery energy storage systems (BESS), supercapacitor energy storage systems (SCES), flywheel energy storage systems (FESS), Superconducting Magnetic Energy Storage (SMES), hydrogen energy storage systems, and Pumped Hydro Energy Storage systems (PHES). For each, the operating principles, grid applications, and market considerations are discussed.

2.1.1 Battery Energy Storage Systems (BESS)

Among the various energy storage technologies, batteries, particularly Lithium-ion (Li-ion), have become the dominant solution due to their high energy density, scalability, and technological maturity. This subsection introduces the operating principles of batteries and highlights key technologies relevant to stationary and grid-scale applications.

2.1.1.1 Operating Principles and Technologies

Batteries are electrochemical devices composed of a cathode (positive electrode) and an anode (negative electrode), separated by a porous membrane that allows ionic transport while blocking electron flow. The electrolyte wets all internal components, enabling the movement of ions between electrodes during charge and discharge [1, 2]. In Li-ion batteries, this process is called the rocking-chair or shuttle mechanism: lithium ions intercalate and deintercalate between the electrodes through the electrolyte while electrons flow through the external circuit. During discharge, lithium ions migrate from the anode to the cathode, generating electrical energy, and the process is reversed during charging. The essential design of Li-ion cells has remained largely unchanged since their commercial introduction by Sony, though materials have evolved [3, 4].

The energy stored or delivered by a BESS is calculated based on the product of voltage, current, and time [5, 6]. It can be expressed as:

$$E_{\text{BESS}} = V \cdot I \cdot t \tag{2.1}$$

Alternatively, if the charge Q is known:

$$E_{\text{BESS}} = V \cdot Q \tag{2.2}$$

Where: E_{BESS} is Energy stored [J or Wh], V is Terminal voltage [V], I is Current [A], t is Time [s or h], and Q is Electric charge [C or Ah].

The SoC indicates the remaining charge in the battery as a percentage of its total capacity. It evolves over time depending on the charging or discharging current:

$$\text{SoC}(t) = \text{SoC}(t_0) - \frac{1}{C_{\text{BESS}}} \int_{t_0}^{t} \frac{I(\tau)}{\eta}\, d\tau \tag{2.3}$$

Where: $\mathrm{SoC}(t)$ is the state of charge at time t, C_{BESS} is the battery capacity [Ah], $I(\tau)$ is the current as a function of time (positive for discharge), η is charging/discharging efficiency, and t_0 is initial time.

Batteries are constructed based on different electrochemical principles and chemistries. The most common types used in grid applications include Li-ion, Na-ion, NaS, NiCd, NiMH, and lead-acid batteries. Li-ion batteries dominate many applications due to their high energy density and favorable cycle life, but emerging chemistries such as sodium-ion and solid-state batteries are gaining attention. While Li-ion, NiCd, Na-ion, and NiMH batteries are usually built from small cells connected in series and parallel to achieve the desired voltage and current, other types, such as lead-acid, NaS, and solid-state batteries, are often produced as larger monolithic units. For modular cell-based batteries, cell balancing technologies are critical to ensure uniform charging and discharging across cells. Passive balancing is widely used due to its simplicity and low cost; however, it is inefficient and can accelerate degradation, particularly in aged batteries. Active balancing improves efficiency but increases complexity and cost, and can still be susceptible to safety issues, such as thermal runaway [7]. Fully power electronics-based Battery Management Systems (BMS) with the ability to dynamically insert or bypass cells offer higher modularity and safety. They can be applied across first-, second-, and third-life battery applications. Table 2.1 provides an overview of key BESS types based on their chemical composition, advantages, and disadvantages.

Table 2.1: Comparison of Battery Energy Storage System (BESS) Types

Battery Type	Chemistry	Key Advantage	Disadvantage
Li-ion (LFP) [8,9]	Lithium Iron Phosphate	High safety, thermal stability, long cycle life	Lower energy density compared to other Li-ion chemistries
Li-ion (NMC) [10]	Nickel Manganese Cobalt	High energy density, good overall performance	Degrades faster at high temperatures; costly materials
Lead-acid [11,12]	Lead-Acid	Low cost, mature and widely available technology	Short cycle life, low energy density, Heavy weight
NaS [11,13]	Sodium-Sulfur	Fast response, long lifespan, high energy density	High operating temperature ($\sim$300°C), safety concerns, high cost
Flow Battery [14,15]	Vanadium Redox, Zn-Br	Scalable capacity, long cycle life, low degradation	Low energy density, complex system design
NiCd / NiMH [16,17]	Nickel-Cadmium / Hydride	Robust performance in extreme temperatures, long life cycle	High cost, high self-discharge rate, environmental issues (cadmium toxicity)

2.1.1.2 Grid Applications

Battery energy storage systems are deployed across a wide range of scales. Residential BESS typically range from 1 kWh to 20 kWh and focus on cost savings and self-consumption. Industrial and commercial BESS generally range from 20 kWh to a few MWh and are often used for grid support, demand management, and backup power. Utility-scale BESSs for power management frequently exceed several MWh and can even reach GWh capacities. Across these applications, BESS can deliver services such as voltage support, frequency regulation, spinning and non-spinning reserves, black start capability, energy arbitrage, power peak-shaving and shifting, and oscillation damping [18, 19]. Li-ion BESSs are especially well-suited to sustained energy delivery thanks to their high energy density and improving cost structures. Still, they also require effective thermal management to avoid overheating and performance degradation [20].

2.1.1.3 Market Perspective

Li-ion batteries are expected to maintain their dominant position in stationary energy storage, driven by continuous cost reductions, advances in material development, and growing deployment. The total annual demand for Li-ion BESS across residential, commercial, and utility sectors is projected to increase from 35.7 GWh in 2022 to approximately 283.8 GWh by 2028, with about 90% of this demand attributed to utility-scale systems. Correspondingly, the annual market value is forecast to grow from around 8.2 billion USD in 2022 to 40 billion USD in 2028 [21, 22]. The battery cell itself represents about 70% of the total battery pack cost. Cathode materials containing cobalt, such as NMC or NCA, are among the most expensive components, but efforts are underway to reduce reliance on critical and toxic materials through chemistries such as Lithium Iron Phosphate (LFP) and sodium-ion alternatives [23].

Overall, several trends can be identified in the development of BESS. These include the continued reduction of cell material costs through improved chemistries and manufacturing processes, as well as the diversification beyond Li-ion toward sodium-ion, NaS, flow batteries, and solid-state batteries [23]. There is also increasing adoption of larger cell formats to enhance energy density and simplify system integration. In parallel, second-life battery applications are expanding as used EV batteries are repurposed for stationary storage. The transition to higher-voltage battery packs, reaching up to 1500 V DC, is underway to enable improved efficiency and faster charging speeds [24]. Furthermore, BMS architectures are evolving from centralized configurations toward more modular and distributed approaches [25], and safety systems are being enhanced, including the replacement of traditional fuses with solid-state circuit breakers [26, 27].

2.1.1.4 Limitations

Despite their growing role in modern power systems, BESS face several key limitations that hinder their long-term effectiveness and economic viability. One of the most critical issues is battery degradation, which occurs due to both cycling and calendar aging [28, 29]. Every charge and discharge cycle gradually reduces a batterys usable capacity and efficiency. This degradation accelerates with higher depth of discharge, rapid power changes, and extreme temperatures, leading to shorter system lifespans and higher replacement costs [30].

Another major constraint is the power density of BESS [31]. While they are excellent for energy balancing, such as frequency regulation, they are less suitable for supplying sustained high-power loads unless significantly oversized, an approach that is often costly [32]. Furthermore, thermal management is essential, as batteries are susceptible to temperature fluctuations. Without adequate cooling or heating systems, performance drops, and safety risks such as thermal runaway increase [33, 34].

Economic and environmental concerns also significantly limit BESS deployment. The upfront investment remains relatively high, factoring in not just the battery cells but also power electronics, safety systems, installation, and integration. Additionally, the environmental footprint of mining and processing raw materials like lithium and cobalt, as well as limited recycling infrastructure, raises sustainability concerns [35, 36].

2.1.2 Supercapacitor Energy Storage Systems (SCES)

Supercapacitors represent a class of energy storage technologies that prioritize power density, rapid response, and cycle life over energy capacity. Unlike batteries, which rely on chemical energy conversion, supercapacitors operate based on electrostatic charge accumulation, enabling ultra-fast charging and discharging [37]. This subsection provides an overview of their operating principles, technology variants, and applications in power systems.

2.1.2.1 Operating Principles and Technology Variants

Supercapacitor energy storage systems, also known as ultracapacitors or Electrochemical Double-Layer Capacitors (EDLC), store energy electrostatically by forming electric double layers at the interface between porous electrodes and the electrolyte. Unlike batteries, which rely on chemical reactions, supercapacitors accumulate charge through the separation of ions, allowing rapid charging and discharging. Both electrodes are typically aluminum foils coated with activated carbon-based compounds, offering a high surface area. A separator moistened with electrolyte

provides electronic insulation while enabling ionic movement. The electric double layer consists of the Helmholtz layer, a compact arrangement of ions directly adjacent to the electrode surface, and a more diffuse layer beyond it. The Helmholtz layer plays a crucial role in determining the capacitance and fast response characteristics of supercapacitors [38, 39].

Compared to conventional electrolytic capacitors, supercapacitors achieve much higher energy density, bridging the gap between traditional capacitors and batteries [40]. In a SCES, the stored energy is a function of the capacitance and the square of the terminal voltage [41]. This relationship is expressed below, where the energy E_{SCES} is given by (2.4):

$$E_{\text{SCES}} = \frac{1}{2} C V^2 \tag{2.4}$$

The charge stored in the supercapacitor is directly proportional to the voltage, as shown in (2.5):

$$Q = CV \tag{2.5}$$

Furthermore, the voltage dynamics are governed by the current flow according to (2.6), which relates the rate of change of voltage to the current:

$$I = C \frac{dV}{dt} \tag{2.6}$$

SCES technologies include pure supercapacitors and hybrid configurations. Hybrid supercapacitors are further divided into battery-supercapacitor designs, which combine electrostatic and faradaic mechanisms to achieve energy densities over ten times higher than pure EDLCs and pseudocapacitors, which rely on redox reactions to enhance capacitance beyond purely electrostatic storage [42]. Unlike EDLCs, which store energy through non-faradaic charge separation, pseudocapacitors store energy via fast and reversible faradaic (redox) reactions occurring at or near the surface of the electrode material. These reactions enable much higher specific capacitance and energy density compared to EDLCs, while still allowing for rapid charge and discharge. Common pseudocapacitor materials include metal oxides such as RuO_2 and MnO_2, as well as conducting polymers like polyaniline [43–45]. While pseudocapacitors have primarily been explored in academic research, hybrid configurations, such as Li-ion capacitors, are commercially available for applications that require higher energy density [46].

The optimal design of the SCES stack, particularly the selection of the discharge ratio, and suitable power converter topologies to boost the output voltage can improve volumetric energy density by up to 50% compared to conventional, non-optimized solutions [47]. To support safe operation and

longevity, integrated balancing technologies are essential, ranging from simple passive balancing to fully power-electronics-based active solutions [48].

2.1.2.2 Grid Applications

Supercapacitors are primarily valued for their high power density, rapid response, long cycle life, and tolerance of wide temperature ranges. In grid applications, SCES are typically used to deliver short-term energy support during transient events, such as voltage sags, faults, and peak power demands. Due to their high-speed charging and discharging capabilities, supercapacitors are commonly integrated with more energy-dense storage systems, such as Li-ion batteries [49, 50].

One widely adopted application is pitch control in wind turbines, where SCES ensure sufficient energy for emergency blade adjustment to prevent mechanical damage during grid faults or shutdowns [51]. Conversely, their deployment in photovoltaic systems remains limited due to cost and lower energy storage capacity relative to batteries.

2.1.2.3 Market Perspective

The global market for supercapacitors approached one billion USD in 2021 and is projected to reach between 3.5 and 6.5 billion USD by 2041, supported by substantial investments from large manufacturers [52]. Grid-related applications are expected to account for nearly 15% of this market.

2.1.2.4 Limitations

While SCES offers compelling advantages in power density and cycle life, adoption is still constrained by challenges, including relatively low energy density and high self-discharge rates. These limitations often necessitate larger systems equipped with dedicated power electronics to ensure safe and efficient operation. Recent developments in balancing and power electronics integration have improved performance, but reliability and cost remain key considerations for broader deployment [53, 54].

2.1.3 Flywheel Energy Storage Systems (FESS)

FESS are mechanical storage devices that convert electrical energy into kinetic energy and vice versa. Known for their high power density, fast response times, and long cycle life, flywheels are

particularly suited for applications involving frequent charge/discharge cycles and short-duration energy delivery [55, 56]. This subsection outlines the underlying operating principles, key design variants, and potential roles of FESS in power systems.

2.1.3.1 Operating Principles and Technology Variants

Flywheel energy storage systems store energy in the form of kinetic energy by rotating a cylindrical mass. The stored energy is linearly proportional to the mass and quadratically proportional to the rotational speed of the flywheel. During charging, electrical energy drives the rotor to accelerate, and the energy is preserved as rotational motion. Discharging involves slowing the rotor and converting kinetic energy back into electrical power through an electrical machine. The overall energy capacity and power delivery characteristics can be adjusted by selecting the flywheels mass, material, and rotational speed [57].

The common flywheel model is developed according to its governing laws [58]. A FESS can store kinetic energy while rotating around its axis, and it is characterized by a fast response to energy peak demands. Flywheel power P and shaft torque T can be expressed by (2.7)-(2.8) [59]:

$$P = T\omega + P_{\text{loss}} \tag{2.7}$$

$$T = J\dot{\omega} \tag{2.8}$$

where J denotes the rotational inertia, P_{loss} represents the total power losses due to factors such as friction and aerodynamic drag, and ω and $\dot{\omega}$ are the angular velocity and acceleration, respectively.

FESS designs vary widely depending on the construction, materials, and bearing technology used. Flywheel disks are typically manufactured from steel for robust, low-speed applications or composite materials for lighter, high-speed designs. For example, Siemens retrofits existing synchronous machines with large steel flywheel masses to provide substantial inertia and grid stability services. However, these systems require significant space and structural support [60]. Conversely, manufacturers such as Stornetic focus on lightweight, high-speed flywheels operating above 45,000 rpm to achieve higher energy densities in more compact installations [61]. Different machine and bearing types of FESS are explained in more detail below.

Classification and Main Components: Flywheel energy storage systems are broadly categorized into two types: low-speed (below 10,000 rpm) and high-speed (10,000-100,000 rpm). Low-speed systems are more cost-effective and suitable for short-duration applications, although they exhibit

higher self-discharge [62]. High-speed flywheels, using magnetic bearings, composite rotors, and vacuum enclosures, achieve greater speeds and lower losses but at higher costs [63, 64]. While low-speed designs are mature, high-speed variants have only recently reached the market stage [65, 66]. The main components of the flywheel are described below.

- **Rotor:** The energy stored in a FESS, denoted as E_{FESS}, depends on the moment of inertia of the rotor J and its rotational speed ω_m, and is given by [63]:

$$E_{\text{FESS}} = \frac{1}{2}\text{J}{\omega_m}^2 \tag{2.9}$$

  Increasing speed has a more significant effect than increasing mass, but the maximum speed is limited by the rotors tensile strength. To maximize energy per unit mass, materials must combine high tensile strength with low density [65, 67]. These properties are found in glass or carbon fiber composites commonly used in high-speed flywheels. In contrast, low-speed systems use steel, increasing mass to store more energy [64, 68]. The rotors geometry, expressed via a shape factor, also affects energy density [67, 69]. Hollow cylinders are typically used for high-speed rotors, while solid ones are common for low-speed designs [69]. The volumetric energy density e_v and specific energy e_m of the flywheel are calculated as:

$$e_v = K\sigma \tag{2.10}$$

$$e_m = \frac{K\sigma}{\rho} \tag{2.11}$$

  where: K is a design-related constant, σ is the tensile strength of the material, and ρ is the material density.

- **Electrical Machine:** The rotor couples to an electrical machine for energy conversion. Low-speed FESS often utilizes asynchronous machines due to their robustness, high torque, and low cost. However, they cannot operate in a vacuum due to cooling limitations. High-speed FESS typically uses Permanent Magnet Synchronous Machines (PMSM), offering high efficiency, power density, and no rotor copper losses [70]. PMSMs are more expensive, have lower tensile strength, and are sensitive to demagnetization at high temperatures [71]. Other machine types, such as switched reluctance, homopolar, and axial-flux machines [72–74], have also been explored, though they are rarely used commercially.

Table 2.2 compares different electrical machine types used in FESS and outlines the main structural distinctions between low-speed and high-speed flywheel energy storage systems. Low-speed designs are a more cost-effective choice, suitable for applications where short discharge durations and higher self-discharge are acceptable. In contrast, high-speed systems incorporate magnetic bearings, composite rotors, and vacuum enclosures to achieve much higher rotational speeds, greater energy capacity, and substantially lower self-discharge rates.

Table 2.2: Comparison of different types of electrical machines used in FESS [62, 75, 76]

Machine Type / Characteristic	Asynchronous	Reluctance	Permanent Magnet Synchronous
Power	High	Medium & Low	Medium & Low
Specific power	Medium (0.7 kW/kg)	Medium (0.7 kW/kg)	High (1.2 kW/kg)
Rotor losses	Copper & iron	Iron (slots)	None
Efficiency	High (93.4%)	High (93%)	Very High (95.2%)
Cost	Low	Low	High

- **Power Converters:** Power converters manage energy flow between the flywheel and the grid, often through back-to-back voltage source converters (VSCs) with DC links [77]. These convert the machines variable-frequency output to grid-compatible AC. Conventional two-level VSCs are widely used, but three-level (neutral-point clamped) converters have been proposed to reduce harmonics and improve efficiency. Matrix converters, which omit the DC link, can reduce volume but add control complexity and harmonic distortion [78,79]. Other configurations, such as Z-source converters, have demonstrated promising efficiency improvements [80]. In high-speed FESS, low machine inductance requires LC filters to limit current ripples and losses [81]. Silicon carbide MOSFETs are being increasingly investigated for improved switching [82].
- **Bearings:** Bearings must support the rotor and minimize losses. Low-speed systems use mechanical bearings, which are simple but suffer from friction, wear, and higher self-discharge [62]. High-speed systems rely on magnetic bearings, which eliminate friction but introduce eddy current, hysteresis, and stray flux losses [83]. Magnetic bearings can be either active, utilizing controlled electromagnets for high stiffness and damping, or passive, employing permanent magnets or HTS [62]. HTS bearings can achieve exceptionally low intrinsic losses [84], though they require cryogenic cooling and have lower stiffness and levitation force. Hybrid configurations combining HTS with active magnetic bearings have

been successfully tested [85–87], although no commercial FESS currently utilizes HTS bearings. Table 2.3 summarizes the advantages and drawbacks of bearing types.

Table 2.3: Comparison of different bearing technologies used in FESS [76]

Bearing Technology	Advantages	Disadvantages
Mechanical	Mature, low cost, high levitation force	High friction losses, short lifetime, requires lubrication
Permanent Magnetic	No power consumption, low losses	Inherently unstable, risk of demagnetization
Active Magnetic	Controllable, high stiffness	Complex, power consumption
HTS Magnetic	Lowest losses, auto-stabilizing	Requires cryogenics, low levitation force

- **Enclosure:** The enclosure contains rotor fragments in case of failure and reduces aerodynamic drag. Low-speed systems require heavy enclosures to contain large steel rotors [88]. High-speed composite rotors disintegrate into smaller pieces, allowing lighter containment. For the same energy content, a high-speed FESS enclosure may weigh half as much as the rotor, whereas low-speed enclosures can weigh twice as much. High-speed FESS enclosures also provide a vacuum to minimize air friction [62].

2.1.3.2 Grid Applications

FESS occupies a unique position between battery and supercapacitor energy storage. Compared to BESS, flywheels provide faster ramp rates and higher power output, typically ranging from tens of kilowatts up to several megawatts, with virtually no degradation over tens of thousands of cycles. Although they store less energy than batteries, they offer higher energy capacity than supercapacitors. This combination makes them especially attractive for applications requiring frequent charge/discharge cycles and rapid response, such as frequency regulation in microgrids, voltage support, and power quality enhancement [89, 90].

FESS are commonly deployed to smooth output power fluctuations from variable renewable energy sources such as wind turbines and photovoltaic systems [91–94]. They are also integrated in hybrid energy storage systems together with high-energy-density batteries to combine fast response with longer-duration energy delivery [95]. Beyond renewable integration, FESS are used in uninterruptible power supplies, voltage sag compensation, and traction applications in transportation systems [96, 97].

2.1.3.3 Market Perspective

Although recent advances in materials and engineering have enhanced performance and reduced some costs, FESS still faces strong cost competition from Li-ion batteries. The upfront capital expenditure for FESS remains significantly higher, sometimes up to ten times greater, than that of Li-ion battery systems with comparable nominal energy capacity. This high initial cost restricts their adoption, particularly in applications where energy capacity is prioritized over power performance. However, due to their rapid response capability and minimal maintenance requirements, FESS continues to attract interest in power-intensive applications requiring short-duration storage [98, 99].

2.1.3.4 Limitations

FESS faces several technical and structural limitations that constrain its broader adoption. The presence of high-speed rotating components introduces mechanical complexity and necessitates precision manufacturing, increasing both cost and maintenance requirements. Composite flywheels, while offering higher energy density, are subject to unpredictable failure mechanisms and catastrophic fracture risks under extreme tensile stress at high rotational speeds [100]. Furthermore, FESS is inherently more suitable for short-duration, high-power applications due to its low energy-to-power ratio, making it less viable for long-duration energy storage. Installation can also be complicated by the need for vibration isolation and robust containment structures, which increase the required infrastructure and footprint [101].

2.1.4 Hydrogen-Based Energy Storage System

Hydrogen has emerged as a key energy carrier in the transition toward decarbonized power systems, offering the potential for large-scale and long-duration energy storage [102]. This subsection introduces the core principles of hydrogen production and utilization technologies, followed by their role in grid applications and the trends in market development.

2.1.4.1 Operating Principles and Technology Variants

Hydrogen can be generated either by splitting water through electrolysis or by processing fossil fuels, and it can be converted back into electricity using fuel cells [103]. Hydrogen storage systems involve producing, storing, and delivering hydrogen to end-users via pipelines, rather than using conventional power lines or marine shipping [104, 105]. Once delivered, hydrogen can be

reconverted into energy through fuel cells or combusted in gas turbines specifically adapted to burn hydrogen. Hydrogen can be produced from a range of feedstocks using diverse manufacturing and processing methods, including both fossil fuels and renewable energy sources [106, 107]. Currently, around 96% of global hydrogen production originates from fossil fuels [108]. Steam Methane Reforming (SMR) is the most commonly applied technique, responsible for approximately 48% of worldwide hydrogen production [109]. Nevertheless, SMR generates substantial amounts of carbon dioxide, contributing notably to climate change [110].

Among the available options, the most environmentally sustainable is the Power-to-Gas process, which relies on water electrolysis powered by renewable energy such as geothermal, hydroelectric, solar, or wave energy [109]. Hydrogen produced through renewable pathways can be stored and transported as needed [111]. Owing to its low self-discharge characteristics and the flexibility to independently scale energy and power capacities, electrolysis combined with hydrogen storage is considered a promising solution for both short-term (lasting several days) and long-term electricity storage applications [112].

Electrolyzers are distinguished by the type of electrolyte materials they use. The three main electrolyzer technologies are Alkaline Electrolysis Cells (AEC), Proton Exchange Membrane Electrolyzer Cells (PEMEC), which use a solid polymer electrolyte, and Solid Oxide Electrolysis Cells (SOEC).

Fuel cells are classified into several types: Alkaline Fuel Cells (AFC), Phosphoric Acid Fuel Cells (PAFC), Molten Carbonate Fuel Cells (MCFC), Proton Exchange Membrane Fuel Cells (PEMFC), and Solid Oxide Fuel Cells (SOFC). Notably, SOFCs operate in reverse as SOECs during electrolysis. Compared to AEC and PEMEC, SOECs have advantages in efficiency, producing hydrogen at higher yields up to twice as efficient as AEC and 1.5 times more efficient than PEMEC systems [113]. The comparison of the fuel cells and electrolysers' material and technology is summarized in the Table 2.4.

2.1.4.2 Grid Applications

Hydrogen-based storage can deliver various ancillary services, including frequency regulation, voltage support, black start capability, and congestion relief in power networks [114–116]. However, there remain open questions about how quickly hydrogen systems can respond dynamically to provide fast services such as primary frequency control. More comprehensive modeling and experimental studies are needed to better understand their impact on power system operations. Hydrogen can also help stabilize grids with high renewable shares by supporting voltage and frequency control and damping power oscillations [117]. Leveraging hydrogens dual role as a

Table 2.4: Overview of Hydrogen Technologies, Production Pathways, and Fuel Cell/Electrolyzer Types

Category	Technology	Key Points
Electrolyzers	Alkaline Electrolysis Cells (AEC)	Conventional, mature technology; uses aqueous alkaline electrolyte
Electrolyzers	Proton Exchange Membrane Electrolyzer Cells (PEMEC)	Solid polymer electrolyte; faster response, compact design
Electrolyzers	Solid Oxide Electrolysis Cells (SOEC)	Operates at high temperatures; higher efficiency
Fuel Cells	Alkaline Fuel Cells (AFC)	Common low-temperature fuel cell type
Fuel Cells	Phosphoric Acid Fuel Cells (PAFC)	Medium-temperature fuel cells, suitable for stationary applications
Fuel Cells	Molten Carbonate Fuel Cells (MCFC)	High-temperature, typically stationary large-scale use
Fuel Cells	Proton Exchange Membrane Fuel Cells (PEMFC)	Low-temperature, fast start-up, common in transport applications
Fuel Cells	Solid Oxide Fuel Cells (SOFC)	High-temperature, can operate in reverse as SOEC during electrolysis; high efficiency

flexible load and energy source can reduce inefficiencies from transporting and converting energy carriers.

2.1.4.3 Market Perspective

Currently, alkaline electrolyzers account for approximately 75% of global production capacity, while PEMEC systems make up roughly 25%. SOEC have a very small market share [115]. By 2050, green hydrogen is projected to supply 60%-80% of total production, equivalent to around 4500 GW of capacity, primarily targeting sectors such as steelmaking, transport, and electricity generation and storage. The expansion of renewable energy is expected to be closely linked with the scaling of green hydrogen production [118].

2.1.4.4 Limitations

Hydrogen-based energy storage systems face several challenges that limit their current widespread adoption. The overall round-trip efficiency is relatively low due to energy losses during electrolysis, compression or liquefaction, storage, and reconversion back to electricity, often reaching

30-50% losses [119]. Additionally, high capital and operational costs, especially for green hydrogen production via electrolyzers, fuel cells, and storage infrastructure, pose economic barriers that require further technological advances and policy support [120].

Furthermore, hydrogens low volumetric energy density necessitates complex and costly storage and transportation solutions, such as high-pressure tanks or cryogenic liquefaction, which also raise safety concerns due to hydrogens flammability and leakage risk. The relatively slow dynamic response of hydrogen systems compared to batteries limits their effectiveness in providing fast grid services like frequency regulations. Moreover, the hydrogen supply chain infrastructure is still underdeveloped, restricting large-scale deployment and integration into existing energy systems [121].

2.1.5 Superconducting Magnetic Energy Storage (SMES)

SMES systems are unique among energy storage technologies in that they store energy in the magnetic field generated by a direct current flowing through a superconducting coil. This method allows for extremely high efficiency, instantaneous power delivery, and minimal energy loss during storage [122]. The following subsection outlines the fundamental operating principles of SMES and the technological variants based on superconducting materials.

2.1.5.1 Operating Principles and Technology Variants

Superconducting Magnetic Energy Storage systems operate by storing energy in a magnetic field created when a direct current flows through a superconducting coil cooled below its critical temperature, allowing nearly lossless conduction. Niobium-titanium is a widely used superconducting material with a critical temperature of 9.2 K [123, 124].

SMES systems employ two main categories of superconductors [125, 126]: (i) Low-Temperature Superconductors (LTS), which require cooling to low temperatures around 30 Kelvin; and (ii) High-Temperature Superconductors (HTS), which can operate at higher temperatures near 77 Kelvin.

2.1.5.2 Grid Applications

Although early concepts envisioned SMES units providing bulk energy storage, charging during off-peak hours, and discharging during peaks to support large power plants, practical deployment has been constrained by high costs and material limitations. As a result, SMES has primarily

been applied to improve power quality, such as stabilizing voltage and mitigating short-term disturbances. Recent research continues to explore SMES as a short-duration storage solution due to its very high efficiency (up to 95%) in large-scale systems [127–129].

2.1.5.3 Market Perspective

While numerous successful SMES pilot projects and demonstrations have been conducted by international organizations and government programs [130–133], the technologys adoption has been limited primarily by the high cost. However, advances in high-temperature superconductors (operating above 77 K) and second-generation superconducting wire hold promise for achieving higher magnetic flux densities, up to 20 Tesla, while reducing costs.

Expanding the supply chain for superconducting coils and related components is also expected to help lower manufacturing expenses [134, 135]. At present, SMES system costs vary considerably depending on design and materials, ranging from 700 $ to 10000 $ per kilowatt-hour of energy capacity, and between $130 and $515 per kilowatt of power capacity [136, 137].

2.1.5.4 Limitations

Despite their excellent efficiency and fast response times, SMES systems face significant challenges that limit their widespread deployment. The requirement to maintain superconducting coils at cryogenic temperatures necessitates complex and costly cooling infrastructure, which increases both capital and operational expenses [122]. Moreover, the energy density of SMES is relatively low compared to chemical batteries or other storage technologies, which restricts their use to short-duration energy storage and power quality applications rather than bulk energy storage [128].

In addition, the high upfront cost of superconducting materials, particularly high-temperature superconductors, and the technical difficulty of manufacturing large-scale superconducting coils remain major barriers [134, 136]. Safety concerns related to the strong magnetic fields and the risk of quenching (loss of superconductivity) require robust engineering controls and monitoring systems. These factors combined mean that SMES is currently best suited for specialized grid services rather than general energy storage, with ongoing research focused on reducing costs and improving scalability.

2.1.6 Pumped Hydro Energy Storage (PHES)

PHES is the most mature and widely deployed form of large-scale energy storage. It provides both energy shifting and grid stability services by leveraging gravitational potential energy in a closed or open hydraulic cycle. PHES has been central to balancing power systems with variable renewable energy and remains a benchmark technology for long-duration storage [138, 139]. The following subsection introduces its operating principles, system configurations, and emerging innovations.

2.1.6.1 Operating Principles and Technology Variants

Pumped hydro energy storage works by converting electricity into gravitational potential energy. During periods of low electricity demand and lower prices, water is pumped from a lower reservoir up to a higher one. When demand increases, the stored water is released back down through turbines to generate power.

There are several configurations and variants of PHES systems. Open-loop systems are connected to a natural body of water, such as a lake, river, or ocean, which serves as one of the reservoirs. In contrast, closed-loop systems, also referred to as off-river systems, employ two artificial reservoirs that are isolated from natural water bodies. This approach reduces environmental impact and provides greater flexibility in site selection. While conventional PHES plants utilize fixed-speed pump-turbines, modern installations are increasingly adopting variable-speed technology, which enables enhanced operational flexibility, improved grid support through frequency and voltage regulation, and smoother transitions between pumping and generating modes [140]. Additionally, underground PHES concepts are emerging, utilizing underground caverns or decommissioned mines as lower reservoirs. These designs create opportunities for deployment in regions that lack suitable surface topography [141, 142].

2.1.6.2 Grid Applications

PHES is widely recognized as one of the most effective technologies for supporting the integration of renewable energy, as it can perform peak shaving and provide dispatchable generation. With an efficiency typically ranging between 70% and 80%, PHES systems can vary in size from several hundred kilowatts to multi-gigawatt capacities [138, 143].

Advantages of pumped hydro include long operational lifespans, rapid response times, large storage capacities, low running costs, and high round-trip efficiency [144–146]. However, their

main limitation is the need for a substantial land area to build reservoirs, ideally near a reliable water source.

2.1.6.3 Market Perspective

PHSE remain the most economically viable option for large-scale energy storage. Nonetheless, they require significant capital investments and depend heavily on appropriate topographic and geological conditions. Simply having enough water nearby does not guarantee that a site will be suitable for development [147, 148].

2.1.6.4 Limitations

Despite its maturity and proven effectiveness, pumped hydro energy storage faces several inherent constraints. The most significant limitation is the dependence on favorable geographic and hydrological conditions, such as suitable elevation differences and abundant water resources, which restrict site availability and limit scalability in many regions [147]. Additionally, the construction of large reservoirs can have substantial environmental and social impacts, including habitat disruption, land use conflicts, and potential displacement of communities.

Furthermore, PHES projects typically require very high upfront capital expenditures and long development times, which can be exacerbated by complex permitting and regulatory processes [148]. While operational costs are low and lifespans are long, the inflexibility of reservoir sizing and limited siting options make PHES less adaptable compared to emerging storage technologies. Innovations such as underground or closed-loop systems aim to alleviate some of these limitations, but these remain less commercially mature.

2.2 Comparison between energy storage technologies

Figure 2.1 illustrates the technical maturity of various ESSs and their suitability for distributed versus bulk energy services. The vertical axis represents the level of technical maturity, ranging from developing technologies at the bottom to mature technologies at the top. The horizontal axis indicates the suitability of each storage technology for distributed services on the left and bulk services on the right.

Pumped hydro storage is depicted as a mature mechanical storage technology that is primarily suited for bulk services, reflecting its century-long history of widespread deployment for grid-scale energy management. BESS is classified as a developed, mature electrochemical technology that covers a wide range of applications, from distributed services to bulk storage, indicating its flexibility and growing role across various scales. FESS is also categorized as a developed mechanical storage system, with a primary focus on distributed services that require fast cycling and high power delivery [149, 150].

SCES and SMES are electrical storage technologies positioned within the developed category. Both are more suitable for distributed services, emphasizing their rapid response characteristics and relatively limited energy storage capacity. Finally, Power-to-Hydrogen is classified as a developing mechanical storage approach, with its primary suitability oriented toward bulk services due to its large-scale seasonal storage potential. However, it is not yet commercially mature [151–153].

To gain a clearer understanding of the potential of power-intensive energy storage systems, it is essential to distinguish them from energy-intensive counterparts. Figure 2.2 illustrates the ranges of specific power (per unit mass), specific energy (per unit energy), and discharge time for various energy storage technologies. Figure 2.3, on the other hand, shows various ESS technologies, their grid applications, and their associated power ratings.

Figure 2.3 also illustrates the relationship between the time horizons of power system phenomena and the typical discharge times of each storage technology in more detail, and Table 2.5 summarizes the ESS characteristics.

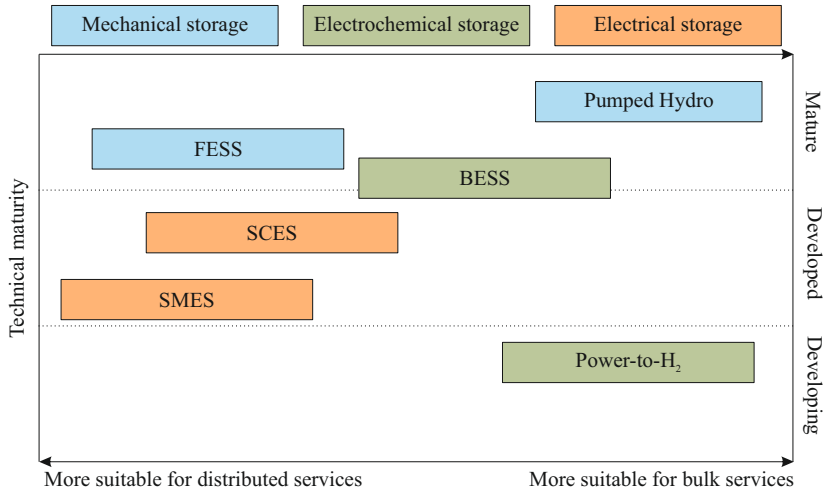

Figure 2.1: Technical maturity of energy storage systems and their suitability

2.3 Hybrid Energy Storage Systems (HESS)

No single energy storage system is without limitations; each technology comes with inherent trade-offs in terms of power density, energy capacity, response time, cost, and lifecycle. To overcome these shortcomings and capitalize on the strengths of different technologies, HESS has been developed. HESS combines two or more types of storage devices with complementary characteristics to enhance overall system performance. Typically, they integrate high power-density technologies, such as FESS and SCES, with high energy-density solutions like Li-ion batteries [166, 167]. This configuration allows high-power devices to quickly respond to transient events and peak loads, while high-energy devices provide sustained energy output for longer durations [168].

The main advantage of HESS lies in its dual capability to offer quick power support and sustained energy output. For instance, supercapacitors can effectively manage rapid, high-power events lasting a few seconds to minutes, such as frequency control in power grids or acceleration in electric vehicles [169, 170]. Meanwhile, batteries or similar long-duration storage technologies ensure a stable energy supply during extended load variations [168]. This complementary interaction enhances overall system performance, minimizes stress on individual components, and extends the operational life of the entire storage system [171].

The operational lifetime of a BESS is a critical factor in determining its economic and technical viability, especially in applications requiring frequent charge and discharge cycles [172, 173].

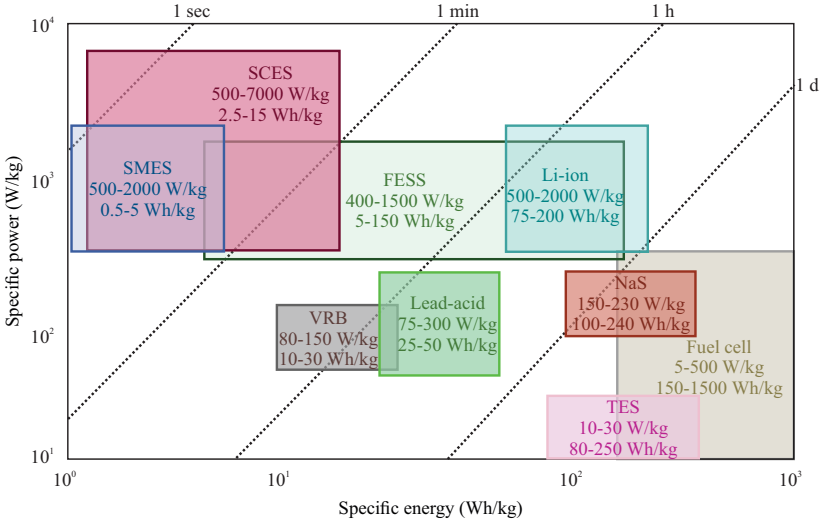

Figure 2.2: Diagram of comparison between specific energy, specific power, and discharge time.

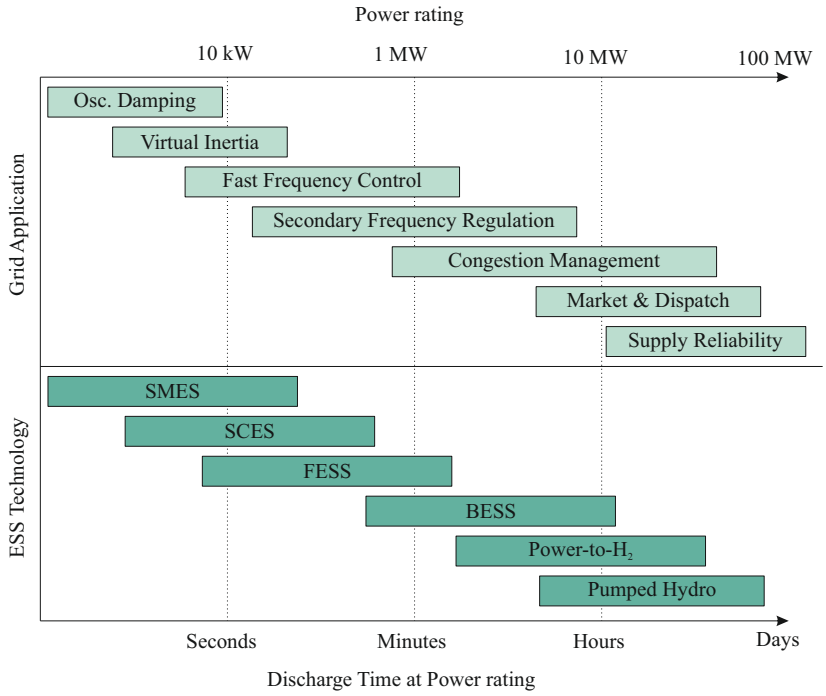

Figure 2.3: Time horizon for power system phenomena and typical discharge times for energy storage systems and the power rating

Battery degradation over time is influenced by multiple stress factors, including high current rates, deep cycling, high temperatures, and frequent power fluctuations. These factors lead to capacity fade and increased internal resistance, ultimately shortening the batterys usable life [174,175]. As such, battery lifetime is increasingly being treated as a performance characteristic for evaluating energy storage strategies.

HESSs, which integrate batteries with fast-response storage technologies such as SCES or FESS, offer a promising approach to mitigating the stress factors that degrade batteries. By assigning rapid power fluctuations and high current transients to the high-power-density auxiliary storage, the battery is effectively shielded from dynamic load conditions. This approach reduces the depth of discharge (DoD), limits peak current loads, and lowers the overall cycling frequency experienced by the battery [176, 177].

In practical applications, various HESS configurations have proven beneficial. For example, combining batteries with supercapacitors in wind power systems has been shown to boost efficiency and lower costs by prolonging battery life [178]. Research has further shown that integrating both short and long-duration storage technologies improves the integration of renewable energy

Table 2.5: Characteristics of some Energy Storage Systems [154]

Technology	BESS [155, 156]				FESS [157, 158]	SCES [159]	Hydrogen (fuel cell) [160–162]	SMES [134, 163]	PHES [164, 165]
	Lead-acid	VRB	Li-ion	NaS					
Specific Energy (Wh/Kg)	25-50	10-30	75-200	150-240	5-150	0.2-10	(30-45) 10^3	0.55	0.51.5
Specific Power (W/Kg)	75-300	80-150	500-2000	150-230	180-1800	7000-18000	500	500-2000	0.01-0.12
Round-trip efficiency (%)	75-85	75-90	85-97	75-90	85-95	80-95	33-42	95-98	70-87
Lifetime Cycles (100% depth of discharge)	200-1000	$<$ 13000	1000-10000	2500-4000	$< 10^6$	$< 10^6$	20000	$< 10^6$	20000-0000
Lifetime Cycles (year)	5-15	5-10	5-15	5-15	15-20	10-30	15-20	20-40	40-80
Self-discharge	Low	Very Low	Medium	Medium	High	High	Very Low	Medium	Very Low
Discharge time (ms-h)	s-h	s-10h	m-h	s-h	ms-15m	$\leq$1 min	s-24h	$\leq$1 min	h-24h+
Average Capital Cost (USD/kW)[a]	2140	2512	2512	2254	867	229	3243	322	1413
Average Capital Cost (USD/kWh)	437	54	546	343	4791	765	540	5350	58

[a] The capital costs are calculated based on each technologys typical discharge time. Average values are medians of published ranges adapted from [160].

sources into the grid [179]. In off-grid wind systems, SCES have demonstrated the ability to enhance battery longevity, a trend supported by predictive models of battery lifespan in similar studies [180,181]. Building on this, we demonstrate the improvement in battery life through HESS by means of state-of-health (SoH) analysis, accompanied by a detailed economic assessment of these benefits presented in Chapter 7.

Figure 2.4 presents the core idea behind the HESS approach for power smoothing and battery life extension. The main principle involves decomposing the original power demand into low-frequency and high-frequency components. The low-frequency portion, representing slower dynamics, is allocated to the battery. At the same time, the high-frequency residual, responsible for rapid power changes, is managed by a secondary storage device such as a supercapacitor or flywheel. This power split reduces the cycling stress on the battery, mitigating degradation. As a result, the battery operates under more favorable conditions, leading to improved SoH over time,

as illustrated in the figure. The comparison demonstrates that integrating HESS significantly enhances battery longevity compared to operating without it.

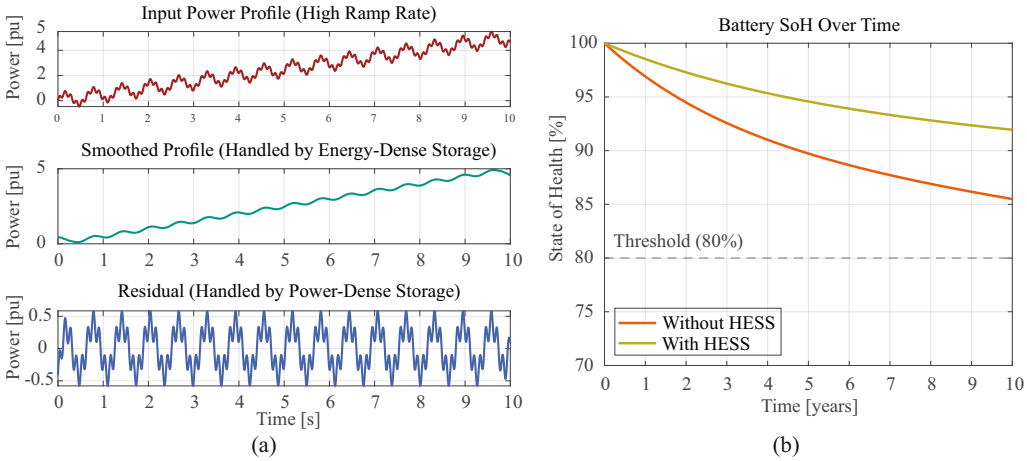

Figure 2.4: HESS concept (a) Main power waveform (b) Smoothed waveform (c) High frequency waveform as residual (d) Battery SoH over time, the cases of with and without HESS

2.3.1 Hybrid Energy Storage System Connections

Designing a HESS involves careful consideration of the energy flow during charging and discharging, as well as the efficient distribution between the different storage components. The goal is to ensure seamless operation and optimize system performance. Since HESS typically integrates two storage technologies with distinct voltage, current, and power characteristics, power electronic converters play a crucial role.

These converters enable the integration of components with different electrical behaviors, whether they act as voltage or current sources, and facilitate precise control of energy exchange. Several connection topologies have been proposed in the literature [182, 183], differing by AC or DC system configurations and the type of interconnection, such as series or multi-level arrangements. Figure 2.5 illustrates four common HESS topologies, each designed to balance performance, complexity, and application-specific requirements.

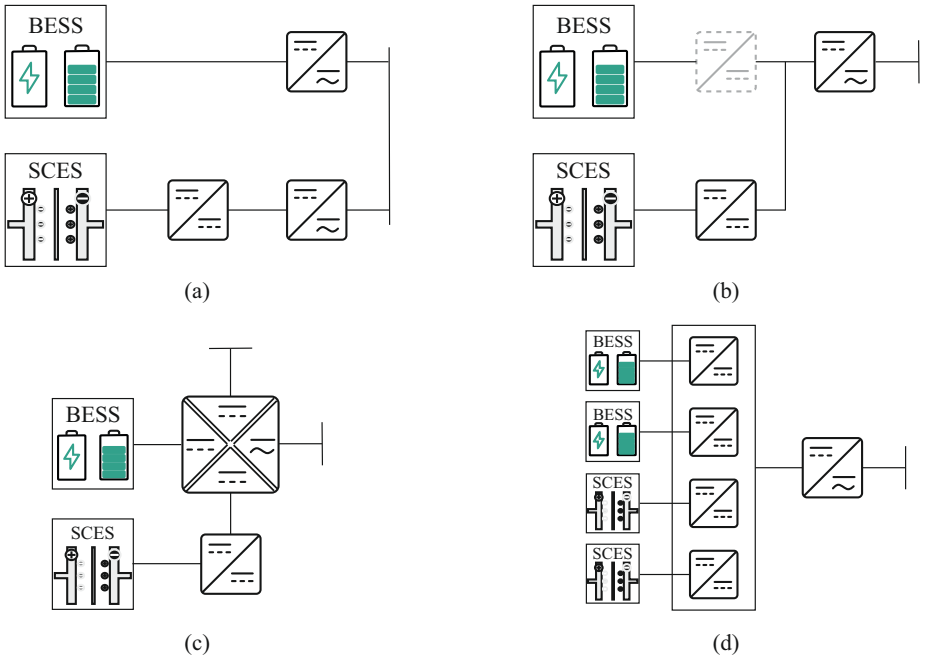

Figure 2.5: HESS connections with Battery Energy Storage System (BESS) and Supercapacitor Energy Storage (SCES) (a) Parallel AC connection, (b) Parallel DC connection, (c) Multi-Port Converter connection, (d) Modular Multi-Level connection.

2.3.1.1 AC-Connected Hybrid Energy Storage Systems

The AC connection architecture is one of the most conventional and widely adopted methods for integrating multiple energy storage systems. In this configuration, each energy storage unit, such as batteries or supercapacitors, operates independently and connects separately to the AC grid. Their coordination occurs purely at the control level through overarching power and energy management strategies.

Although this approach typically involves multiple power conversion stages, most commonly a DC/DC converter for internal power regulation and a DC/AC inverter for interfacing with the grid, which offers substantial modularity. This architecture offers substantial modularity and flexibility because each storage unit can be integrated independently using standardized inverters, allowing for heterogeneous technologies, scalable deployment, and easy upgrades without major system redesign [184]. One of its key advantages is that each storage component is a standard, off-the-shelf product that can be integrated for tailored solutions. This makes the AC connection architecture particularly attractive for scalable and flexible deployments.

2.3.1.2 DC-Connected Hybrid Energy Storage Systems

Given that most energy storage technologies, such as batteries, supercapacitors, and fuel cells, naturally operate on DC power, integrating them at the DC level presents a logical and efficient system design. Connecting storage units directly to a common DC bus eliminates the need for one stage of AC/DC conversion, thereby improving overall system efficiency up to 96% and lowering both hardware complexity and cost [185–187].

DC connections in HESS can be configured in several ways [188–190]. These include:

- **Passive connection:** where storage devices are directly tied to the DC link without intervening converters.
- **Semi-active connection:** where one energy storage unit is interfaced through a power converter for control, while others remain directly connected.
- **Active connection:** in which all storage elements are interfaced via dedicated power electronic converters, offering precise control over energy flow and system dynamics.

While active configurations provide superior control and flexibility, passive and semi-active setups can reduce component count, simplify the architecture, and offer rapid access to stored energy, which is particularly useful when capacitors are directly connected to the DC bus. Figure 2.6 illustrates the different DC-connected configurations of HESS with BESS and SCES.

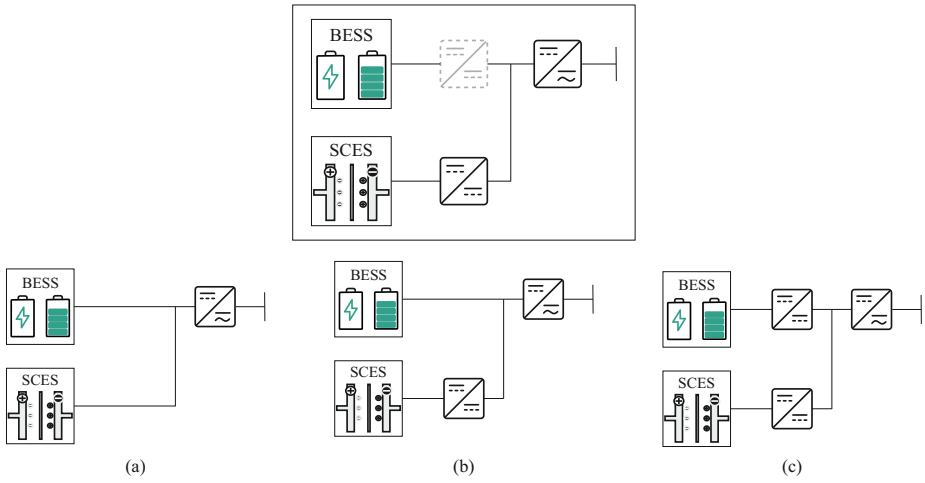

Figure 2.6: HESS DC-connections with Battery Energy Storage System (BESS) and Supercapacitor Energy Storage (SCES) (a) Passive connection, (b) Semi-active connection, (c) Multi-Port Converter connection, (d) Active connection.

2.3.1.3 Multi-Port Converter Connection

An alternative to conventional AC or DC coupling of various energy storage systems, such as batteries and supercapacitors, is the use of a single, integrated multi-port power converter. These converters can be non-isolated, commonly applied in mobile or onboard systems where compactness and weight are priorities [191], or isolated, which are better suited for stationary applications where electrical isolation is required for safety and protection [192, 193]. This approach offers a centralized and potentially more compact control structure for managing multiple storage devices within a hybrid system.

2.3.1.4 Modular Multi-Level Connection

A promising recent development involves using Modular Multi-level Converters (MMCs) to integrate various energy storage technologies at the sub-module level. Initially applied in battery energy storage systems [194], this architecture has also been extended to hybrid energy storage configurations [195, 196]. This topology enables greater modularity in both power and energy handling, while also enhancing the overall performance of the DC/AC conversion process. However, one notable limitation is the potential safety concern due to the absence of intermediate power electronics stages. To mitigate risks such as short circuits at the energy storage unit level, additional protective components, such as circuit breakers, are often necessary.

2.3.2 Services and Application of Hybrid Energy Storage Systems:

This subchapter outlines the key services offered by HESS and highlights several recent industrial projects that incorporate HESS technology.

2.3.2.1 Services provided by HESS

HESSs are uniquely suited to bridge the gap between power and energy demands across a broad range of modern applications. By integrating complementary storage technologies, such as batteries, supercapacitors, and flywheels, HESS can effectively manage short-term power dynamics and long-term energy storage, thereby enhancing system performance, reliability, and lifespan. The following sections elaborate on several high-impact sectors where HESS provides a strategic advantage.

- **Renewable Energy Integration:** One of the primary applications of HESS lies in supporting the integration of variable renewable energy sources such as wind and solar power. These resources are inherently intermittent, affected by meteorological conditions and diurnal cycles, leading to supply-demand imbalances and potential grid instability. HESS mitigates these challenges by decoupling generation and consumption: energy-dense batteries can store surplus energy during peak generation, while power-dense components like SCES or FESS can deliver fast response to sudden load changes or frequency deviations [197–200]. This dual-action capability enables grid operators to balance frequency, mitigate voltage sags/swells, and ensure smoother renewable power dispatch.

- **Electric Vehicles (EVs):** In electric mobility, the deployment of HESS enhances both driving performance and energy efficiency. Electric vehicles powered by battery-only systems face limitations in delivering high power bursts required during acceleration or regenerative braking due to thermal constraints and cycle life degradation. Integrating SCES or FESS alongside batteries provides a dual-layer storage mechanism, supercapacitors handle high current events while batteries ensure cruising-range energy provision. This results in reduced stress on batteries, extended battery life, improved acceleration response, and greater overall efficiency [201, 202]. Such configurations are increasingly adopted in hybrid electric vehicles (HEVs), plug-in hybrids (PHEVs), and fuel cell electric vehicles (FCEVs), offering superior energy management under dynamic operating conditions.

- **Electric Railways and Trains:** Electrified railway systems demand robust, high-frequency energy exchange for both traction and regenerative braking. Traditional energy storage systems like batteries, though widespread, often fall short in terms of response speed and cycle life. HESS enables the simultaneous accommodation of high regenerative braking energy and steady traction demands. SCES or FESS can absorb energy peaks during braking events and support traction acceleration, while batteries handle average load demands over longer durations [168, 203–205]. This combination improves energy utilization, reduces peak power draw from substations, and leads to cost savings on rail infrastructure.

- **Marine Transportation:** The maritime sector is undergoing a paradigm shift toward decarbonization, with all-electric and hybrid-electric propulsion systems gaining traction as alternatives to diesel-driven ships. These vessels require reliable and resilient onboard energy storage solutions. However, conventional battery systems alone are vulnerable to rapid current surges, which can accelerate degradation and compromise operational reliability. HESS solutions, combining Li-ion batteries with SCES, offer a more resilient system. Supercapacitors buffer high-power transients from propeller load changes or maneuvering operations, while batteries provide the baseline energy [206, 207]. This reduces the total

cost of ownership, enhances safety, and aligns with environmental compliance targets by reducing Nitrogen oxides (NOx) and Sulfur oxides (SOX) emissions.

2.3.2.2 Existing Projects with HESS

Real-world implementations of HESS are gaining momentum as the energy industry increasingly prioritizes systems capable of managing both energy density and power delivery. The following projects underscore the diverse applicability and technical sophistication of HESS across different domains.

- **Duke Energy HESS, Rankin Substation, Gaston County:** This pilot project demonstrates the viability of HESS for renewable integration and load shifting at the substation level. The system combines 100 kW/300 kWh Aqueous Hybrid Ion batteries from Aquion Energy with ultracapacitors from Maxwell Technologies. The dual-storage configuration improves response speed and energy throughput, reducing the reliance on peaker plants and enhancing solar smoothing capabilities [208]. It stands as a benchmark for substation-level hybrid deployments tailored for distributed solar PV environments.
- **Skeleton Technologies SuperBattery HESS:** Skeleton Technologies has introduced a hybrid energy solution that combines the high power density of ultracapacitors with the energy density of conventional batteries. Known as the SuperBattery, this technology offers rapid charge/discharge capability, operational durability in harsh climates, and excellent cycle lifemaking it highly suitable for grid applications, electric buses, and industrial use cases [209]. The innovation lies in the custom electrode design that enhances conductivity and thermal stability, addressing critical limitations of standard Li-ion systems.
- **Beyonder & ABB Li-ion Capacitor HESS:** In a strategic partnership, Beyonder and ABB are commercializing Li-ion capacitors for large-scale grid integration. By leveraging ABBs power electronics and Beyonders advanced capacitor technology, the project aims to deploy modular, sustainable, and fast-responding HESS units. These are envisioned for use in grid edge applications, including zero-emission airport logistics, electric port cranes, heavy-duty EV charging, and fast frequency regulation [210]. The system is designed to minimize total harmonic distortion and provide ancillary grid services such as synthetic inertia and short-circuit support.
- **V-ACCESS (Vessel Advanced Clustered and Coordinated Energy Storage Systems):** Funded under the European Union framework, V-ACCESS exemplifies the state-of-the-art in marine hybrid storage. The project integrates a coordinated cluster of 100 kW battery, SCES, and SMES units aboard electric vessels to optimize energy flow in real-time based

on operational profiles. The inclusion of superconducting storage offers ultra-fast response for critical maritime maneuvers. The project not only targets emission reduction but also improves onboard power system stability. It incorporates advanced power flow control strategies, DC bus integration techniques, and rigorous safety and marinization standards to ensure the robustness of hybrid systems in harsh marine conditions [211].

- **Calistoga Resiliency Center Hydrogen+BESS:** It is a long-duration energy storage and generation facility that combines Li-ion battery storage with a hydrogen fuel cell power plant. This hybrid setup delivers a total peak power of 8.5 MW and stores up to 293 MWh of energy. Under typical load conditions, the system can supply uninterrupted power to the city for up to 48 hours. The facility operates using green hydrogen produced through electrolysis, meeting Californias Renewable Portfolio Standard. Once fully commissioned, it is expected to become the largest green hydrogen-based long-duration energy storage project in the U.S [212].
- **Pyhäsalmi mine Hybrid PHES-BESS in Finland:** Developed by Sustainable Energy Solutions Sweden Holding (SENS), is a fully established HESS that integrates a 75MW underground PHES storage facility with a 170 MW Li-ion BESS. Originally designed with an 85 MW battery component, the systems storage capacity was doubled in early 2025 thanks to advances in battery technology. This HESS setup combines the long-duration capabilities of PHES with the fast response and flexibility of battery storage, enabling the system to participate effectively in both frequency regulation and energy arbitrage markets [213].

The summary of the existing HESS project is also presented in Table 2.6.

Table 2.6: Overview of selected real-world HESS projects

Project	Technology Mix	Key Features
Duke Energy HESS (2016, USA)	100 kW/300 kWh AHI + Ultracaps	Substation-level solar smoothing and load shifting
Skeleton SuperBattery (2023, EU)	Li-ion + Ultracaps	High power density, fast charging, long cycle life
Beyonder & ABB (2024)	Li-ion Capacitors	Grid-edge support, fast response, synthetic inertia
V-ACCESS (2023, EU)	BESS + SCES + SMES	Marine HESS with real-time coordination and ultra-fast response
Calistoga Resiliency (2025, USA)	8.5 MW BESS + H_2 Fuel Cell	293 MWh long-duration backup, green H_2
Pyhäsalmi Mine HESS (2025, Finland)	75 MW PHES + 170 MW BESS	Long-duration and fast-response hybrid; market-ready

2.4 Summary

This chapter provides an overview of energy storage technologies and the rationale for integrating them into Hybrid Energy Storage Systems (HESS). First, it surveys the characteristics, strengths, and limitations of energy storage technologies, such as BESS and FESS. It then provides a comprehensive comparison of the Energy Storage Systems (ESS), including their characteristics, applications, and costs. Next, the chapter introduces HESSs, which combine complementary technologies to balance energy capacity and power capability by assigning high-power transients to fast-response devices and sustained loads to high-energy devices. Several power electronics integration topologies for HESS are detailed, which enable precise control and efficient energy flow between diverse storage technologies.

The chapter further outlines key applications and services provided by HESS, emphasizing their role in renewable energy integration, electric vehicles, electrified railways, and marine transport. Several real-world projects demonstrate the deployment of HESS across various sectors, showcasing technological maturity and practical benefits.

3 Experimental Setup

Power Hardware-in-the-Loop (PHIL) testing has become a powerful methodology to bridge the gap between simulation and field deployment. By combining real-time numerical simulation of grid and system dynamics with physical power exchange, PHIL allows researchers and engineers to assess hardware components and controllers under controlled, repeatable, and highly dynamic scenarios.

At the Karlsruhe Institute of Technology (KIT), the EnergyLab facility offers a state-of-the-art PHIL environment that can simulate complex low-voltage distribution grids, renewable energy generation profiles, and demanding load conditions. The platform integrates a high-performance real-time simulator, power amplifiers, and comprehensive monitoring and safety infrastructure. This chapter describes the experimental environments used to evaluate the Flywheel Energy Storage System (FESS) and Supercapacitor Energy Storage (SCES) as the main Devices Under Test (DUT) within PHIL-based studies.

3.1 Power Hardware-in-the-Loop (PHIL) Concept and Architecture

PHIL is a real-time simulation technique that enables the interaction between simulated models and physical hardware components. Unlike purely software-based simulations or traditional Hardware-in-the-Loop (HIL) setups, PHIL incorporates actual power exchange, allowing the real-world testing of power equipment under controlled and repeatable scenarios [214, 215]. This methodology is especially valuable for the development, validation, and testing of power electronics, control strategies, and complex systems such as Hybrid Energy Storage Systems (HESS).

PHIL setups as shown in Figure 3.1 consist of three main components: (1) a Real-Time Digital Simulator (RTDS), (2) a Power Interface, and (3) the Device Under Test (DUT). At the core of PHIL is the real-time simulator, which plays a pivotal role in replicating the dynamic behavior of electrical systems. Real-time simulation is a critical methodology in modern power system

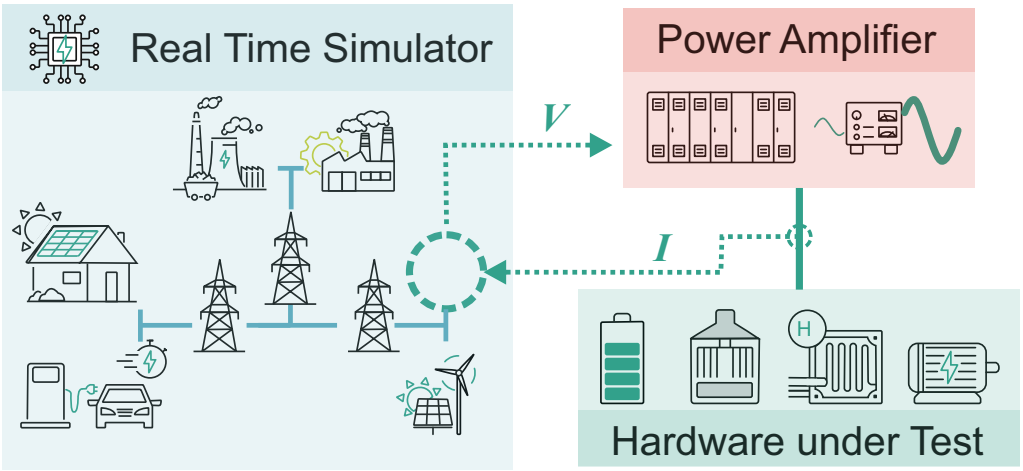

Figure 3.1: Power Hardware In the Loop concept

analysis and testing. By definition, real-time simulations require that the computational model representing the physical system be updated at every fixed, small time step, enabling the simulation to reflect the real-world behavior of the system with high fidelity [216]. Unlike traditional (offline) simulations, which may take minutes or hours to simulate a few seconds of system behavior, real-time simulations must operate synchronously with actual time, meaning that one second of simulation time must be computed within one second of wall-clock time.

At the heart of real-time simulation lies the hard real-time constraint: all mathematical calculations and I/O communications, often involving large sets of differential and algebraic equations, especially in Electromagnetic Transient (EMT) models, must be completed within a predefined simulation time step. In power system simulations, especially those dealing with transient events, this time step can be as small as 10 to 50 microseconds, depending on the system dynamics and the required resolution [217].

To satisfy the hard real-time constraint, fixed-step solvers are employed. Unlike variable-step solvers used in offline simulations, which adjust the time step based on the complexity of system dynamics at a given moment, fixed-step solvers maintain a constant step throughout. This ensures deterministic timing but significantly increases the computational burden. Any violation of this time constraint is referred to as an overrun. This condition occurs when the simulation takes longer than the available time step to complete a cycle [218]. Overruns lead to incorrect or unstable simulation results and must be strictly avoided [219].

To ensure real-time capability in PHIL setups, particularly those modeling detailed EMT phenomena, the simulator must solve large sets of differential equations efficiently. This becomes

especially challenging in low-voltage distribution networks with high levels of converter-interfaced Distributed Energy Resources (DERs) [76]. These systems:

- Lack long transmission lines that could provide natural propagation delays for model decoupling, as used in transmission system simulations [220],
- Often requires detailed models of inverters, power electronic interfaces, and control systems, which significantly increase the computational load,
- Must maintain accuracy despite limited time for computation.

3.1.1 PHIL Test Case Development

Before conducting PHIL testing, it is essential to prepare the necessary models and define appropriate test cases. This process involves several key steps to ensure the hardware is thoroughly understood, the simulation environment is suitably configured, and the test scenarios accurately reflect real-world conditions. The main stages of test case development are summarized below:

- **Initial Modeling and Simulation:** Model and simulate the hardware under test to understand its behavior before conducting physical experiments. This step helps prevent unexpected issues during testing and supports the design of safe and effective test cases. The required modeling detail depends on the study objectives. Although offline simulations are helpful, real-time simulations allow direct integration with the grid model used later in actual tests. Developed models should be validated with measurements from the real hardware whenever possible.
- **Grid Modeling in Real-Time Simulation:** Implementing the grid where the hardware will be tested within a real-time simulation environment. Ensure the model detail and simulation step size are appropriate to accurately represent the real power system. The simulation sampling rate should be at least 10-20 times higher than the highest dynamic of transients requiring accurate representation (model bandwidth) [221]. The model bandwidth also determines the minimum amplifier bandwidth needed, helping select a suitable power amplifier for the PHIL setup.
- **Defining Test Scenarios:** Develop and define scenarios for PHIL testing. Simulate these scenarios using the hardware and grid models, preferably in a real-time simulation environment. This provides an accurate prediction of hardware behavior for each scenario. Incorporate PHIL-related delays and latencies into the simulation to improve accuracy.

Once the real-time simulation models and test scenarios have been prepared and the stability and accuracy of the PHIL setup have been thoroughly assessed, the hardware under test can be connected using the selected interfacing algorithm.

Although theoretical stability analysis offers helpful insights into the expected stability margins, it is important to recognize that unforeseen instabilities may still arise during experiments, potentially damaging the hardware or the PHIL installation itself [222]. Inaccurate modeling or parameter settings can compromise the reliability of the stability assessment. For example, as demonstrated in [223], total loop delays within the PHIL system can fluctuate over time due to the interactions among discrete system components. To address these risks, both hardware and software safety mechanisms must be in place to immediately disconnect the system if excessive voltages, currents, or instability are detected.

When executing the PHIL tests, the grid simulation should be started in real time first. It is advisable to close the feedback loop only when there is no or minimal power exchange between the hardware and the amplifiers. This precaution helps prevent potential damage caused by incorrect configurations or instability. Once the loop has been safely closed and stable operation is confirmed, the predefined test scenarios can be carried out. In the following sections, the two main PHIL setups in KIT EnergyLab are discussed in detail, and the ESS is explained as the DUT for each PHIL setup.

3.2 KIT 1-MW Power Hardware in the Loop Setup with Egston Amplifier

An illustration of this PHIL configuration is provided in Figure 3.2. At the heart of the system is an Opal-RT 5700 real-time digital simulator, which features eight Intel Xeon processor cores alongside an Xilinx Virtex-7 FPGA mounted on a VC707 board. The simulator integrates multiple analog and digital input/output boards. It is equipped with 16 high-speed fiber-optic Small Form-factor Pluggable (SFP) ports capable of data rates up to 5 GBps. These interfaces enable direct connections both to the power amplifiers and to several OP4520 Kintex7 FPGA and I/O expansion modules through Opal-RTs Multi-System Expansion (MUSE) link.

Model compilation, deployment, and execution on the real-time target are managed using RT-LAB software, which generates C code from simulation models. RT-LAB further supports real-time monitoring of model execution, identification of overruns, mapping of I/O signals to model variables, and adjustment of model parameters during runtime.

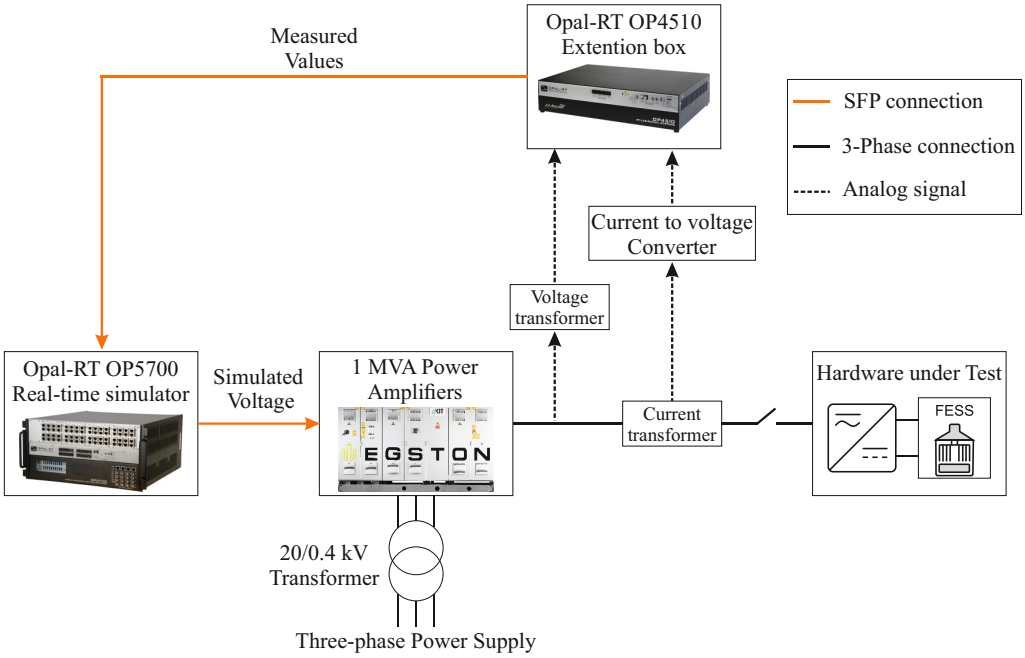

Figure 3.2: Overview of the 1-MW PHIL setup at KITs EnergyLab.

Voltage reference signals generated by the simulated grid are transmitted digitally to five 200 kVA switched-mode power amplifiers via the Aurora communication protocol developed by Xilinx. This high-speed digital link minimizes latency by removing the need for digital-to-analog conversion stages and their anti-aliasing filters, while also mitigating issues related to signal noise and grounding. The amplifiers employed are the COMPISO System Unit (CSU) GAMP6 units from Egston Power, each rated at 200 kVA. Their technical specifications are summarized in Table 3.1. Each amplifier cabinet contains six COMPISO Digital Amplifiers (CDAs), which can be flexibly configured. For emulating a 4-wire three-phase network typical of European low-voltage grids, the system is set up in a three-phase plus neutral mode, where each phase uses a single CDA, and the neutral connection uses three CDAs to handle higher neutral currents.

The five CSU amplifiers, depicted in Figure 3.3, can be operated in series or parallel configurations to achieve higher voltage or current capacities, supporting up to 1 MW of total output power. In such configurations, set points are routed first through an Egston control unit before distribution to each amplifier.

To complete the PHIL feedback loop, voltage and current signals from the hardware under test are captured and routed to two OP4520 Kintex7 I/O expansion units equipped with 16-channel, 16-bit analog input cards with a 2.5 μ s conversion time. These measurements are relayed via

Figure 3.3: Five 200 kVA GAMP6 Egston switched-mode power amplifiers (1 MVA in total).

high-speed fiber-optic connections back to the simulator. Current sensing is carried out using Danisense current transducers capable of measuring up to 640 A, 2 kA, and 5 kA, depending on the channel.

Additionally, the PHIL setup incorporates a comprehensive emergency shutdown system that can trip amplifier output breakers and isolate the equipment when needed. Besides hardware-level protections, software-based safeguards run on the real-time simulator to detect unstable conditions or abnormal voltages and currents, initiate protective trips to the amplifiers and the hardware under test, open the simulation loop, and reset set points to zero to prevent damage.

3.2.1 DUT Example Installation: FESS at KIT EnergyLab

The principles, market perspective, and grid applications of Flywheel Energy Storage Systems (FESS) have already been discussed in Chapter 2 alongside other energy storage technologies. In this subsection, the FESS is described in greater detail because this thesis involves experiments

Table 3.1: The characteristics of each Egston amplifier at KIT EnergyLab.

Parameter	Value
Nominal apparent power	200 kVA
Nominal AC Voltage (phase to phase)	450 V_{RMS}
Amplifier bandwidth	5 kHz
Maximum AC current	252 A_{RMS}
Maximum DC voltage	725 V
Maximum DC current (unipolar operation)	900 A
Controller time step	4 μs

with a real high-speed flywheel system. The focus here is on the installed high-speed FESS in KIT EnergyLab.

The FESS installed at the Energy Lab of KIT plays a crucial role in the university's research on grid-interactive storage technologies. This setup serves as a practical testbed for evaluating control strategies and operational performance under realistic conditions.

The configuration of a FESS includes the integration of all its essential subsystems. Figure 3.4 depicts the component-level architecture of a high-speed FESS. This layout is based on a commercial high-speed FESS rated at 120 kW/8 kWh. Figure 3.5 provides an internal view of the container housing the 120 kW unit along with its auxiliary equipment, and Table 3.2 shows the parameters of the FESS.

As shown in Figures 3.4 and 3.5, a high-speed FESS incorporates a PMSM mechanically coupled to a high-inertia rotor. It also features two Voltage Source Converters (VSC): the Machine-Side Converter (MSC) and the Grid-Side Converter (GSC), each with dedicated controllers and AC-side filters. Because the PMSM in this system has exceptionally low inductance, an LC filter is installed between the PMSM and the machine-side converter to mitigate current and torque ripple [224].

In essence, a FESS operates on principles comparable to those of a variable-speed wind turbine that uses a PMSM [225]. Nonetheless, the flywheel differs in several key aspects: it exhibits significantly faster dynamic behavior, it does not rely on any mechanical input torque, and it is designed to both store and release energy as needed. PMSMs are typically selected for high-speed FESS applications, whereas asynchronous machines are more commonly used in low-speed configurations. The lack of field windings makes PMSMs especially well-suited for operation in the vacuum chambers of high-speed systems, where convection cooling of the rotor is not feasible. Additionally, their simple and robust construction contributes to improved reliability. Compared

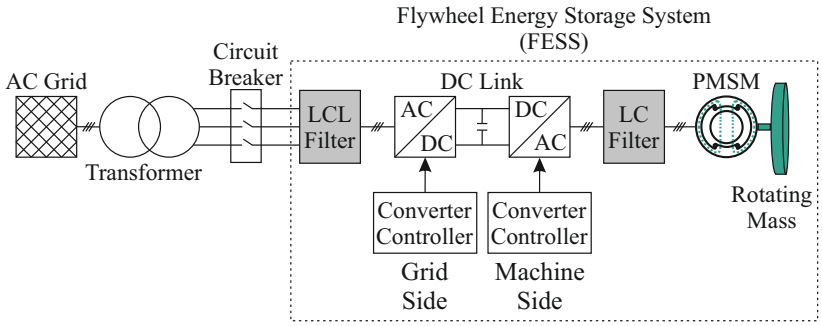

Figure 3.4: Structure of a high-speed Flywheel Energy Storage System (FESS).

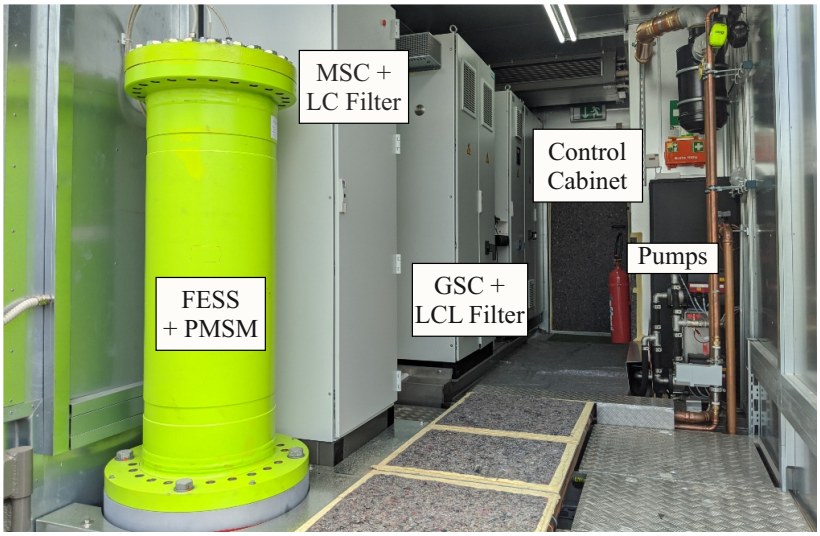

Figure 3.5: The inside view of the container of the 120 kW high-speed FESS.

to other types of electrical machines, PMSMs offer high power-to-weight and torque-to-mass ratios, along with a comparatively straightforward control design [70].

Table 3.2: Flywheel Energy Storage Parameters

Parameter	Value
Nominal power	120 kW
Nominal energy	8 kWh
Max current	160 A
AC voltage	400 V
DC voltage	720 V
Max cooling power	16 kW
Max speed	750 Hz

3.3 KIT 15-kW Power Hardware in the Loop with Spitzenberger Amplifier

Another PHIL setup at the Karlsruhe Institute of Technology has been employed, with a grid emulator as a RTDS system and three APS 15000 linear amplifiers from Spitzenberger & Spies, as shown in Figure 3.6 with a SCES as a DUT.

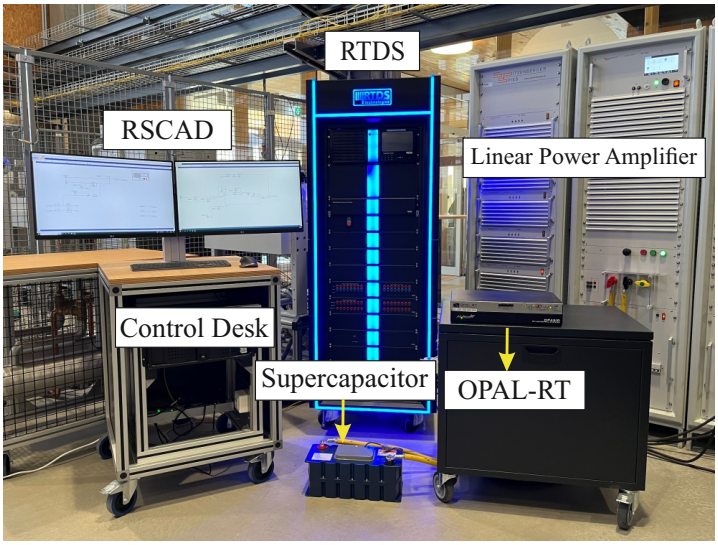

Figure 3.6: Experimental setup for the supercapacitor SoC estimation.

The employed 4-quadrant amplifiers enable full control of all electrical parameters such as voltage, current, frequency, and phase angle. This capability offers two main advantages: experiments can be reproduced under identical conditions, and, in conjunction with a real-time simulator, arbitrary connection scenarios can be investigated. The main components can be categorized into a rectifier, DC-link, linear amplifier, resistor bank, internal current and voltage measurement, and digital control. These components are illustrated in Figure 3.7.

The amplifier operates based on a controlled linear voltage amplifier. The rectifier, the DC-link with resistor bank, and the linear amplifier can be regarded as a single unit. This unit outputs a controllable voltage, which is detected by the current and voltage measurement system. The digital control system then regulates the output voltage to match the setpoint. The rate of change required for voltage regulation is low in linear amplifiers (in this case, 50 V/μ s). For example, a voltage step from 0 to 230 V_{RMS} results in a delay of less than 5 μ s. The maximum voltage slew

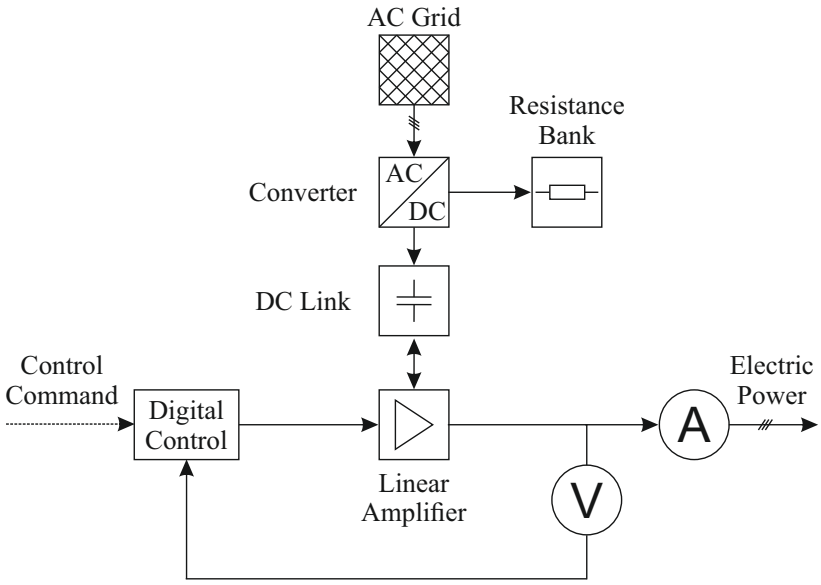

Figure 3.7: Overview of the internal structure of the power amplifier

rate also determines the maximum output AC voltage frequency. The manufacturer, Spitzenberger & Spies, specifies a maximum sinusoidal frequency of 10 kHz [226].

With an electrical power rating of 5 kVA per phase, the three-phase power amplifier can support any operating condition. The power fed into the amplifier is not returned to the grid but is dissipated in internal resistor banks. The maximum absorbable power is also 5 kVA per phase. The maximum continuous power (>1 hour) decreases with a declining power factor. With a maximum output voltage of 270 V (RMS), the amplifier is also capable of conducting overvoltage tests. The 4-quadrant power amplifiers used allow for both motoring and generating operation of DUT.

The power amplifier is controlled via an analog voltage signal. Depending on the real-time simulator used, the input level can range from ± 10 V to ± 16 V. Here, 10 V or 16 V corresponds to the full-scale RMS output voltage of 270 V from the amplifier.

3.3.1 DUT Example Installation: SCES at KIT EnergyLab

Another DUT in the smart charging energy storage platform at the KIT EnergyLab is the EATON XLR-48R6167-R supercapacitor module, also known as the XLR 166F, shown in Figure 3.8. This commercially available module is designed for high power applications and is characterized

by a nominal capacitance of 166 F and a maximum working voltage of 48.6 V. With an Equivalent Series Resistance (ESR) of only 5 mΩ, the device offers a peak power output of up to 118 kW, enabling it to handle demanding pulse load profiles with a pulse current capability of up to 2200 A. The continuous current rating is 86 A, with a nominal leakage current of approximately 5.2 mA.

Figure 3.8: EATON XLR-48R6167-R supercapacitor in KIT EnergyLab

The module is constructed from 18 individual XL60 cells, each rated at 2.7 V, and includes active cell balancing and integrated voltage management. This modular configuration results in a stored energy capacity of approximately 54 Wh, calculated using the classical energy storage formula $E = \frac{1}{2}CV^2$.

Designed with robust mechanical housing and IP65 ingress protection, the supercapacitor module is suitable for harsh environments and is compliant with Restriction of Hazardous Substances (RoHS) and Underwriters Laboratories (UL) safety standards. It can operate within a temperature range of $-40°\mathrm{C}$ to $+65°\mathrm{C}$, with extended functionality up to $+85°\mathrm{C}$ under derated voltage conditions. The module supports a rated lifetime of 1500 hours at maximum voltage and temperature, and a cycle life exceeding 1 million cycles with minimal performance degradation.

In the SCES setup, the module is controlled and evaluated using a PHIL framework, allowing real-time emulation of dynamic grid conditions. Table 3.3 summarizes the nominal specifications of the EATON XLR 166F supercapacitor as provided by the manufacturer [227].

Table 3.3: EATON XLR 166F Supercapacitor Specifications

Parameter	Value
Capacitance (F)	166
Maximum working voltage (V)	48.6
Equivalent Series Resistance (mΩ)	5
Nominal leakage current (mA)	5.2
Stored energy at maximum voltage (Wh)	54
Nominal continuous current (A)	86
Peak power (kW)	118
Pulse current (A)	2200

3.4 Summary

This chapter details the experimental environment used to evaluate Hybrid Energy Storage Systems (HESS) and related control strategies through Power Hardware-in-the-Loop (PHIL) testing.

PHIL combines real-time simulation with actual power exchange to test hardware under realistic and repeatable conditions. Unlike traditional Hardware-in-the-Loop (HIL), PHIL setups emulate real grid conditions by exchanging power with the Device Under Test (DUT). The key components of PHIL are: a real-time digital simulator that solves complex differential equations within strict time constraints (often microseconds), a power interface (amplifiers) that reproduces voltage and current waveforms, and the DUT itself.

At KITs EnergyLab, one of the PHIL platforms consists of an Opal-RT 5700 real-time simulator, five Egston GAMP6 200 kVA switched-mode power amplifiers configured for a total output of up to 1 MVA, high-speed fiber-optic connections for low-latency data exchange, and robust safety systems for hardware protection. This setup allows high-fidelity emulation of low-voltage grids, including detailed converter dynamics and transient behavior. As the main DUT, the Flywheel Energy Storage System (FESS) deployed in the EnergyLab is a commercial high-speed unit rated at 120 kW/8 kWh. It consists of a Permanent Magnet Synchronous Machine (PMSM) mechanically coupled to a high-inertia rotor, a Machine-Side Converter, and a Grid-Side Converter with dedicated controllers.

To explore hybrid configurations, there exists another PHIL environment with a supercapacitor-based storage system. The supercapacitor DUT is supplied via a Spitzenberger & Spies APS 15000 4-quadrant amplifier, which provides precise voltage and current control across all operating quadrants. Real-Time Digital Simulator (RTDS) is used in this setup as a grid emulator.

Together, the FESS and supercapacitor setups provide a versatile platform to investigate the integration of hybrid energy storage.

4 Power Management and Control of Hybrid Energy Storage Systems (HESS)

HESSs combine complementary energy storage technologies, typically high-power and high-energy devices, to address the diverse requirements of modern power systems. As described in Chapter 2, no single ESS meets all performance criteria for grid applications; hence, HESS has emerged as a promising solution for balancing power and energy demands. However, integrating multiple storage technologies increases the complexity of power management and control, particularly under dynamic conditions. This chapter provides an overview of the control and power management challenges associated with HESS and the techniques employed to address these challenges.

4.1 Challenges in HESS Control

The control of HESS presents a complex array of challenges stemming from its intrinsic heterogeneity, dynamic behavior, and operational constraints. One of the primary difficulties lies in coordinating multiple storage devices with fundamentally different characteristics. Batteries are optimized for high energy capacity but are susceptible to degradation when exposed to frequent, high-power transients [104, 228]. In contrast, supercapacitors and flywheels can absorb and deliver large bursts of power but have limited energy storage. The control strategy must therefore dynamically allocate power in a way that minimizes battery stress while ensuring that fast load fluctuations are smoothed, an objective that often conflicts with maintaining optimal SoC levels in all subsystems [159, 229].

Another major challenge is the accurate estimation and prediction of SoC and SoH. Conventional battery SoC estimation algorithms, such as Kalman Filters or Coulomb Counting, may not be directly applicable to supercapacitors due to their nonlinear voltage, charge relationships, and self-discharge behavior [230, 231]. Moreover, inaccuracies in SoC estimation can lead to suboptimal or even unsafe power allocation decisions [232]. This challenge becomes particularly pronounced

in real-time applications where control algorithms must respond within milliseconds to grid disturbances.

The design of control strategies that balance performance objectives such as efficiency, lifetime extension, and grid support services also introduces complexity. Among the most commonly used control strategies, rule-based controllers are often simple to implement but may not yield optimal results under varying load conditions. Conversely, optimization-based methods such as Model Predictive Control (MPC) or dynamic programming can deliver superior performance but are computationally intensive and require accurate system models. For instance, MPC must solve constrained optimization problems in real time, often under uncertainty due to load forecasting errors or parameter variability. This trade-off between computational burden and control quality remains a key barrier to widespread deployment [233].

Furthermore, HESS control is complicated by the need to handle operational constraints and safety limits. Each storage component has voltage, current, and thermal limits that must be respected. For example, excessive charging currents can overheat batteries or supercapacitors, accelerating degradation and posing safety hazards [234]. Implementing constraint handling robustly under rapidly changing conditions requires sophisticated algorithms and reliable sensor data, both of which increase system complexity and cost.

Interfacing HESS with power electronics introduces additional challenges. Bidirectional DC/DC converters must be controlled to deliver or absorb power rapidly and efficiently, while also maintaining DC bus voltage stability [235, 236]. In grid-connected applications, the power management strategy must synchronize with the inverter control to comply with grid codes, such as providing frequency regulation or reactive power support, further increasing the burden on the control system.

Finally, the uncertainty inherent in real-world environments, including unpredictable renewable generation, fluctuating loads, and component aging, requires that control strategies be adaptive and robust. While adaptive controllers or machine learning approaches offer potential solutions, they introduce new challenges related to training data requirements, interpretability, and ensuring stability [237].

The control of HESS demands solutions that can reconcile conflicting objectives, respect diverse physical constraints, and operate reliably under uncertainty and real-time constraints. Addressing these challenges is crucial to unlocking the full potential of HESS in applications ranging from renewable energy integration and microgrids to electric vehicle charging and provision of ancillary services. In following some of the important control strategies, addressing these challenges is discussed in more detail. Some of the literature that utilizes these strategies and their objectives is also presented.

4.2 Control Strategies

Depending on the system configuration and application, various control strategies can be employed, ranging from simple rule-based methods to advanced optimization and intelligent approaches. Each strategy offers trade-offs between complexity, adaptability, and computational requirements [238, 239]. In this context, selecting or designing an appropriate control strategy is crucial for achieving optimal operation of HESS under varying grid conditions, load demands, and operational constraints [240]. Below are the control architectures or approaches used to manage the energy and power flow in a HESS.

Figure 4.1 illustrates the main categories of control techniques commonly applied in HESS and their corresponding subsections.

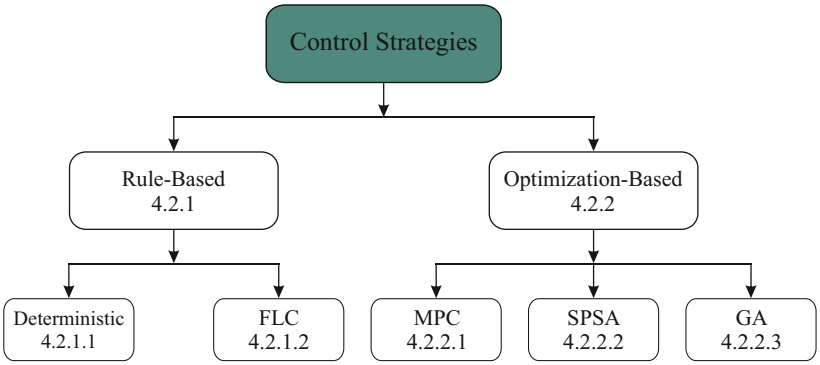

Figure 4.1: Control Strategies with their most common techniques

4.2.1 Rule-Based Control

Rule-based control strategies represent some of the earliest and most widely implemented approaches for managing power flows in HESS. Their popularity stems from their conceptual simplicity, intuitive design, and relatively low computational demands, making them attractive for applications where real-time responsiveness is prioritized over strict optimality [241]. Despite the increase of model-based and optimization-based methods, rule-based control remains highly relevant, particularly in industrial contexts where transparency, ease of tuning, and deterministic behavior are essential [242].

At their core, rule-based controllers use predefined heuristics or logical conditions to allocate power among storage devices. These rules are typically based on knowledge of the storage

technologies and the applications load profile. For example, in battery-supercapacitor systems, it is common to assign low-frequency power demands to the battery and reserve the supercapacitor for fast, high-power transients. This principle underpins many practical implementations of rule-based HESS control. A common approach involves SoC threshold-based rules, which limit charging and discharging based on each devices SoC to keep them within safe ranges and prolong their lifespan [243]. These thresholds can be combined with power splitting to create hybrid rule sets.

Priority-based allocation is also popular, designating one device (often the battery) as the primary energy source, while the high-energy ESD provides peak support during acceleration or load spikes. Adaptive rule-based schemes further enhance flexibility by adjusting filter parameters or SoC thresholds in real time [159, 229]. The two main groups of rule-based control are described in the following.

4.2.1.1 Deterministic (if-then rules)

Deterministic control, often referred to as rule-based or if-then logic, is one of the simplest and most intuitive control strategies used in HESS. It involves predefined rules and thresholds to manage the power flow between different storage devices such as batteries, supercapacitors, or flywheels [244, 245]. In these schemes, control actions are triggered directly by measurable variables, typically the power demand, the SoC of each storage component, and sometimes temperature or current limits.

In practice, deterministic controllers often incorporate threshold logic to ensure each device operates within safe and optimal ranges. For instance, if the SoC of the supercapacitor exceeds an upper threshold, surplus regenerative energy will be directed to the battery or curtailed, while if the SoC drops below a minimum threshold, the system will prevent further discharge to avoid deep depletion. These if-then rules can be implemented in real time with minimal computational effort, making them particularly attractive for embedded controllers in electric vehicles, microgrids, and renewable energy integration [246].

4.2.1.2 Fuzzy Logic Control (FLC)

FLC is a control strategy for managing HESS, especially when the system dynamics are complex, nonlinear, or uncertain with conflicting objectives. Unlike deterministic rules, fuzzy logic enables gradual decisions rather than binary (yes/no) outputs, making it ideal for coordinating multiple storage units, such as batteries, supercapacitors, and flywheels [247–249]. In FLC, expert knowledge and heuristic strategies are encoded in the form of linguistic rules (e.g., If the battery

SoC is low and load power is high, then increase supercapacitor contribution), which are evaluated using membership functions that assign degrees of truth to input variables [250].

This approach enables the controller to generate smooth and adaptive control actions that reflect the uncertain or imprecise nature of real-world operations. For example, instead of sharply switching power flows between storage units, FLC can proportionally adjust their contribution depending on how closely each input variable matches its fuzzy sets (such as low, medium, or high SoC) [251]. Typical input variables include battery SoC, supercapacitor SoC, load power demand, and sometimes the rate of change of power, while the output determines how the power is split among the devices. The design process involves defining appropriate membership functions, constructing a rule base, and selecting a defuzzification method to generate crisp control commands [252, 253]. A block diagram of a fuzzy logic control system is shown in Figure 4.2 [254].

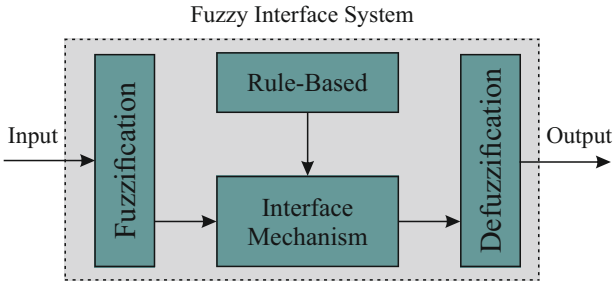

Figure 4.2: The basic structure of a fuzzy logic-based controller

Fuzzy logic controllers are particularly valued for their ability to handle nonlinearity, parameter uncertainties, and conflicting objectives (e.g., balancing battery aging with performance). They have been applied successfully in applications such as electric buses, grid-connected HESS, and microgrids [255].

While rule-based controllers offer many advantages in terms of simplicity, transparency, and low computational requirements, they also have notable limitations that can restrict their effectiveness in more demanding or dynamic scenarios. One of the most significant drawbacks is their lack of explicit optimization. Because rules are predefined and static, they cannot guarantee optimal performance in terms of minimizing energy losses, maximizing battery lifespan, or reducing operating costs under varying operating conditions [256].

Additionally, deterministic rules and FLCs rely heavily on expert knowledge and extensive tuning during the design phase. Developing an effective set of rules or membership functions often requires iterative testing and empirical adjustment, which can be time-consuming and may not generalize well to different system configurations or use cases. This manual tuning process also

complicates maintenance and scalability, particularly in applications where the system must adapt to aging components, environmental variability, or evolving operational constraints. Furthermore, because conventional rule-based controllers react only to real-time measurements, they are inherently reactive rather than predictive, lacking the capability to plan actions based on forecasts of future demand or renewable generation [168].

To overcome these limitations, research and industrial practice have increasingly turned to optimization-based control strategies, which formulate power management as a mathematical optimization problem subject to system constraints and objectives. Unlike rule-based approaches, optimization-based methods can explicitly consider multiple competing goals, such as minimizing battery degradation and improving efficiency [257]. In the following subsection, optimization-based Control is discussed in more detail.

4.2.2 Optimization-Based Control

Optimization approaches can be either offline or online. Offline optimization refers to an optimization approach where control strategies or decision rules are computed in advance (offline) using historical data, simulations, or known system models. The resulting control policy is then stored and used during real-time operation, without solving complex optimization problems online [258, 259]. It is widely used in HESS to balance power allocation, minimize battery degradation, or optimize cost and efficiency, especially when computational resources are limited during operation [260, 261].

Online optimization in HESS refers to real-time decision-making strategies that dynamically allocate power between multiple energy storage components based on continuously changing system states and external conditions [262, 263]. Some of the online optimization methods are explained in the following.

4.2.2.1 Model Predictive Control (MPC)

MPC is among the most widely adopted online optimization techniques for HESS due to its ability to handle multivariable systems with constraints. In MPC, an internal predictive model of the system is used to forecast future states, such as SoC trajectories and power demands, over a defined prediction horizon. At each control interval, the optimizer solves a constrained optimization problem to determine the control inputs (e.g., power split between two ESDs) that minimize a cost function, which often includes terms for battery aging, energy losses, or deviation from desired SoC setpoints [264, 265]. Only the first step of the computed control sequence is implemented before the optimization is repeated at the next time step, enabling continuous

feedback and adaptation. MPC offers a high degree of flexibility and can incorporate forecasts of load or renewable generation; however, it requires substantial computational resources and accurate system models to ensure real-time feasibility [266, 267].

Figure 4.3 schematically depicts the MPC process. At each control instant, the MPC controller first measures the current system state. It then employs numerical optimization to determine the control input that optimizes performance over a prediction horizon of steps, according to a specified objective function. The control action computed for the first step of this horizon is applied to the system. Subsequently, the system evolves to a new state, and the process repeats from this updated state [268].

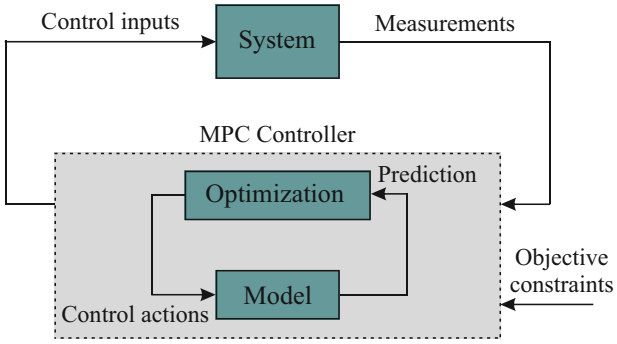

Figure 4.3: Illustration of model predictive control

4.2.2.2 Simultaneous Perturbation Stochastic Approximation (SPSA)

SPSA is a gradient-free optimization algorithm well-suited for systems with uncertain or noisy measurements. Unlike classical gradient descent methods that require gradients of the objective function with respect to all variables, SPSA perturbs all decision variables simultaneously using random perturbations and estimates the gradient from only two objective function measurements [269, 270]. This makes SPSA computationally efficient, particularly in high-dimensional problems. In HESS, SPSA can adaptively tune power allocation policies or control gains to minimize losses, balance state-of-charge levels, and improve dynamic response [271].

The increasing complexity of managing non-programmable power generation sources demands real-time, efficient computation of power shares among renewable sources, hybrid energy storage devices, and the grid. Consequently, power management strategies require suitable optimization algorithms [270]. Various approaches, including linear, nonlinear, dynamic, stochastic algorithms, and artificial intelligence techniques, have been proposed to minimize objectives such

as emissions and costs [272]. However, artificial intelligence methods often face challenges related to convergence and dependence on initial estimates, limiting their applicability in real-time optimization.

Within this context, multivariate stochastic optimization techniques offer effective solutions for engineering system management and control [273]. In particular, gradient-based stochastic algorithms like SPSA and Lyapunov methods demonstrate strong potential for real-time power management, as they operate without requiring future knowledge, mathematical uncertainty models, or forecast error considerations.

SPSA, introduced by Spall in 1992 and recently proposed by the authors [177, 274], represents a fast convergent alternative for the global optimization problem of an unknown system's performance (i.e., the loss function) [275]. Advantages such as easier performance function selection, no necessity for loss function gradient, ease of implementation, lower computational burden, robustness to noise in the loss measurements, and the ability to find a global minimum make SPSA suitable for a wide range of applications [276–280].

SPSA is formulated by an initial estimation of the parameter vector ($\hat{\theta}$), determining the optimal solution by means of iterations, simultaneously perturbing all the parameters involved within the current estimate. Algorithm parameters are updated during each iteration through equations (4.1)-(4.2). Parameters a, c, α, γ are selected to guarantee algorithm convergence [270, 281].

$$a_k = \frac{a}{(A + k + 1)^{\alpha}} \tag{4.1}$$

$$c_k = \frac{c}{(k + 1)^{\gamma}} \tag{4.2}$$

During each iteration, two different estimates of the vector $\hat{\theta}$ are calculated by perturbing the current estimation, as reported in (4.3). The perturbation vector elements (Δ_k) follow a Bernoulli distribution.

$$\hat{\theta}_k^{\pm} = \hat{\theta} \pm c_k \Delta_k \tag{4.3}$$

The solution provides a vector of parameters able to minimize the loss function gradient. The estimate of $\hat{g}(\hat{\theta})$ at the kth iteration is calculated by (4.4), where $\Delta_k \in \mathbb{R}^p$ is the vector of p mutually independent average zero random variables.

$$\hat{g}_k(\hat{\theta}_k) = \frac{\partial L_k}{\partial \theta_k} = \frac{y(\hat{\theta}_k^+) - y(\hat{\theta}_k^-)}{2c_k} \begin{bmatrix} \Delta_{k1}^{-1} \\ \Delta_{k2}^{-1} \\ \vdots \\ \Delta_{kp}^{-1} \end{bmatrix} \tag{4.4}$$

Finally, (4.5) is used to update the current estimate, and the loss function is re-evaluated.

$$\hat{\theta}_{k+1} = \hat{\theta}_k - a_k \hat{g}_k(\hat{\theta}_k) \tag{4.5}$$

The iterative process terminates once either the maximum number of iterations or the convergence condition is reached.

4.2.2.3 Genetic Algorithm (GA) or Particle Swarm Optimization (PSO)

Metaheuristic optimization techniques, such as GA and PSO, have also been employed for HESS control, particularly in contexts where the optimization problem is highly nonlinear or discontinuous [282]. Genetic Algorithms mimic natural selection by evolving a population of candidate solutions through selection, crossover, and mutation operators. Over successive generations, the population converges toward high-quality solutions according to a defined fitness function, which can combine objectives such as efficiency, battery lifespan, and cost [283]. Similarly, PSO is inspired by the collective behavior of swarms and involves a set of particles exploring the search space by adjusting their trajectories based on individual and collective experience [284, 285].

These methods are particularly well-suited to offline optimization, such as generating lookup tables or optimal policy maps used during real-time operation. While metaheuristics are flexible and robust against complex landscapes, they can be computationally demanding and may not be practical for time-critical online control without simplification or hybridization with faster algorithms [286].

Overall, these optimization-based control approaches enable HESSs to dynamically adapt to variable loads, fluctuating renewable generation, and evolving system states in a way that rule-based strategies cannot. By explicitly considering objectives, constraints, and predictions, they provide a systematic framework for improving performance and prolonging the lifetime of energy storage assets. However, their implementation requires careful attention to computational complexity, model accuracy, and real-time feasibility to ensure that theoretical benefits translate into practical gains in deployed systems.

Steps of a GA are shown in Figure 4.4 and described below [287, 288]:

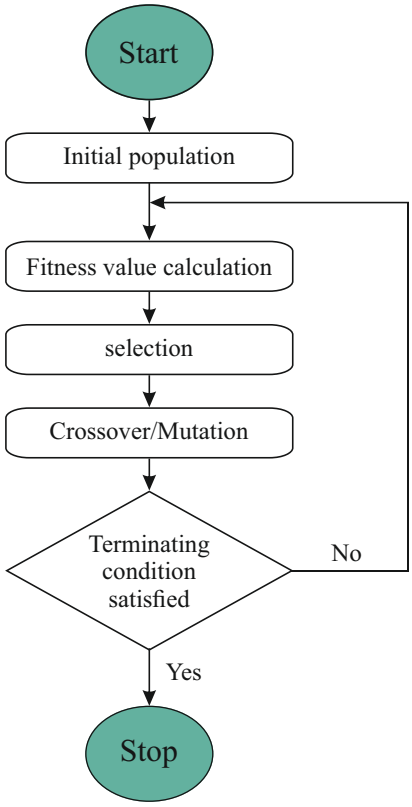

Figure 4.4: Flow chart of a typical GA

1. **Initialization:** Generate a random initial population of individual solutions.
2. **Fitness Evaluation:** Evaluate the fitness of each individual in the population using a defined fitness function to measure how well it solves the problem.
3. **Selection:** Select the fittest individuals based on their fitness values to serve as parents for the next generation.
4. **Reproduction (Crossover and Mutation):** Create a new generation by applying crossover (recombining parent chromosomes) and mutation (introducing random variations) to generate offspring.
5. **Termination Check:** Repeat steps 2-4 until a termination condition is met, such as reaching a maximum number of generations or achieving a satisfactory fitness level.

Table 4.1 summarizes selected studies on these control approaches, highlighting whether each work employed real-time simulation or PHIL experiments to validate their controllers.

Table 4.1: State of the art on hybrid energy storage systems

Reference	Objective	ESS Type	Type of Control	SoC as control parameter	RTS[a]	PHIL[b]
[247]	Power fluctuations	Lead acid BESS-FESS	Rule-based	✓	✗	✗
[289]	Power fluctuations	BESS-FESS	Rule-based	✓	✓	✗
[238]	Decrease power rating of the converter	BESS-UC	Rule-based	✗	✗	✗
[290]	Increase BESS Lifetime	BESS-SCES	Rule-based	✓	✗	✗
[291]	Control power distribution	BESS-UC-Fuel cell	Rule-based	✓	✗	✗
[292]	Power sharing	BESS-SCES	Rule-based	✓	✗	✗
[293]	Power fluctuations	BESS-SCES	Rule-based	✓	✗	✗
[294]	Supply uninterrupted power	Multiple ESDs	Rule-based	✓	✓	✗
[239]	Voltage regulation	BESS-SCES	Optimization	✗	✓	✗
[295]	Power sharing	BESS-UC	Optimization	✓	✓	✗
[296]	Electricity usage minimization	BESS-SCES	Optimization	✓	✗	✗
[286]	Increase BESS Lifetime	BESS-SCES	Optimization	✓	✓	✗

✓= investigated ✗= not investigated

[a]Used real-time simulation
[b]Used power hardware in the loop

Having introduced the various control strategies employed in HESS, it is now essential to explore in detail the specific parameters these strategies are designed to monitor, regulate, and optimize. Understanding the role of each parameter provides deeper insight into how control algorithms ensure the efficient operation of the overall system.

4.3 Key Control Parameters

A major task of the control strategy is to achieve optimal energy management, which entails determining the most efficient way to allocate and dispatch energy among the storage units. This requires a thorough consideration of the systems power and energy demands, the storage capacities and dynamic behaviors of each ESS, and the interconnection topology of the overall

system. The goal is to utilize the complementary strengths of different technologies, such as combining high energy density batteries with high power density supercapacitors or flywheels, to effectively satisfy both short-term and long-term energy requirements [256, 297].

In addition, the control system must handle the estimation of critical internal states and performance indicators that are not directly measurable. These include the SoC, SoH, and remaining useful life based on RR or other indicators of storage components [176, 298]. Accurate estimation of these indicators is vital for making informed operational decisions and for maintaining system reliability over time [229, 299, 300].

Ensuring safe operation is another crucial responsibility. This involves continuously monitoring key parameters, such as current, voltage, temperature, and SoC, for each storage element to keep them within predefined safety thresholds. Maintaining these variables within optimal ranges not only protects the components from damage but also enhances their efficiency and extends their operational lifespan [301].

The control strategy also plays a role in the regulation of system variables, ensuring that the system can follow reference signals with precision. Many storage technologies are sensitive to fluctuations in voltage or temperature, and the ability to regulate these variables contributes significantly to the overall stability and performance of the system [302, 303].

Another important aspect is grid integration and power quality management. The control algorithms must manage the interaction between the HESS and the grid, ensuring smooth power exchanges and supporting grid services, including frequency regulation, voltage control, and load balancing. This contributes not only to the stability of the HESS itself but also to the reliability of the broader power network [289, 293, 294].

Lastly, effective communication and coordination among the various storage technologies are vital. The control system must ensure that all components work in synergy, leveraging their complementary characteristics to enhance overall performance. This involves synchronizing charge and discharge cycles, balancing load contributions, and dynamically adjusting control parameters in response to changes in operating conditions.

Table 4.2 summarizes the key control parameters important for control of HESSs.

Figure 4.5 depicts an example of HESS architecture combining a battery and flywheel, both interfaced with a power management system. The controller responds to frequency and voltage contingencies (Δf and ΔV), generating active and reactive power references (P and Q) for each ESS. Control signals are dispatched based on ramp rate constraints and SoC conditions, ensuring optimal utilization of both storage technologies.

Table 4.2: Key Control Parameters for HESS Management

Control Parameter	Description
Energy Management	Optimal allocation and dispatch of energy among storage units, considering power/energy demands, system topology, and complementary strengths of different ESS technologies.
State Estimation	Estimation of unmeasurable states like SoC, SoH, and remaining useful life using RR and other indicators.
Safety Monitoring	Continuous tracking of current, voltage, temperature, and SoC to ensure operation within safety thresholds, protecting components, and enhancing lifespan.
System Regulation	Ensuring that system variables (e.g., voltage, temperature) follow reference signals precisely for maintaining system stability and performance.
Grid Integration	Managing power exchange and providing grid services such as frequency regulation, voltage support, and load balancing.
Coordination and Communication	Synchronizing charge/discharge cycles, balancing load between ESS units, and adjusting parameters dynamically in response to operating conditions.

Besides the power management of the HESS, there are management systems for the BESS and FESS. The Battery Management System (BMS) supervises the operation of the battery energy storage unit by performing the following essential functions [304–306]:

- **Voltage Monitoring:** Tracks cell and module voltages to ensure they remain within safe operating limits (e.g., 2.5 V - 4.2 V per cell).
- **Temperature Monitoring:** Uses thermal sensors to detect overheating and to maintain cells within the optimal temperature range (e.g., $0°\text{C}$ - $45°\text{C}$).
- **Current Control:** Limits the charge and discharge current to prevent overcurrent damage, based on battery specifications.
- **State Estimation:** SoC, which can be estimated using Coulomb counting or model-based observers such as Kalman filters, SoH, which can be evaluated from capacity degradation or increased internal resistance, and Remaining Useful Life (RUL), which can be predicted using usage history and degradation models.
- **Cell Balancing:** Ensures voltage uniformity across cells using passive (resistive) or active balancing strategies to maximize battery life and performance.
- **Protection Functions:** Engages protective measures under fault conditions such as overvoltage or undervoltage, overtemperature, overcurrent, and Short circuit.

- **Communication Interface:** Provides real-time data (e.g., SoC, SoH, temperature) to the central controller for energy management decisions.

In the HESS setup, the BMS communicates with the central power management system to regulate power flow to and from the battery. For example, if SoC drops below 20%, the BMS signals the controller to limit discharge or shift load to alternative storage units like the flywheel or supercapacitor.

Moreover, the FESS management system is responsible for supervising and controlling the operation of a flywheel energy storage unit [307, 308]. Key functions include:

- **Rotor Speed Monitoring:** Ensures flywheel operates within safe RPM ranges (e.g., 20,000-60,000 RPM).
- **SoC Estimation:** Calculates stored energy as $E = \frac{1}{2} J\omega^2$.
- **Vacuum and Containment Monitoring:** Maintains a low drag environment and detects seal failures.
- **Bearing Condition Monitoring:** Detects vibration or misalignment in magnetic or mechanical bearings.
- **Thermal Management:** Prevents overheating of motor-generator and mechanical components.
- **Power Interface Control:** Manages converter operation for fast charge/discharge events.
- **Protection Logic:** Initiates isolation in case of overspeed, mechanical failure, or fault conditions.

The FESS management system also communicates with the overall HESS controller to participate in grid support operations such as frequency regulation and transient power compensation.

Chapter 6 presents a method for estimating the SoC as a key parameter in energy storage systems using a Kalman filter, specifically applied to a supercapacitor.

4.4 Summary

This chapter explains how Hybrid Energy Storage Systems (HESS) are controlled and managed to balance power and energy needs. Combining different storage technologies, such as batteries and flywheels, increases flexibility but also adds complexity to control and management. A major

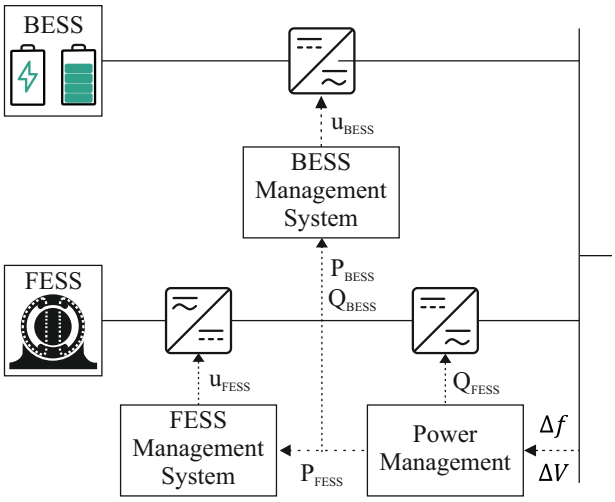

Figure 4.5: General HESS management system architecture

challenge is determining how to share power between the devices while maintaining them within safe operating limits and preventing premature wear. For example, using flywheels excessively can quickly drain them, while ignoring the state of charge risks overcharging or deep discharging the batteries.

Different control approaches are available. Rule-based methods utilize predefined thresholds to trigger actions, whereas fuzzy logic provides smoother, more adaptable decisions when system behavior is uncertain. Optimization-based strategies can be planned in advance (offline) or calculated in real time (online). Techniques like Model Predictive Control or Simultaneous Perturbation Stochastic Approximation dynamically adjust power allocation as conditions change.

In addition, the chapter emphasizes that effective control is not only about deciding how to split power but also about managing the key control parameters of the system. These include energy management (optimally dispatching energy between devices), state estimation (SoC, SoH, and RUL), safety monitoring (current, voltage, temperature), system regulation (keeping variables such as voltage and temperature within reference limits), grid integration (providing services like frequency regulation and voltage support), and coordination among storage technologies to exploit their complementary strengths.

The chapter also highlights the role of device-level management systems. The Battery Management System (BMS) monitors voltages, temperature, and current, estimates battery health indicators, performs cell balancing, and protects against unsafe conditions, while the FESS management system supervises rotor speed, stored energy, vacuum conditions, bearing health, thermal

limits, and protection against overspeed or mechanical faults. Both subsystems communicate with the central HESS controller, ensuring that the battery, flywheel, or supercapacitor responds in a coordinated way to grid requirements and system contingencies.

5 Control and Power Management of Hybrid Energy Storage Systems Using Moving Average and Fuzzy Logic

Building on the previous discussion of general control challenges and established power management techniques, this chapter focuses on a rule-based control strategy tailored explicitly to battery-flywheel configurations. In particular, it explores a novel combination of moving average filtering and fuzzy logic controller to coordinate power allocation between two energy storage systems effectively. These methods are designed to leverage the complementary characteristics of the two storage technologies. The control strategies presented here explicitly consider key operational parameters, including the ramp rate of the and the state of charge of the FESS. This chapter details the modeling, implementation, and experimental evaluation of the proposed power management technique.

5.1 Proposed Control Strategy

This section outlines the control methodology employed for managing the power distribution in a HESS consisting of a battery and a flywheel. The overall control scheme is illustrated in Figure 5.1, which is divided into three main components:

a) **Power Signal Separation:** The first stage involves separating the input power signal using a moving average (MA) filter. This filter smooths short-term fluctuations, revealing long-term trends in the power profile. As a result, the signal is decomposed into slow and fast-changing components, which is critical for assigning the appropriate energy storage device, battery or flywheel, based on their respective dynamic characteristics.

b) **RR and SoC Monitoring:** The second stage involves calculating the Ramp Rate (RR) of the battery and the State of Charge (SoC) of the flywheel. The RR is a measure of

how rapidly the battery can charge or discharge, and controlling it is essential to prevent degradation and extend battery life. Meanwhile, the flywheels SoC is monitored to ensure it operates within safe energy bounds. Given the flywheel's suitability for fast response due to its mechanical nature, it is tasked with managing rapid power fluctuations. The flywheels SoC is estimated by integrating its power over time.

c) **Adaptive Window Selection via Fuzzy Logic:** In the third stage, a Fuzzy Logic Controller (FLC) dynamically determines the window size of the moving average filter (n_t). This adaptive approach ensures that the decomposition of the input power profile into fast and slow components is optimized according to the real-time condition, specifically the flywheels SoC and the battery's RR. The FLC facilitates the maintenance of the flywheels SoC within desired limits while minimizing stress on the battery, thus promoting both system responsiveness and component longevity.

Each component of the control strategy is detailed in the subsequent subsections, highlighting the rationale and implementation behind the hybrid power management approach.

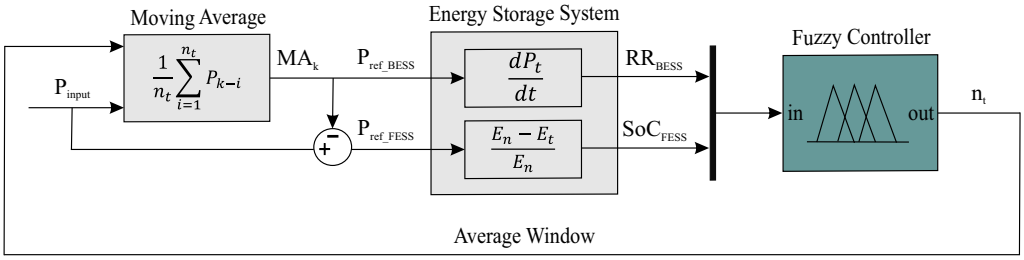

Figure 5.1: Control scheme for HESS including the moving average and fuzzy logic stages

5.2 Control Components

We have seen an overview of the control strategy. This subsection explains the components of the control strategy and their responsibilities.

5.2.1 Moving Average (MA)

Moving average filter is a widely utilized signal processing technique that plays a pivotal role in analyzing trends and smoothing time-series data. At its core, MA involves computing the average of a sequence of consecutive values over time, achieved through a mathematical convolution

operation [309]. This technique effectively reduces short-term fluctuations and highlights long-term trends within the data, making it invaluable in various fields, including finance, control systems, and electrical engineering.

Historically, the MA strategy has been employed extensively in financial analysis, particularly for monitoring stock prices and forecasting market trends [310, 311]. MA strategy utilizes both short-term and long-term moving averages to detect trend reversals and generate trading signals. A buy signal is typically produced when the short-term average crosses above the long-term average, whereas a sell signal is indicated when the opposite occurs. This principle, comparing fast and slow trends, finds a direct analogy in power systems. In power quality analysis, load forecasting, and signal conditioning, MA serves as a low-pass filter, isolating slow dynamics while filtering out high-frequency components. This makes it especially useful for applications in energy management and storage control.

In the context of HESS, which combines energy-dense and power-dense storage technologies, MA-based filtering offers a practical and computationally efficient method for decoupling fast and slow power variations. This enables distinct energy storage elements, such as batteries and flywheels, to be allocated roles that align with their physical characteristics. Specifically, the MA filter is employed to extract the slow-changing component of the power demand, which is then assigned to the BESS. In contrast, the residual signal, representing the high-frequency and rapid power variations, is delegated to the FESS.

The most basic implementation of the moving average is the Simple Moving Average (SMA), defined as:

$$\text{SMA}(t) = \frac{1}{n_t} \sum_{i=1}^{n_t-1} P_{t-i} \tag{5.1}$$

- $SMA(t)$ is the simple moving average at time t
- n_t is the window size or period length (number of previous time steps considered),
- P_{t-i} represents the power value at past time step $t - i$
- P is the power demand or signal to be filtered.

By adjusting n_t the filter can be tuned to define what constitutes a slow variation. A larger n_t results in a smoother, slower-changing average, whereas a smaller window captures more rapid changes. The difference between the original power signal $P(t)$ and the moving average output $SMA(t)$ defines the fast component power setpoint:

$$P_{fast}(t) = P_t - \text{SMA}(t) \tag{5.2}$$

This differential signal can then be routed to the fast-acting storage system (e.g., FESS), while the smoothed signal is assigned to the battery.

While a fixed-window SMA is effective, more advanced HESS control strategies may implement adaptive or variable-length moving averages. In such configurations, the window size n_t can be dynamically adjusted based on system conditions, such as the SoC of the storage or the rate of change in power demand. This enables filtering, ensuring the optimal division of power tasks between the BESS and FESS over time. Such dynamic filtering schemes form the basis of hybrid control strategies that enhance the efficiency of hybrid energy storage configurations.

5.2.2 Fuzzy Logic Controller

As explained in subsection 4.2.1, fuzzy logic as a rule-based control is a powerful control methodology well-suited to systems with inherent uncertainties, nonlinearities, or vague operating rules. Unlike traditional controllers that require precise mathematical models and operate on binary logic, FLCs use linguistic rules to make decisions, mimicking human reasoning [312,313]. These controllers handle imprecision by defining fuzzy sets for inputs and outputs and using a rule base to determine control actions based on approximate reasoning [314, 315].

In energy management systems, where decisions often depend on dynamic conditions such as storage states and power profiles, fuzzy logic is particularly advantageous. It allows the controller to react flexibly to changing conditions and smooth out abrupt transitions in power flows.

In this study, the FLC is employed to optimize the coordination between the BESS and the FESS. Specifically, the FLC dynamically determines the length of the MA window, which directly affects how quickly or gradually power is transferred between the two storage units. The goal is to reduce BESS stress by managing its RR and to maximize the utilization of FESS when its SoC allows.

The inputs of the FLC are the RR of the BESS and the SoC of the FESS, while the output is the average window length of the moving average filter. The use of fuzzy logic enables the controller to balance short-term power fluctuations and long-term energy availability without requiring a detailed mathematical model of the system.

5.2.2.1 Membership Functions

Instead of using precise numerical values, fuzzy logic describes inputs and outputs using linguistic terms and approximate reasoning. These linguistic variables are mapped to fuzzy sets through membership functions, which provide a flexible framework for decision-making. In this study, the inputs to the FLC are the RR of the BESS and the SoC of the FESS, while the output is the average window length used by the MA filter. Figure 5.2 illustrates the membership functions of these variables, and Table 5.1 defines the associated fuzzy sets in linguistic terms.

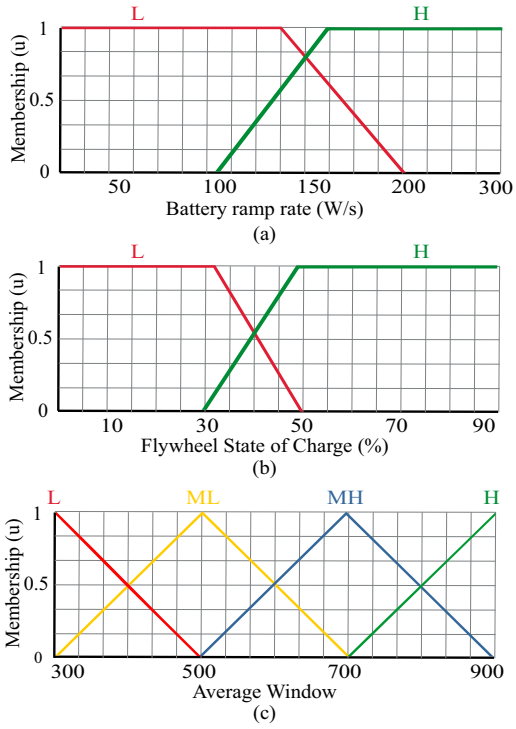

Figure 5.2: Membership Functions (a) Battery Energy Storage Ramp Rate (b) Flywheel Energy Storage State of Charge (c) Average window of Moving Average

This work adopts the Mamdani inference method, implemented in MATLAB/Simulink, which is widely recognized as a standard approach in fuzzy control applications [316, 317]. For simplicity and effectiveness, both input variables, RR and SoC, are classified into two categories: "Low" and "High." This design choice simplifies rule creation and ensures faster and more intuitive decision-making, aligning with the specific needs of our HESS strategy. The dual-category scheme targets the most critical scenarios: high RRs that can strain the BESS, and SoC levels

Table 5.1: Fuzzy sets and their linguistic variables

Sets	Linguistic Variables
L	Low
ML	Medium Low
MH	Medium Low
H	High

that either risk depleting the FESS or affect its efficiency when too high. Introducing additional categories would increase computational complexity without delivering substantial performance gains for the intended application.

Keeping the FESS SoC above 30% is essential to ensure adequate torque and rotational speed and maintain the flywheels ability to deliver high power when needed. Although a high SoC does not pose a risk to the FESS, distinguishing between "Low" and "High" SoC enhances the systems responsiveness, particularly in cases where both the ramp rate of BESS and SoC of FESS are high.

The controllers output, which is the average window length, is divided into four categories to allow more refined control over power smoothing and distribution. Trapezoidal membership functions are used for the inputs (RR and SoC), offering smooth transitions between fuzzy regions. The output employs triangular membership functions, allowing sharper control adjustments over the window length.

Thanks to this fuzzy logic framework, the system continuously adapts the average window length in response to real-time conditions, enabling more efficient and balanced power sharing between the battery and flywheel. The full range definitions for each input and output membership function are presented in Table 5.2.

Table 5.2: Membership functions sets and their range

Battery Ramp Rate (RR)		Flywheel SoC		Average Window (AW)	
Set	**Range**	**Set**	**Range**	**Set**	**Range**
L	RR<200	L	SoC<50%	L	AW<500
				ML	300<AW<500
H	RR>100	H	SoC>30%	MH	500<AW<900
				H	AW >900

5.2.2.2 Rules of Fuzzy Controller

The core of the FLC lies in its rule base, which consists of a set of decision-making rules. Each rule consists of an antecedent, which describes the current system state using fuzzy sets and variables, and a consequent, which specifies the appropriate system response. These fuzzy rules define how the controller should react under various conditions, with the overall system output derived by aggregating the results of all applicable rules. The number of rules and linguistic terms used depends on the complexity of the system and the level of control required. FLCs offer an effective solution for managing nonlinear and uncertain systems due to their adaptability and fine-tuned decision-making capability.

In this study, the FLC rule base is outlined in Table 5.3. For instance, when the batterys RR is low and the flywheels SoC is also low, the FLC reduces the average window length, thereby relying more on the battery to handle power demands. Conversely, suppose the battery experiences a high RR while the flywheels SoC is high. In that case, the controller increases reliance on the flywheel to absorb power fluctuations, thus easing the load on the battery and improving overall system stability.

These fuzzy rules enable the controller to dynamically modulate the power distribution between the BESS and FESS based on real-time conditions. Through this rule-based approach, the system balances the energy flow, optimizing the performance and longevity of both energy storage components.

Table 5.3: Rules of fuzzy logic controller

		Flywheel SoC	
		L	**H**
Battery Ramp Rate	**L**	L	MH
	H	MH	H

5.3 Experimental Validation

This section introduces the input power profile used to validate the proposed control strategy and presents the experimental validation using this profile.

5.3.1 Input Power Profile

To validate the performance of the proposed control strategy, a real-world power profile was employed as the target signal for the HESS. This reference power profile was derived using an enhanced motif discovery algorithm as detailed in [318]. The algorithm identifies the most recurrent daily load patterns from historical data, providing a representative and repeatable profile for evaluating storage control techniques. The dataset used for this analysis features a temporal resolution of 1 second.

The input data was collected during the summer of 2018 in South Germany from four different 10/0.4 kV distribution substations. This period was strategically chosen to capture peak photovoltaic (PV) generation, which is crucial for realistic sizing and operation of energy storage systems under high renewable penetration scenarios. The four substations were selected based on their voltage sensitivity to active power variations, according to the methodology presented in [319].

High-resolution measurements were recorded using the "PQI-DA Smart" power quality monitoring device from A-Eberle [320], which was installed on the low-voltage side of the transformer at each substation. This setup enabled the acquisition of the total active and reactive power from all downstream feeders. Due to the high resolution and data storage limitations, each substation contributed approximately two weeks of measurements.

The identified motif-based load profile served as the reference signal for the HESS control system. The goal was to dynamically regulate the energy flow within the HESS to follow this power trajectory while minimizing battery stress and optimizing system performance. Figure 5.3 presents an example of the control behavior when a 10-minute moving average filter is applied to the reference input. The filtered output power lies within the range of ± 160 kW, while the difference between the raw input and the smoothed output, the component assigned to fast-response storage such as the flywheel, is within ± 30 kW. This separation demonstrates the temporal decoupling enabled by the moving average, allowing short-term fluctuations to be managed by high-power devices and slower trends to be assigned to high-energy devices.

5.3.2 Experimental Results

To empirically validate the proposed control strategy, the controller was deployed on a 120 kW, 8 kWh high-speed FESS, as detailed in subsection 3.2.1, within a PHIL setup described in Section 3.1. The implementation involves integrating a controller based on the combination of a moving average and fuzzy logic. Figure 5.4 illustrates a schematic diagram of the setup created to assess the performance of the proposed control design.

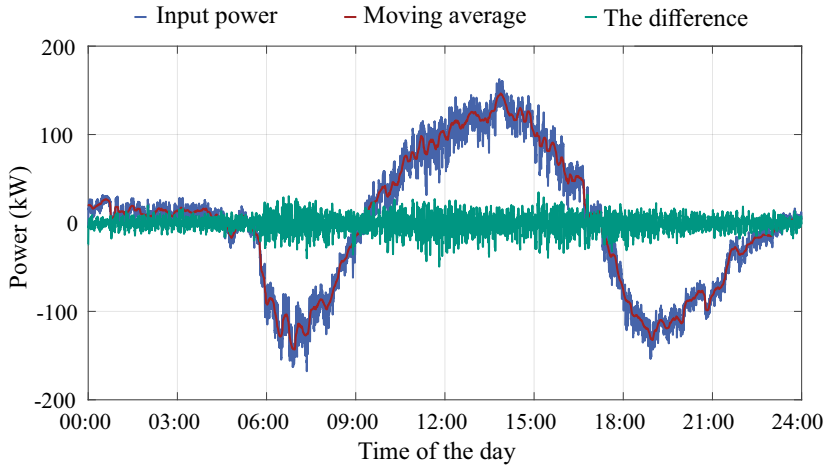

Figure 5.3: The input power pattern, the filtered signal via moving average, and the resulting difference.

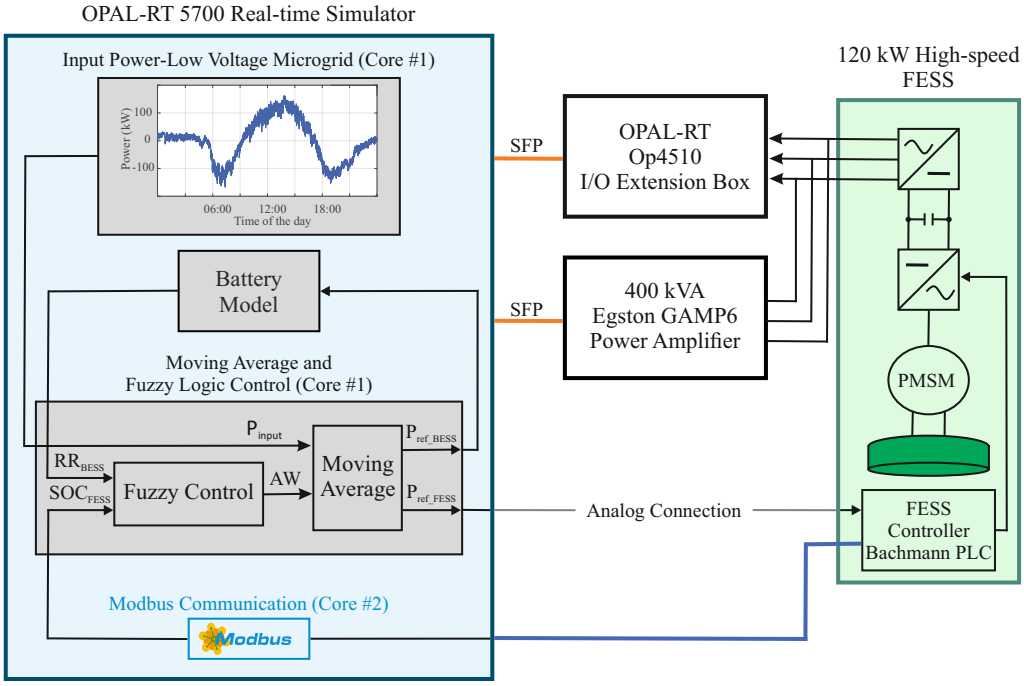

Figure 5.4: Configuration for prototyping the proposed controller and conducting PHIL simulations using the 120 kW high-speed FESS.

The setup consists of three main parts. The simulated part in the real-time simulator, the actual device, and the communications and connections between these two parts. Opal-RT OP5700 real-time simulator simulates the proposed control in real-time. The controller controls the input power mentioned in section 5.3.1, integrated into a low-voltage microgrid, and generates the active power references for both the BESS and FESS.

The active power reference of BESS is sent to the battery model within the real-time simulator. For the parameters to be controlled, the SoC of the flywheel is obtained by the device, while the RR of the battery is derived from its power, as shown in equation (5.3) in the simulation environment.

$$RR = \frac{dP(t)}{dt}. \tag{5.3}$$

In the battery model, the nominal capacity E_n is crucial in determining the number of cells in a Li-ion battery and the maximum rotational speed and inertia in a flywheel. Calculating the nominal capacity involves integrating the power profile of the ESS and assessing the maximum change in resulting energy variations, as outlined in equations (5.4) and (5.5). However, to extend the lifespan of an ESS, particularly Li-ion batteries, oversizing is commonly adopted as a strategy.

$$E(t) = \eta^{-sgn(P(t))} \int_0^t P(\tau)\, d\tau, \tag{5.4}$$

$$E_n = \frac{maxE(t) - minE(t)}{SoC_{max} - SoC_{min}}. \tag{5.5}$$

For Li-ion batteries, research has indicated that avoiding high SoC values can significantly mitigate the cells' cathode degradation and calendar aging. Likewise, deep discharging has been shown to elevate the internal resistance of the cells [321]. Consequently, allocating a specific non-usable capacity is advisable to prevent extreme SoC values, denoted as SoC_{min} and SoC_{max}. Thus, the nominal capacity can be determined by considering the minimum and maximum SoC, assuming 10% and 90%, respectively. The round-trip efficiency of the battery (η) is assumed to be 90%.

The proposed controller requires knowledge of the BESS's RR and the FESS's SoC. The RR of the battery is calculated from its power derivative in its model presented in the real-time simulator. FESS's SoC, measured internally in the FESS controller, is sent to the real-time simulator using an Ethernet connection and the Modbus TCP/IP protocol from the industrial controller of the FESS.

In this setup, which is explained in detail in section 3.1 , the Ethernet connection can transmit reference commands, including the active power reference, to the FESS. However, due to the slow and non-deterministic nature of the Modbus protocol [322], a faster analog signal transmission method is preferred in this particular study. Specifically, a 4-20 mA current signal is used to transmit the active power reference to the FESS, ensuring more efficient and reliable communication.

Figure 5.5 presents the comparison between the actual measured power output of the FESS and the corresponding reference signal derived from the experimental trials. The close alignment between the curves indicates the high accuracy of the control strategy in ensuring the FESS tracks the target power trajectory. In parallel, Figure 5.6 shows the time-varying behavior of the moving average window length as modulated by the FLC during the test period.

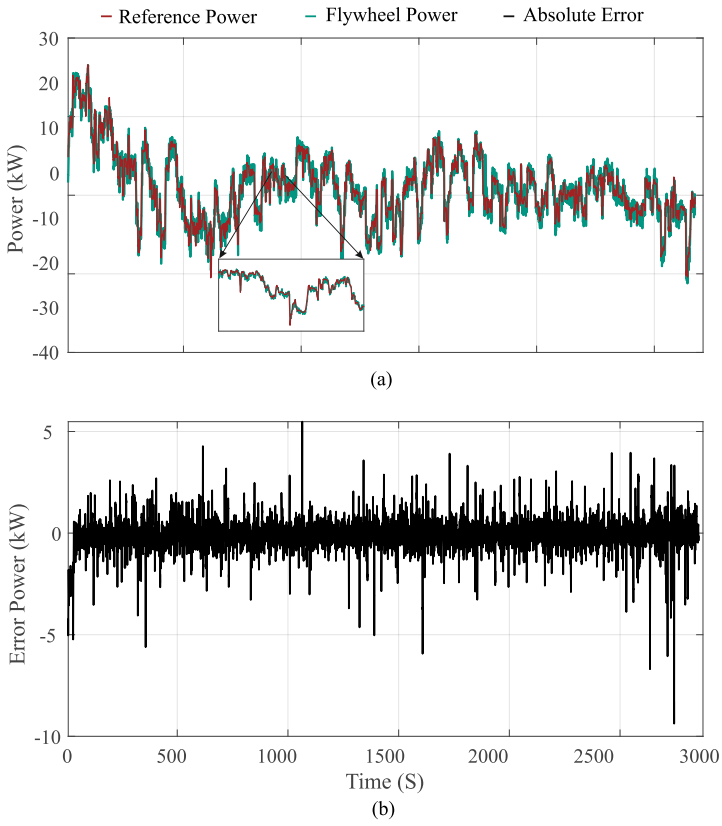

Figure 5.5: Comparison between reference and hardware-measured power in the flywheel system:(a) Reference and measured power profiles (b) Absolute error between the two signals

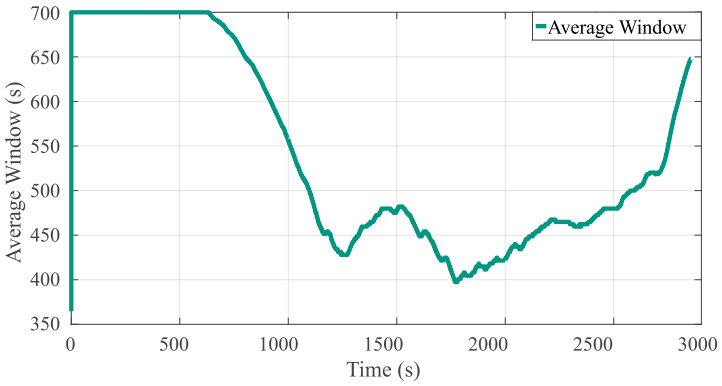

Figure 5.6: Average Window of the moving average

For comparative analysis, the proposed fuzzy-moving average controller is evaluated against a LPF-based controller, which is commonly used in energy management literature [247, 282, 292, 293, 323–325]. The LPF controller splits the input power between the BESS and the FESS using frequency-domain separation:

$$\text{Filter} = \frac{1}{1 + \text{T}s} \tag{5.6}$$

Where s is the Laplace operator and $\text{T} = \frac{1}{f_{cut-off}}$ .A cut-off frequency of $f_{cut-off}$= $2.5mHz$ was selected to balance the storage system dynamics and ensure positive SoC levels for both BESS and FESS. The architecture of the LPF-based controller is shown in Figure 5.7.

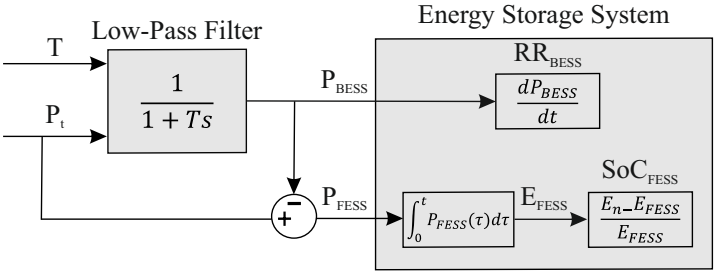

Figure 5.7: Low-pass filter-based control architecture

Figure 5.8 illustrates how the total input power is distributed between the BESS and FESS under both control strategies. The FLC-MA controller demonstrates a more dynamic and responsive power allocation, successfully attenuating high RR demands from the BESS while preserving sufficient SoC in the FESS.

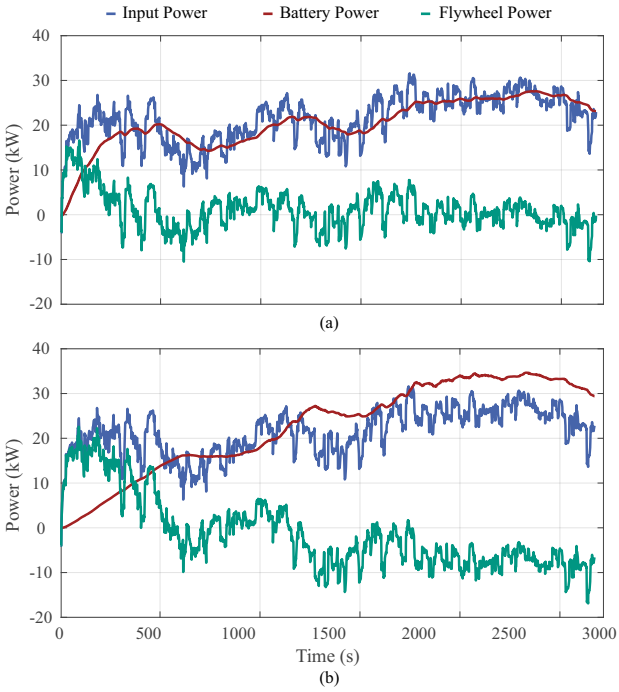

Figure 5.8: Experimental comparison of power in two methods (a) Filter method (b) Fuzzy-Moving average Method

This is further validated in Figure 5.9, where the SoC trajectory of the FESS and the ramp rate of the BESS are depicted. Under the proposed controller, the FESS SoC consistently remains above the 40% threshold, and the ramp rate of the battery is significantly smoother, indicating reduced stress and potential enhancement of battery life. In contrast, the LPF controller allows SoC levels to drop below 30%, a critical point at which the flywheel's maximum power output becomes constrained due to reduced rotational speed.

Moreover, unlike basic filtering methods, the FLC-MA controller accounts for the auxiliary power demand of the flywheel system, which varies with the SoC. The intelligent control of SoC in the proposed strategy ensures this parasitic load is managed effectively, thereby preserving available energy for active power delivery.

5.4 Parameter Variation Analysis

Fuzzy logic controllers inherently rely on parameter tuning that is often guided by a heuristic understanding of the system. Since such tuning can significantly affect performance, a parameter

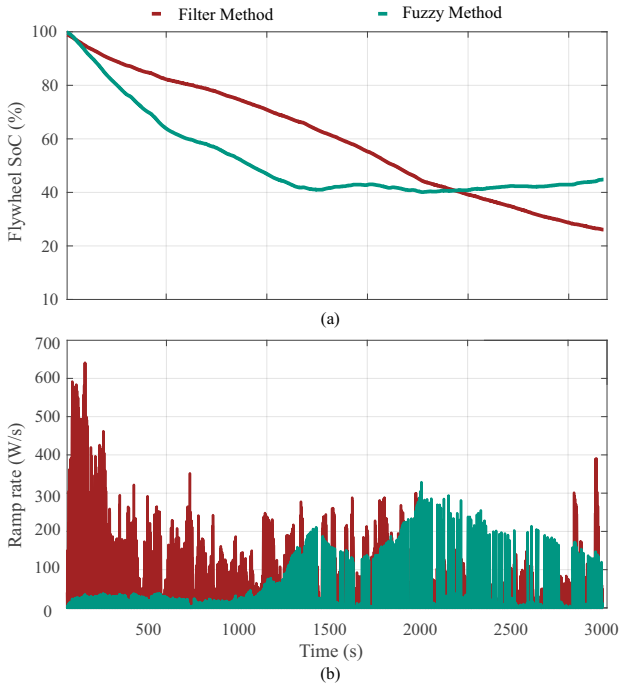

Figure 5.9: Comparison of the Filter Method and the Fuzzy-Moving average method (a) Flywheel SoC from experimental results (b) Battery ramp rate derived from post-analysis of experimental data

sensitivity study was conducted to analyze the impact of the two core design parameters: the moving average window width in the proposed controller and the cut-off frequency in the LPF approach.

5.4.1 Moving Average Window Width

The moving average window length plays a key role in determining the balance between smoothing the input power and maintaining the responsiveness of the HESS. Simulation results using the real daily power profile and battery models (subsection 5.3.1) reveal the performance trade-offs of varying the window width.

A lower range for the average window length restricts the controllers decision-making flexibility, leading to suboptimal smoothing of the power signal. On the opposite, a higher range can result in operational inefficiencies, with the system responding too frequently to minor fluctuations. Figure 5.10 illustrates these trade-offs, considering simulations for two window width ranges: 300–900 s (the proposed one) and 100–1300 s (higher range). The results show that increasing

the average window length from 300-900 s to 100–1300 s significantly increases the ramp rate of the BESS, potentially affecting its lifetime. This is attributed to the larger window length introducing excessive variability into the moving average calculation. Consequently, the chosen window width strikes a balance, minimizing ramp rate fluctuations while maintaining efficient smoothing for optimal SoC dynamics.

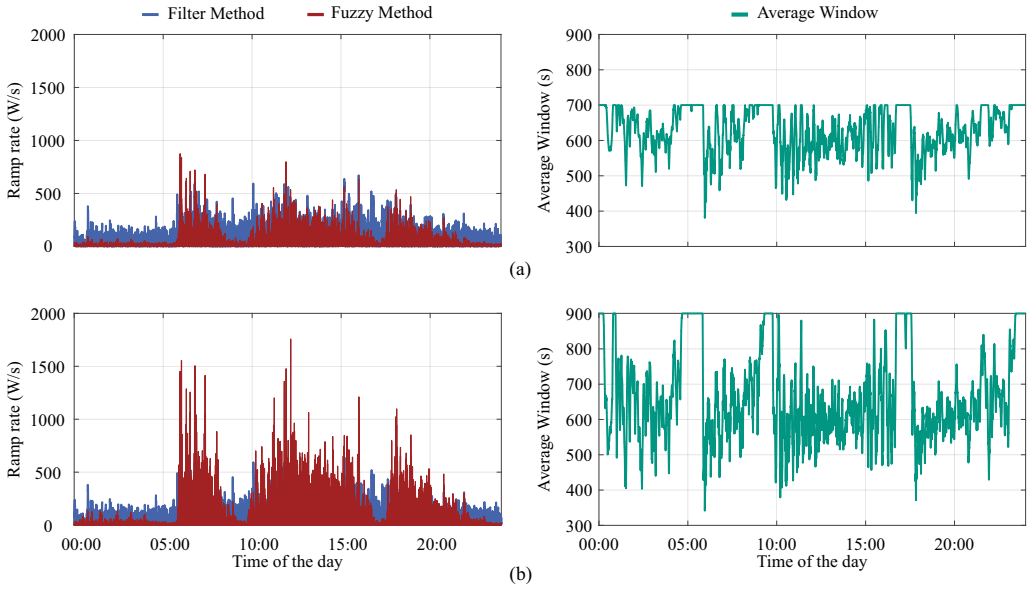

Figure 5.10: Effect of different membership functions on the ramp rate and the average window (a) Average window between 300 - 900 s (b) Average window between 100 - 1300 s

The works in [326–328] underline that the parameter acquisition in fuzzy logic systems is often guided by the specific requirements of the target application, reinforcing the validity of our approach to defining parameters based on the systems operational characteristics. To further demonstrate the adaptability of the proposed fuzzy logic controller, we tested the system with two additional power profiles: one scaled to double the existing power profile and another scaled to half of it. For each case, the ramp rate of the power profile changes, necessitating modifications to the membership function and storage sizes to accommodate the altered dynamics.

The results in Figure 5.11 compare each power profiles RR and SoC behavior with its corresponding filter range. The results confirm that the controller consistently balances the RR and SoC independently from the power profile dynamics.

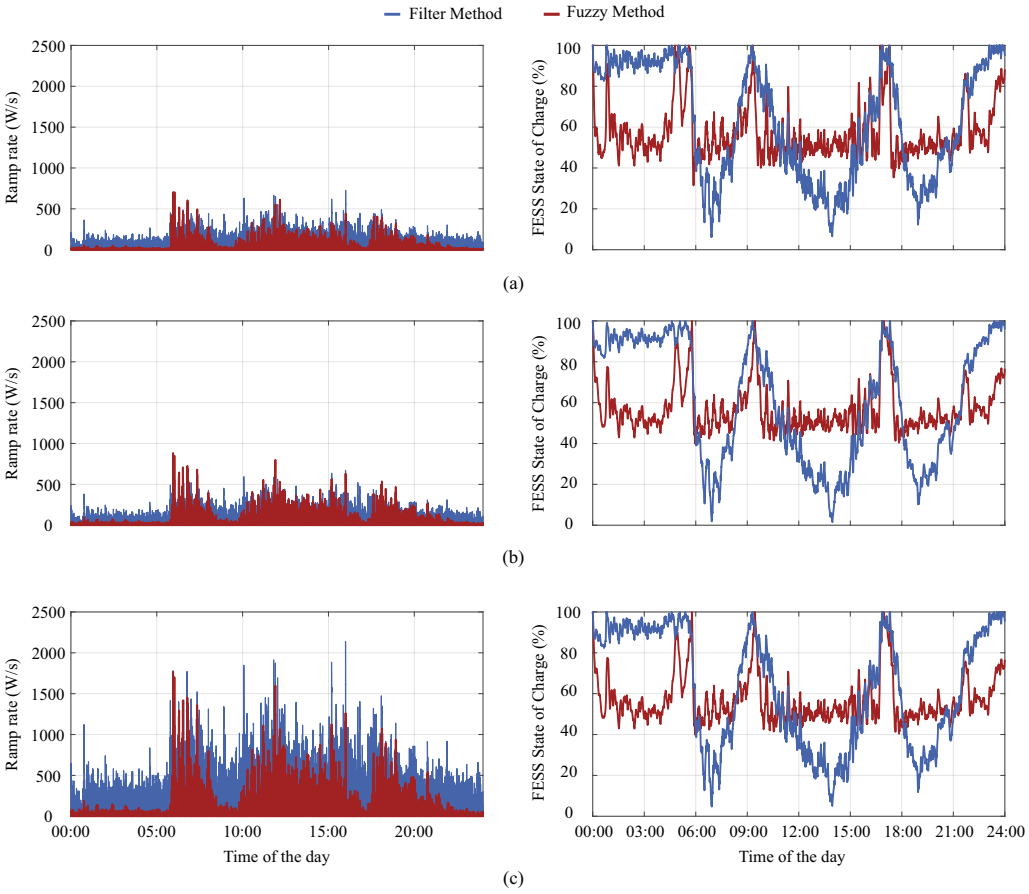

Figure 5.11: Comparison of the controller on different power profiles (a) half of the original power profile (b) original power profile (c) twice the original power profile

5.4.2 Low-pass Filter Cut-Off Frequency

In addition to the moving average window width, the cut-off frequency of the low-pass controller was analyzed in the same simulation setup. A higher cut-off frequency allows the controller to respond more quickly to fluctuations, improving the SoC dynamics of the FESS by allocating more of the high-frequency power variations to the BESS. However, this comes at the cost of increased ramp rates for the BESS (similarly to the larger moving average window width), as the battery is more exposed to components of the power demand.

Conversely, a lower cut-off frequency effectively smooths the BESS ramp rate but compromises the SoC performance. Figure 5.12 depicts these trade-offs. It can be seen that for the chosen cut-off frequency of 2.5 mHz, the ramp rate of the BESS is comparable with the proposed controller, while the SoC of FESS is kept positive. It also demonstrates how a higher cut-off frequency of 3.5 mHz improves the SoC utilization of the FESS while simultaneously increasing the ramp rate of the BESS. A lower cut-off frequency of 1.5 mHz, on the other hand, achieves the opposite effect of a lower ramp rate of BESS but leads to an empty FESS, highlighting the importance of selecting an intermediate frequency that balances the trade-offs between the parameters.

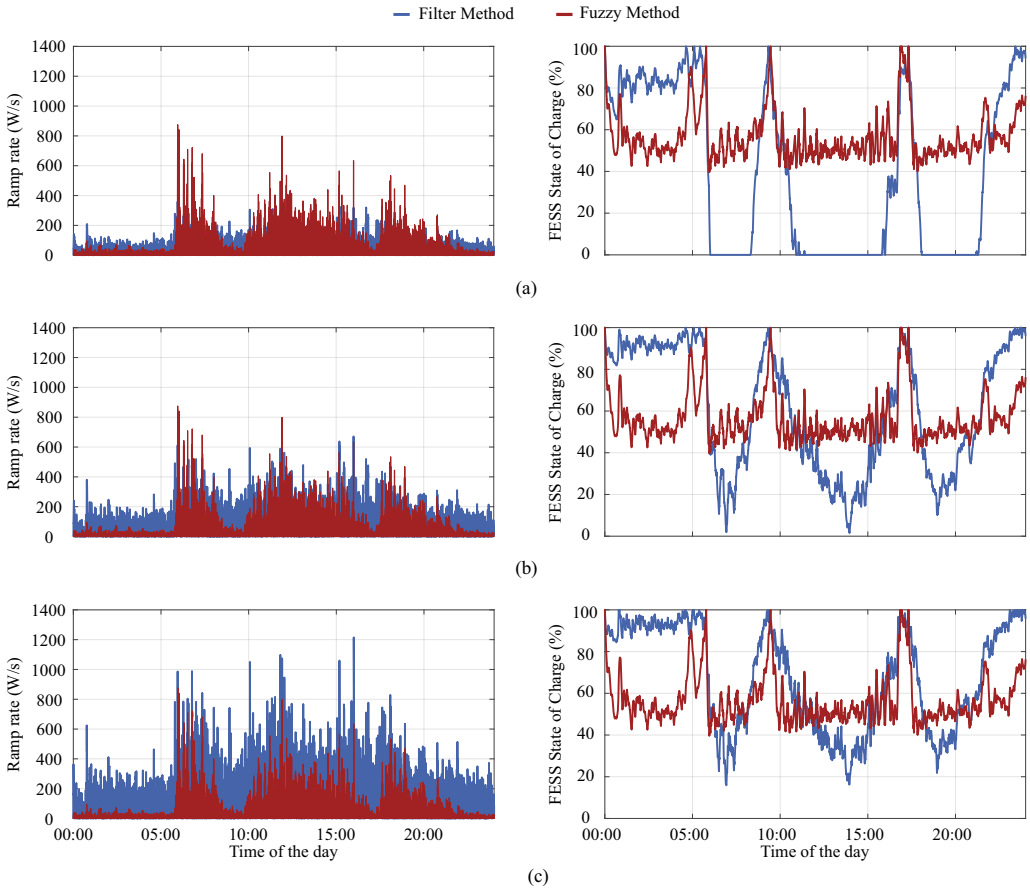

Figure 5.12: Comparison of the different cut-off frequency (a) 1.5 mHz (b) 2.5 mHz (c) 3.5 mHZ

5.5 Summary

This chapter presented a control strategy for managing power distribution in a Hybrid Energy Storage System (HESS) combining a battery and a flywheel. The approach uses a moving average filter to split the power signal into slow and fast components, assigning them to the battery and flywheel, respectively. A fuzzy logic controller dynamically adjusts the moving average window size in real time based on the battery ramp rate and the flywheels state of charge (SoC), allowing the system to adapt to changing conditions and balance performance.

The proposed method was experimentally validated using real load profiles and a Power Hardware-in-the-Loop (PHIL) setup with a 120 kW flywheel. Results demonstrated accurate tracking of power references, effective smoothing of battery ramp rates, and maintenance of adequate flywheel SoC levels. Comparisons with a conventional low-pass filter controller confirmed that the fuzzy-moving average strategy provided improved control performance and better utilization of storage capacities.

Finally, a sensitivity analysis highlighted the impact of tuning key parameters such as moving average window length and low-pass filter cut-off frequency, showing the importance of selecting appropriate settings to balance responsiveness and stability. Overall, the proposed adaptive control strategy enhanced the efficiency and reliability of hybrid energy storage operation.

6 Supercapacitor SoC Estimation in Hybrid Energy Storage Systems

Thanks to their high specific power and long life cycle, supercapacitors are highly suitable for use alongside batteries in HESS. As explained in Section 4.3, one of the key challenges in their integration is accurately estimating the state of charge (SoC), which is essential for reliable energy management and overall system performance. SoC serves as the primary indicator of the energy stored within a device, and accurate tracking is crucial to ensure safe and efficient operation. Inaccurate estimation can lead to overcharging, degradation, or underutilization of the storage device, which are particularly critical risks for high-power components such as supercapacitors.

This chapter presents a detailed overview of algorithms used for SoC estimation in supercapacitors, with a focus on Kalman filter-based methods. In particular, an adaptive square-root unscented Kalman filter (ASR-UKF) approach is introduced to enhance estimation accuracy. To support the implementation of these algorithms, equivalent electrical circuit models of the supercapacitor are developed and used as the basis for applying the Kalman filtering (KF) techniques.

6.1 Overview of Estimation Methods

Estimation methods play a crucial role in accurately determining system states and parameters that are not directly measurable. These methods enable effective monitoring, control, and optimization of complex systems by providing reliable state information based on available measurements and models. In the following subsections, the conventional estimation methods and the Kalman Filtering (KF) Method are explained in detail. The mathematical formulation of the Kalman filters is provided separately in Appendix A.

6.1.1 Conventional Methods

Traditional approaches for estimating the SoC in supercapacitors often begin with simplified models. One of the most widely used techniques is the simple capacitive model, which treats

the supercapacitor as an ideal capacitor. In this approach, the SoC is calculated as the ratio of the energy currently stored to the maximum possible energy, derived directly from the measured terminal voltage. The stored energy is obtained from the capacitor voltage, while the maximum energy is based on the rated capacitance and nominal voltage [329, 330]. This results in the following State of Art (SoA) expression:

$$SoC_{SoA} = \frac{\frac{1}{2}C_n V_{SCES}^2}{\frac{1}{2}C_n V_n^2} = \frac{V_{SCES}^2}{V_n^2} \tag{6.1}$$

Where V_{SCES} is the measured terminal voltage, and C_n and V_n are the rated capacitance and nominal voltage, respectively. This method is favored for its simplicity and ease of implementation. However, it fails to capture the non-linear behaviors of real supercapacitors, such as internal losses and charge redistribution, which can lead to significant estimation inaccuracies.

To address these shortcomings, a more detailed representation can be used through a multi-branch RC model, which includes multiple internal capacitance branches. In this model, the SoC is computed by summing the energy stored across all internal capacitive elements, thereby accounting for internal charge redistribution effects [331]. In detail, the SoC given by a multi-branch model, namely SoC_{MB}, results as follows:

$$SoC_{\text{MB}} = \frac{\sum_{i=1}^{n} \frac{1}{2}C_i v_i^2}{E_{\text{max}}} \tag{6.2}$$

where n represents the number of internal RC branches, C_i and v_i denote the internal capacitance and its corresponding voltage, and E_{max} is the total maximum energy characterized across all branches.

Another commonly applied technique, especially in real-time applications, is the Coulomb Counting method. This approach estimates the SoC by integrating the measured current over time, starting from a known initial SoC value SoC_0. The estimated SoC at time t, denoted as SoC_{CC}, is given by:

$$SoC_{\text{CC}} = SoC_0 - \frac{1}{C_{\text{Ah}}} \int_0^t I_{SCES}(t)\, dt \tag{6.3}$$

where C_{Ah} is the rated capacity in ampere-hours, and I_{SCES} is the measured current. While this method is suitable for online estimation, it is sensitive to sensor noise and cumulative integration errors. Moreover, its accuracy heavily depends on the correctness of the initial SoC value.

To correct accumulated errors, a relationship between SoC and Open-Circuit Voltage (OCV) is often used. The initial SoC is interpolated from OCV data obtained during rest conditions. However, this approach requires prior offline characterization and assumes a linear OCV-SoC relationship, which does not account for the voltage-dependent capacitance and non-linear behavior typical of supercapacitors. Additionally, observing a true open-circuit voltage requires extended rest periods with zero current, which may not be practical in real-world operation.

Overall, while these conventional methods are adequate for applications where simplicity is prioritized over precision, they are often insufficient for the demands of HESS applications. In such systems, high accuracy is critical for effective energy management. Phenomena like internal charge redistribution and self-discharge can significantly affect the available energy, necessitating more advanced estimation techniques to ensure reliable SoC tracking.

6.1.2 Kalman Filtering (KF) Method

The Kalman Filter (KF) is an optimal state estimation algorithm for systems with linear dynamics and Gaussian noise. It combines a system model with noisy sensor measurements to estimate hidden states (e.g., position, velocity, or SoC) with minimum mean squared error [332, 333].

The system model and KF steps are summarized as follows:

- **System model:** Discrete-time statespace form:

$$x_{k+1} = Ax_k + Bu_k + w_k, \quad w_k \sim \mathcal{N}(0, Q) \tag{6.4}$$

$$y_k = Cx_k + Du_k + v_k, \quad v_k \sim \mathcal{N}(0, R) \tag{6.5}$$

  with:

  - x_k: state vector (e.g., SoC, voltage states).
  - u_k: input/control (e.g., current, power).
  - y_k: measurement (e.g., voltage, current sensors).
  - A, B, C, D: system matrices.
  - w_k, v_k: process and measurement noise, Gaussian with covariances Q, R.

- **Prediction step:** Propagates state and covariance:

$$\hat{x}_{k|k-1} = A\hat{x}_{k-1|k-1} + Bu_{k-1} \tag{6.6}$$
$$P_{k|k-1} = AP_{k-1|k-1}A^T + Q \tag{6.7}$$

  where: $\hat{x}_{k|k-1}$: predicted state, $\hat{x}_{k-1|k-1}$: updated state from previous step, $P_{k|k-1}$: predicted covariance, $P_{k-1|k-1}$: previous covariance.

- **Update step:** Corrects prediction with new measurement:

$$K_k = P_{k|k-1}C^T(CP_{k|k-1}C^T + R)^{-1} \tag{6.8}$$
$$\hat{x}_{k|k} = \hat{x}_{k|k-1} + K_k(y_k - C\hat{x}_{k|k-1}) \tag{6.9}$$
$$P_{k|k} = (I - K_kC)P_{k|k-1} \tag{6.10}$$

  where: K_k: Kalman gain, $y_k - C\hat{x}_{k|k-1}$: innovation (measurement-prediction error), $\hat{x}_{k|k}$: updated state, $P_{k|k}$: updated covariance.

Its efficiency, low computational cost, and ability to run in real time have made it a standard tool in control, navigation, and energy storage state estimation [332].

Initially introduced in 1960 for linear systems [334], the KF has since become a foundational technique for optimal state estimation. Over the years, its application has expanded to various nonlinear systems through adaptations such as the Extended Kalman Filter (EKF), which incorporates nonlinear models using a first-order Taylor series expansion [335].

In the context of supercapacitor SoC estimation, an EKF-based method employing a three-branch equivalent circuit model was proposed in [329]. This method was validated across several charge/discharge cycles, although its comparison was limited to the basic capacitive model, leaving out more complex or nonlinear alternatives.

To address the limitations of linearization, the Unscented Kalman Filter (UKF) was developed. It introduces a deterministic sampling strategy, improving estimation robustness in highly nonlinear systems [336]. Its application to supercapacitor SoC estimation using a first-order dynamic equivalent circuit model has been demonstrated in [337], where experimental validation confirmed resilience to parameter variations. However, this work did not include a comparison with alternative estimation algorithms or supercapacitor models, leaving open questions regarding relative performance.

A further refinement of this approach is the Square-Root Unscented Kalman Filter (SR-UKF), which offers enhanced numerical stability and computational efficiency [338]. An adaptive

extension of this filter, referred to as ASR-UKF, was proposed in [339], and shown to improve estimation accuracy in other domains [340]. Despite its advantages, its use for supercapacitor SoC estimation has not yet been addressed in the existing literature.

Similarly, adaptive laws can be defined for the process noise covariance Q to reflect model uncertainties and variations in system dynamics. By updating Q and R online, the ASR-UKF achieves improved robustness and accuracy in the presence of time-varying or uncertain noise statistics [341, 342].

An alternative modeling strategy involves the use of fractional-order models, leading to the development of fractional KF methods [343]. While promising in terms of accuracy, these approaches demand extensive parameter identification. Moreover, implementations such as the hybrid Kalman Filter-Particle Filter (KF-PF) significantly increase algorithmic complexity. Although good estimation accuracy was reported in [343], the testing was performed offline on a host PC, without confirming real-time execution capability. In addition, comparisons were limited to the conventional Ampere-hour integration method.

Another notable approach is the multiobserver estimation scheme presented in [344]. This technique combines multiple model observers to achieve robust and accurate SoC estimation. However, it requires substantial modeling effort and complexity, and although experimental validation was performed using MATLAB/Simulink, its suitability for real-time applications remains unverified.

On the other hand, intelligent modeling techniques such as data-driven Artificial Neural Networks (ANN) and fuzzy logic offer strong modeling capability [345]. Their adoption is limited by high training effort and the requirement for large datasets to ensure robustness and accuracy [346].

Table 6.1 summarizes the main state-of-the-art approaches for supercapacitor SoC estimation, covering both classical Kalman filtering variants and intelligent modeling techniques. The comparison highlights whether each method has been applied to supercapacitors, implemented in real time, compared across different supercapacitor models, or requires training data. While classical Kalman-based methods (KF, EKF, UKF, SR-UKF), which are explained in more detail in Appendix A, generally offer real-time feasibility and do not require training data, their ability to handle different models is often limited, and some have not yet been applied to supercapacitors. Hybrid approaches such as the KF-PF and multi-observer frameworks provide higher modeling accuracy at the cost of increased complexity and lack of real-time validation. Intelligent methods (ANN, fuzzy logic) demonstrate strong modeling capability but are constrained by their dependence on extensive training datasets.

The adaptive algorithm originally proposed in [339, 347] for SoC estimation of Li-ion batteries has been adapted and implemented for supercapacitor applications in this work. The adaptive scheme

dynamically updates the process and measurement covariance matrices at each iteration, based on the residual covariance of the terminal voltage, defined as the error between the measured voltage and the model output estimated by the filter. This approach eliminates the need for manual tuning of initial parameters and enhances both accuracy and robustness under realistic operating conditions [338, 347].

Table 6.1: State of the art on supercapacitor SoC estimation methods

Reference	Method	Supercap application	Real-Time	Different models comparison	Training data required
[334]	KF	✓	✓	✗	✗
[329, 335]	EKF	✓	✓	✗	✗
[336, 337]	UKF	✓	✗	✗	✗
[338–340]	SR-UKF	✗	✓	✗	✗
[343]	KF-PF	✓	✗	✗	✗
[344]	Multi-observer	✓	✗	✗	✗
[345, 346]	ANN/ Fuzzy Logic	✓	✗	✗	✓
Proposed method	ASR-UKF	✓	✓	✓	✗

6.1.2.1 Kalman Filter Initialization

For KF algorithms to achieve optimal performance and robustness, a proper initialization phase that aligns with the system dynamics is essential. In particular, the key covariance matrices, namely the measurement noise covariance R, the process noise covariance Q, and the initial state covariance S_0 are typically initialized as diagonal matrices. This assumption implies that only the auto-covariance terms are considered and that the noise sources are uncorrelated.

Since these parameters directly affect the filters convergence behavior and estimation accuracy, they must be carefully calibrated. To facilitate this process, a representative charge/discharge current profile can be employed to test and refine the initialization values. As part of the modeling workflow, optimal calibration is achieved by aligning the filter-estimated state trajectories with reference simulations using the Parameter Estimator app in MATLAB-Simulink®. This toolbox

applies a nonlinear least-squares solver to minimize discrepancies between selected model outputs and reference data. The resulting optimized parameters offer a reliable initialization of the KF under specified operating conditions.

6.2 Supercapacitor Model

To implement a reliable and effective model-based state estimation method, such as KF, a representative model of the physical system is required. For supercapacitors, two widely adopted Equivalent Circuit Models (ECMs) are typically used to describe their dynamic behavior: the three-branch ECM and the first-order ECM.

The three-branch model has been demonstrated as an effective compromise between accuracy and computational efficiency, making it a suitable option for real-time applications [348–350]. However, a key limitation of this model is the absence of a direct mathematical expression for the SoC, which complicates its integration into SoC estimation algorithms and necessitates additional identification procedures.

In contrast, first-order dynamic ECMs incorporate an explicit relationship between the SoC and the modeled OCV, along with other circuit parameters. This structure facilitates SoC estimation by allowing it to be directly computed as part of the models internal state. While these models generally offer lower fidelity in capturing the nonlinear behavior of supercapacitors compared to more detailed multi-branch models, their reduced complexity and straightforward implementation make them attractive for SoC estimation tasks [337, 351].

Despite the widespread use of both modeling approaches, comparative studies analyzing their respective impacts on SoC estimation performance remain limited. Therefore, this section investigates the modeling of supercapacitor behavior using both the three-branch and first-order ECMs. Their applicability to SoC estimation is assessed, along with an evaluation of how model selection influences the performance and reliability of the model-based estimation process.

6.2.1 Three-Branch Equivalent Circuit Model

Figure 6.1(a) shows the electrical schematic of the three-branch equivalent circuit model, as proposed in [352]. This structure consists of a main nonlinear RC branch and two parallel RC sub-branches that capture the internal diffusion dynamics of the supercapacitor.

In the main branch, the capacitor $C(v)$ models the voltage-dependent capacitance and is connected in series with resistor R. The variation of capacitance with voltage is described by:

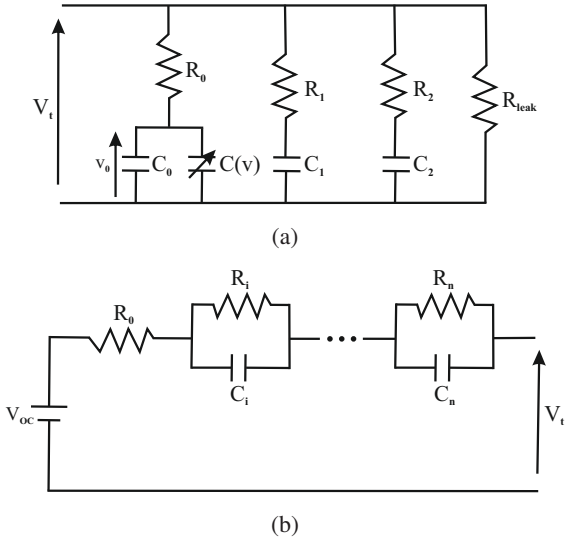

Figure 6.1: Supercapacitor equivalent models: (a) Three-Branch Electric Circuit Model and (b) Generic n-Order Dynamic Equivalent Circuit Model.

$$C(v) = C_0 + K_v \cdot v_0 \tag{6.11}$$

where C_0 is the base (constant) capacitance, v_0 is the voltage across the main branch capacitor, and K_v is a coefficient that quantifies the voltage dependency. The sub-branches R_1-C_1 and R_2-C_2 represent two different time constants associated with ion diffusion [352]. A leakage resistor R_{leak} is also included to model self-discharge, with its value typically provided in manufacturer datasheets.

According to Kirchhoff's laws, the state-space representation of the system can be written as:

$$\begin{cases} C(v_0)\dfrac{dv_0}{dt} = -\dfrac{R_p}{R_0}\left(\dfrac{1}{R_1}+\dfrac{1}{R_2}\right)v_0 + \dfrac{R_p}{R_0R_1}v_1 + \dfrac{R_p}{R_0R_2}v_2 + \dfrac{R_p}{R_0}I \\ C_1\dfrac{dv_1}{dt} = \dfrac{R_p}{R_0R_1}v_0 - \dfrac{R_p}{R_1}\left(\dfrac{1}{R_0}+\dfrac{1}{R_2}\right)v_1 + \dfrac{R_p}{R_1R_2}v_2 + \dfrac{R_p}{R_1}I \\ C_2\dfrac{dv_2}{dt} = \dfrac{R_p}{R_0R_2}v_0 + \dfrac{R_p}{R_1R_2}v_1 - \dfrac{R_p}{R_2}\left(\dfrac{1}{R_1}+\dfrac{1}{R_0}\right)v_2 + \dfrac{R_p}{R_2}I \\ V_t = \dfrac{R_p}{R_0}v_0 + \dfrac{R_p}{R_1}v_1 + \dfrac{R_p}{R_2}v_2 + R_pI \end{cases} \tag{6.12}$$

where $\mathrm{R}_p = R_0 \parallel R_1 \parallel R_2 \parallel R_{\text{leak}}$, and v_1 and v_2 are the voltages across capacitors C_1 and C_2, respectively.

To enable real-time implementation of the KF, the model is discretized with a sampling time T_s. Defining the state vector as $x = [v_0, v_1, v_2]^T$, the discrete-time state-space equations are expressed as follows:

$$\begin{bmatrix} V_{0,k+1} \\ V_{1,k+1} \\ V_{2,k+1} \end{bmatrix} = \begin{bmatrix} \left(1 - \frac{R_p T_s}{R_0 C(v)} \left(\frac{1}{R_1} + \frac{1}{R_2}\right)\right) V_{0,k} + \left(1 + \frac{R_p T_s}{R_0 R_1 C(v)}\right) V_{1,k} + \left(1 + \frac{R_p T_s}{R_0 R_2 C(v)}\right) V_{2,k} + \frac{R_p T_s}{R_0 C(v)} I_k \\ \left(1 + \frac{R_p T_s}{R_0 R_1 C_1}\right) V_{0,k} + \left(1 - \frac{R_p T_s}{R_1 C_1} \left(\frac{1}{R_0} + \frac{1}{R_2}\right)\right) V_{1,k} + \left(1 + \frac{R_p T_s}{R_1 R_2 C_1}\right) V_{2,k} + \frac{R_p T_s}{R_1 C_1} I_k \\ \left(1 + \frac{R_p T_s}{R_0 R_2 C_2}\right) V_{0,k} + \left(1 + \frac{R_p T_s}{R_1 R_2 C_2}\right) V_{1,k} + \left(1 - \frac{R_p T_s}{R_2 C_2} \left(\frac{1}{R_1} + \frac{1}{R_0}\right)\right) V_{2,k} + \frac{R_p T_s}{R_2 C_2} I_k \end{bmatrix} \tag{6.13}$$

$$V_{t,k} = \frac{R_p}{R_0} v_{0,k} + \frac{R_p}{R_1} v_{1,k} + \frac{R_p}{R_2} v_{2,k} + R_p I_k \tag{6.14}$$

These equations define the evolution of internal capacitor voltages at each discrete time step k, where T_s is the time step and I_k is the input current.

Although the model is highly effective for internal voltage tracking, ideal for voltage monitoring and observer-based estimation, there is no direct link between these internal voltages and the SoC. To enable SoC estimation, the energy stored in the capacitors can be used, as defined in Eq. (6.2). To provide a normalized SoC representation, especially when considering a minimum operational voltage (typically half the rated voltage), an indication of SoC definition as below is used:

$$SoC_{3B} = \frac{\sum_{i=1}^{n} \frac{1}{2} C_i v_i^2 - E_{\text{min}}}{E_{\text{max}} - E_{\text{min}}} \tag{6.15}$$

where E_{min} is the minimum required energy to keep the supercapacitor in its operational range, calculated as:

$$E_{\text{min}} = \sum_{i=1}^{n} \frac{1}{2} C_i v_{\text{min}}^2 \tag{6.16}$$

6.2.2 First-Order Dynamic Equivalent Circuit Model

Equivalent circuit modeling is a widely adopted approach in battery research to represent electrochemical behavior through simplified electrical networks. A similar approach can be applied to supercapacitors, with necessary adjustments for their distinct voltage characteristics. As shown

in Figure 6.1(b), the typical structure consists of an ideal voltage source (V_{oc}) in series with an internal resistance R_0 and one or more R_iC_i branches in parallel.

In this work, a first-order ECM is selected due to its favorable balance between modeling accuracy and implementation simplicity. Compared to higher-order models, the first-order structure offers adequate fidelity for capturing the key electrical behavior of supercapacitors, while remaining computationally efficient for real-time applications [330].

The model includes [337, 353]:

- An open-circuit voltage (V_{oc}), which reflects the SoC-dependent terminal voltage under no-load conditions
- A series resistance R_0 accounting for contact and electrode losses
- A single R_1-C_1 parallel branch to capture charge redistribution and diffusion dynamics

A key advantage of this configuration is that it yields a locally observable model, with the SoC explicitly included as a state variable. The SoC is updated through Coulomb Counting, allowing real-time energy tracking during both charge and discharge cycles. The continuous-time model equations are given as:

$$\begin{cases} SoC = SoC_0 - \dfrac{1}{3600 \cdot C_{Ah}} \displaystyle\int_0^t I_{sc}(t)\, dt \\ \dfrac{dv_1}{dt} = -\dfrac{v_1}{R_1C_1} + \dfrac{I_{sc}}{C_1} \\ V_t = V_{oc} - R_0 \cdot I_{sc} - v_1 \end{cases} \tag{6.17}$$

where v_1 is the voltage across the R_1-C_1 branch, and I_{sc} is the current through the supercapacitor, considered positive during discharge and negative during charge.

For implementation in a discrete-time framework, the state vector is defined as $x = [SoC, V_1]^T$, and the discretized equations using a sampling interval T_s are:

$$\begin{bmatrix} SoC_{k+1} \\ V_{1,k+1} \end{bmatrix} = \begin{bmatrix} SoC_k - \dfrac{T_s}{3600 \cdot C_{Ah}} \cdot I_{sc,k} \\ \left(1 - \dfrac{T_s}{R_1C_1}\right) \cdot V_{1,k} + \dfrac{T_s}{C_1} \cdot I_{sc,k} \end{bmatrix} \tag{6.18}$$

$$V_{t,k} = V_{oc} - R_0 \cdot I_{sc,k} - V_{1,k} \tag{6.19}$$

6.2.3 Model Parameters Extraction

The models described in subsections 6.2.1 and 6.2.2 were experimentally characterized using an EATON XLR-48R6167-R supercapacitor (model 166F) as the DUT, which is explained in subsection 3.3 where Table 3.3 presents the key nominal specifications of the tested component, as provided by the manufacturer.

In the three-branch equivalent circuit model, the identified parameters remain constant across different SoC levels. The variation in capacitance with respect to voltage is modeled by the K_v coefficient, which, when multiplied by the voltage v_0, accounts for the voltage dependency of the capacitance.

A charging/discharging repeating cycle has been experimentally performed by imposing constant current steps on the device to calibrate the three-branch model. In this way, the DUT is charged and discharged four times between a selected minimum voltage level and its nominal value, applying a 20-second rest period between each phase of the test. The supercapacitor voltage and current measurements during the experimental characterization are illustrated in Figure 6.2(a). The extraction of the model parameters has been made by means of the "Parameter Estimator" tool in Matlab-Simulink®. It allows for fitting the model voltage curve to the measured one by selecting the same current input given by the experimental test. As a solver, the nonlinear least square method has been selected, and the obtained parameters are reported in Table 6.2.

Table 6.2: Fitted parameters for the three-branch supercapacitor model

Parameter	$C_0\,(F)$	$K_v\,(^F/_V)$	$R_0\,(m\Omega)$	$R_1\,(\Omega)$	$C_1\,(F)$	$R_2\,(\Omega)$	$C_2\,(F)$	$R_{leak}\,(k\Omega)$
Value	132.78	1.08	5.2	11.01	6.61	159.96	2.38	9.5

The second model in this analysis includes SoC-dependent parameters to enable direct observability of the SoC as a state variable. Therefore, a dedicated parameter identification procedure is required. This model is widely used in Li-ion battery applications, where the standard approach is the Hybrid Pulse Power Characterization (HPPC) [354], which involves applying 20-second current pulses at incremental SoC levels, assuming negligible SoC variation during each pulse.

However, for supercapacitors, due to their significantly lower capacity, this assumption becomes less valid. Hence, a similar procedure known as the Positive Pulsed Current (PPC) method [355] is adopted. In this method, shorter current pulses are applied to incrementally increase the supercapacitors SoC while simultaneously identifying the model parameters.

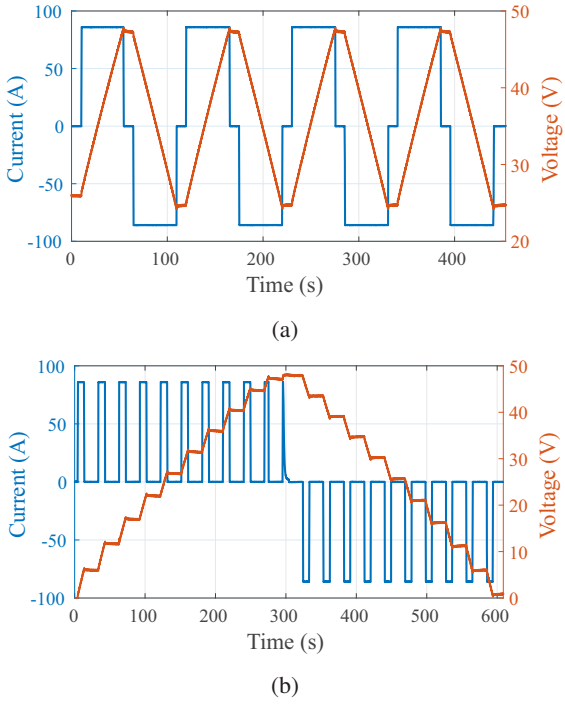

Figure 6.2: Experimental characterization of the supercapacitor: measured current and corresponding terminal voltage during the procedure related to (a) three-branch model and (b) first-order dynamic Equivalent Circuit Model.

The procedure was performed at various charging and discharging current levels. Figure 6.2(b) presents an example of current and voltage measurements obtained during a test using the nominal current. Each current pulse is designed to change the SoC by approximately 10%, and a 20-second rest period is inserted between consecutive pulses. The voltage recorded during each rest phase is used for parameter estimation, as it reflects the SoC reached at the end of the previous pulse.

The series resistance R_0 is determined from the instantaneous voltage drop ΔV observed immediately after the current pulse ends, calculated as ΔV divided by the pulse amplitude. The remaining voltage relaxation is modeled using an exponential fit corresponding to an RC response, enabling the estimation of R_1 and C_1.

Both modeling procedures were carried out using a nominal current of $86\,\mathrm{A}$ for both charging and discharging. The parameters identified through the PPC characterization procedure are summarized in Table 6.3 and Table 6.4, with separate listings for the charging and discharging phases to account for any asymmetric behavior or hysteresis in the supercapacitor's electrical response.

Table 6.3: Extracted parameters during **discharge** using PPC procedure for the first-order ECM

SoC (%)	V_{oc} **(V)**	R_0 **(mΩ)**	R_1 **(mΩ)**	C_1 **(KF)**
10	6.08	2.7	2.6	4.77
20	11.28	2.7	2.1	5.47
30	16.28	2.7	1.9	5.97
40	21.09	2.7	1.8	5.79
50	25.73	2.6	1.7	5.65
60	30.27	2.7	1.6	5.63
70	34.73	2.8	1.4	5.75
80	39.14	2.8	1.1	5.52
90	43.51	2.6	0.8	3.90

Table 6.4: Extracted parameters during **charge** using PPC procedure for the first-order ECM

SoC (%)	V_{oc} **(V)**	R_0 **(mΩ)**	R_1 **(mΩ)**	C_1 **(KF)**
10	5.98	2.8	1.2	7.55
20	11.62	2.8	1.6	6.23
30	16.92	2.7	1.8	5.95
40	21.92	2.7	2.1	5.64
50	26.71	2.7	2.5	5.25
60	31.34	2.7	2.8	4.82
70	35.85	2.6	3.2	4.42
80	40.26	2.8	3.3	4.31
90	47.03	2.6	4.0	3.78

6.3 Results and Validation

This section presents the numerical and experimental results, along with their validation under a realistic grid power profile.

6.3.1 Numerical Results

To compare their performance, all SoC estimation methods described in the previous section were implemented in MATLAB-Simulink. The three-branch model and the first-order ECM

were employed as plant models to simulate the supercapacitor behavior, with random noise added to both voltage and current measurements to emulate a realistic acquisition environment.

The model equations presented in Sections 6.2.1 and 6.2.2 were incorporated into two distinct ASR-UKF frameworks to evaluate the influence of each modeling approach on the proposed adaptive estimation algorithm. Furthermore, all SoC estimation results were scaled to reflect the relative SoC with respect to the supercapacitors voltage operating range, allowing for practical interpretation and a fair comparison across methods.

To quantify estimation performance, the absolute estimation error relative to the reference SoC, computed as in (6.20), was used:

$$\varepsilon = |SoC_{est} - SoC_{ref}| \tag{6.20}$$

where SoC_{est} is the estimated state of charge, and SoC_{ref} is the reference computed from ideal internal voltages.

As in the model characterization process, a constant current was applied to pre-charge the device to its minimum operating voltage. After a rest period, a sequence of charging and discharging current pulses was imposed to test the estimation performance.

The numerical SoC estimation results from four different methods are shown in Figure 6.3(a), where SoC_{ref} is the true reference which has been computed on the basis of the ideal internal supercapacitor voltages. SoC_{SoA} and SoC_{CC} correspond to the State-of-the-Art and Coulomb Counting methods, as described by (6.1) and (6.3), respectively. The proposed adaptive methods based on ASR-UKF combined with the first-order ECM and the three-branch model are labeled as ASR-UKF$_{\text{ECM}}$ and ASR-UKF$_{\text{3B}}$, respectively.

The corresponding estimation errors are illustrated in Figure 6.3(b). It can be observed that the conventional methods and the ASR-UKF$_{\text{ECM}}$ produce comparable accuracy, with absolute errors exceeding 8%. This limited accuracy can be attributed to the small capacity and high current rates characteristic of supercapacitors, which differ significantly from typical battery applications. Specifically, the Coulomb Counting approach performs poorly due to its inability to account for nonlinear behaviors such as voltage-dependent capacitance and internal redistribution effects.

In contrast, the proposed ASR-UKF$_{\text{3B}}$ approach demonstrates significantly improved performance by effectively modeling the supercapacitors dynamic behavior. This results in estimation errors remaining below 1% throughout the entire testing profile, confirming the suitability of the three-branch model for high-accuracy SoC estimation.

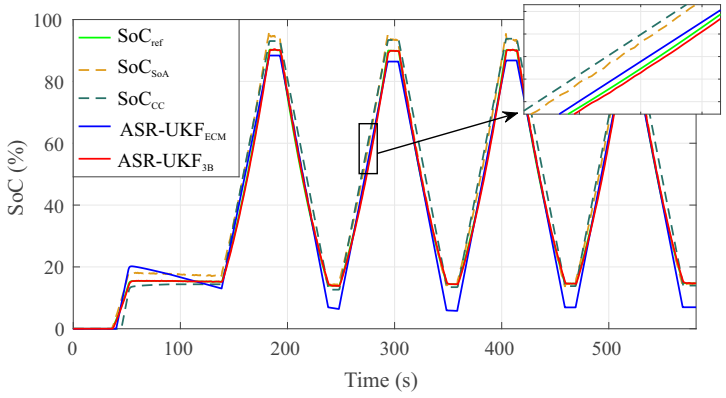

(a)

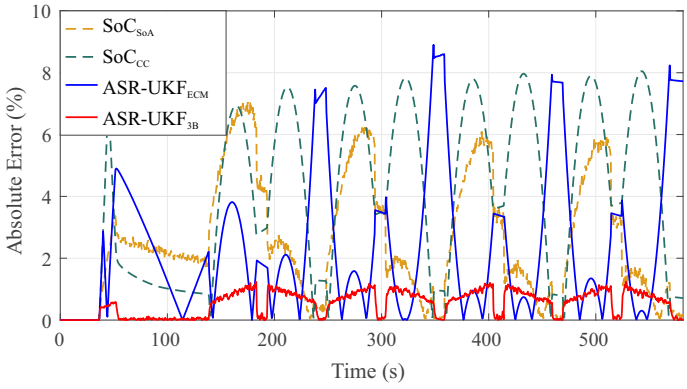

(b)

Figure 6.3: Numerical results for SoC estimation: (a) SoC estimation results and (b) errors with respect to the ideal SoC reference.

6.3.2 Experimental Results

An experimental setup, which is explained in subsection 3.3, was developed to validate the numerical findings and assess the real-time performance of the proposed SoC estimation algorithm. The ASR-UKF was implemented using the models introduced in Sections 6.2.1 and 6.2.2, and a real-time comparison was carried out against conventional methodsnamely the simple SoC definition and Coulomb Counting.

The same EATON supercapacitor used in the numerical simulations was employed as the DUT for experimental validation. As illustrated in Figure 6.4, the supercapacitor was connected to a Spitzenberger&Spies DM 15000 PAS amplifier, acting as a bidirectional current source driven by the desired current profiles.

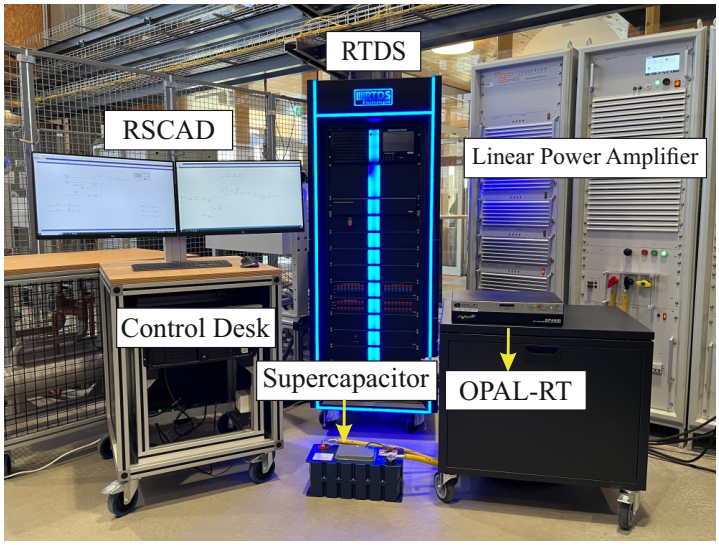

Figure 6.4: Experimental setup for the supercapacitor SoC estimation.

All estimation algorithms, described in Section 6.1, were deployed on an Opal-RT OP4510 real-time simulator, which also managed the acquisition of voltage and current measurements along with the estimation outputs. The ASR-UKF-based SoC estimation was performed with a sampling time of 0.5 s, while the Coulomb Counting and simple SoC computation methods were executed at 50 μs to replicate high-frequency data acquisition.

The complete experimental setup is depicted in Figure 6.5, which highlights both the estimation and measurement components integrated within the Opal-RT system. The power amplifier

was controlled using a NovaCor Real-Time Digital Simulator (RTDS), which generated the control signals required to automatically execute the test procedure. The current profile used for characterizing the three-branch model (see Figure 6.2) was also applied here for consistency across all estimation methods.

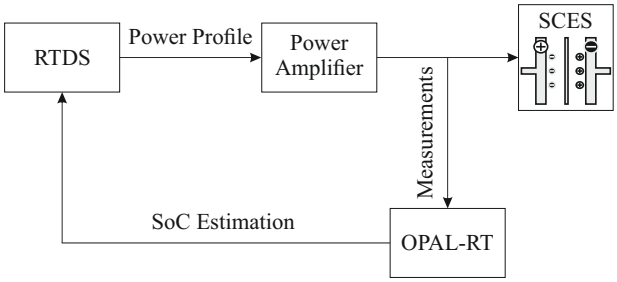

Figure 6.5: Supercapacitor SoC estimation hardware diagram.

To emulate realistic measurement conditions, voltage dividers and current transducers were included. The experimental SoC estimation results are presented in Figure 6.6, where each estimation method is compared to the ideal SoC reference. The absolute estimation error is used as a performance metric.

Additionally, the supercapacitor's internal temperature was continuously monitored using a thermistor embedded within the device, as provided by EATON. The temperature variation throughout the test remained below $3^{\circ}\mathrm{C}$ relative to ambient, and was thus considered negligible in terms of its impact on SoC estimation accuracy.

The results confirm the advantage of the proposed ASR-UKF when paired with the three-branch model. As shown in Figure 6.6(b), this combination achieved the lowest estimation error, remaining below 2% throughout the entire experiment. In contrast, both the simple SoC and Coulomb Counting methods resulted in errors ranging from 6% to 8%. Moreover, the SoC_{SoA} method exhibited noticeable noise, primarily due to voltage measurement disturbances in the experimental setup. The ASR-UKF implementation using the first-order ECM also showed improved results compared to conventional methods, but its peak error still exceeded 6%.

Although a slight performance degradation was observed in the experimental results compared to the numerical simulations, the three-branch ASR-UKF consistently delivered superior accuracy. These findings validate the robustness and real-time applicability of the proposed estimation approach using the three-branch ECM for supercapacitor SoC monitoring.

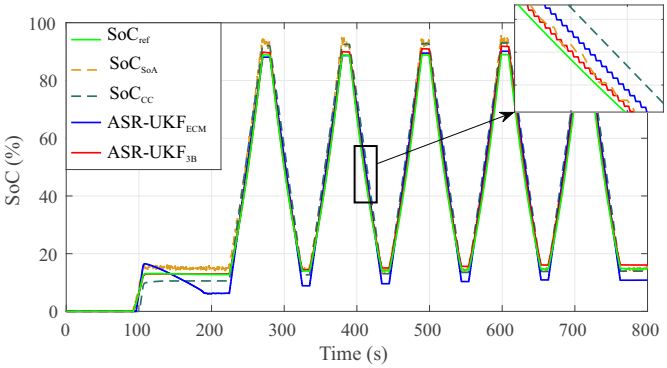

(a)

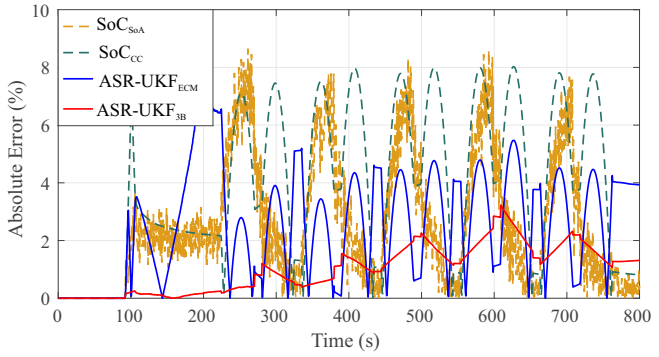

(b)

Figure 6.6: Experimental results for real-time SoC estimation: (a) SoC estimation results and (b) errors with respect to the ideal SoC reference.

6.3.3 Validation under Realistic Grid Power Profiles

Additional experimental tests were conducted using a 1-hour time window extracted from a standard daily power profile measured at a German MV/LV substation [318], explained in detail in Subsection 5.3.1, representing realistic conditions typically encountered by a HESS.

The plant model consisted of a HESS integrating a supercapacitor module and a Li-ion battery pack. A LPF control strategy was employed to allocate power between the energy storage technologies: low-frequency current variations were assigned to the battery, while the supercapacitor was tasked with damping current transients and supplying the high-frequency power demands.

To reproduce this scenario in the real-time experimental setup, the supercapacitor reference power profile was scaled to match the voltage and current operating ranges of the EATON supercapacitor. Figure 6.7 shows the daily power profile, with the selected 1-hour test window highlighted. The extracted power allocations for the battery and supercapacitor using the LPF are displayed in Figure 6.7(b) and 6.7(c), respectively.

Figure 6.8(a) presents the supercapacitor current imposed by the power amplifier during the experiment, obtained by scaling the power profile to the device's operating range and dividing by its rated voltage.

In Figure 6.8(b), the ideal SoC reference (computed under ideal conditions) is compared with SoC estimations from conventional methods and the proposed ASR-UKF algorithm. Consistent with prior tests, Figure 6.8(c) shows that the simple capacity model is affected by voltage measurement noise, while the Coulomb Counting method exhibits errors within the 6%-8% range. Conversely, the proposed ASR-UKF combined with the three-branch model reduces the error to below 1.5% over the entire test duration, demonstrating superior accuracy and robustness under realistic grid power conditions.

6.4 Summary

This chapter introduces a novel approach for estimating the State of Charge (SoC) of supercapacitors using an Adaptive Square-Root Unscented Kalman Filter (ASR-UKF), originally developed for batteries and adapted here to handle the highly variable charge and discharge currents typical of supercapacitors. The method incorporates both three-branch and first-order dynamic electric circuit models to accurately represent the behavior of supercapacitors. Using MATLAB-Simulink, the Kalman filter was optimally calibrated, and the approach was experimentally validated with an EATON 166 F supercapacitor. Real-time simulators, including Novacor RTDS and Opal-RT OP4510, were employed to control the system and implement the SoC estimation. Compared to traditional methods such as Coulomb Counting and simple capacitive models, the ASR-UKF demonstrated superior estimation accuracy. Additional tests using realistic power profiles from a German MV/LV substation further confirmed the methods applicability within Hybrid Energy Storage Systems (HESS), using a classic low-pass filter for power allocation.

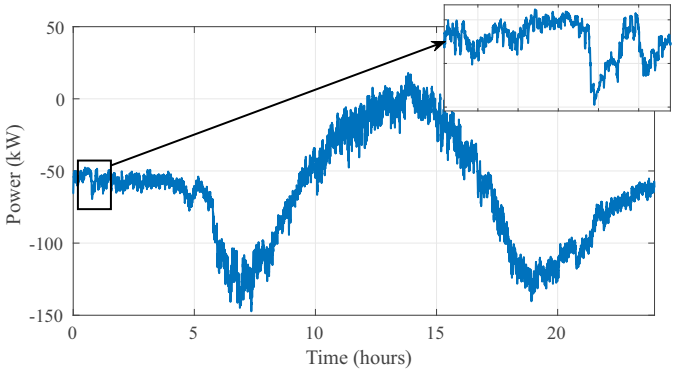

(a)

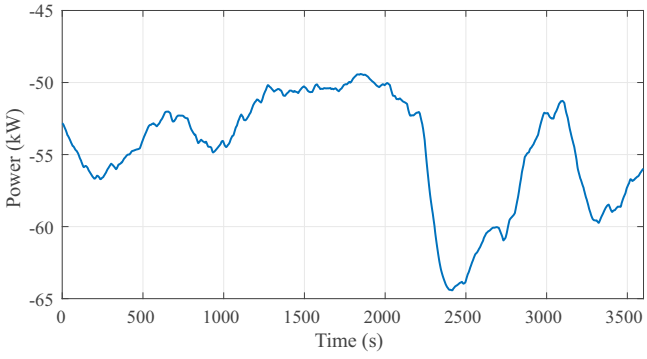

(b)

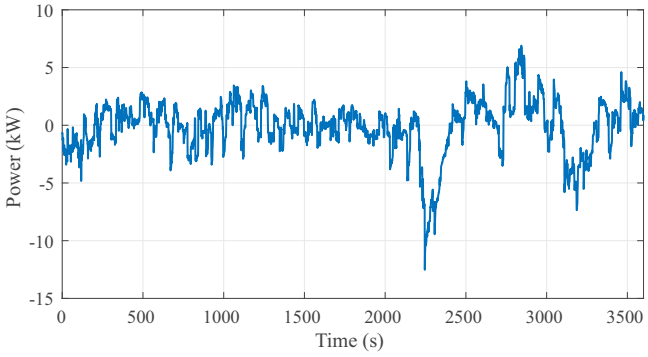

(c)

Figure 6.7: Experimental results for supercapacitor SoC estimation in a HESS: (a) daily power reference profile in a German MV/LV substation with selected 1-hour window; (b) power profile allocated to the battery; (c) power profile allocated to the supercapacitor.

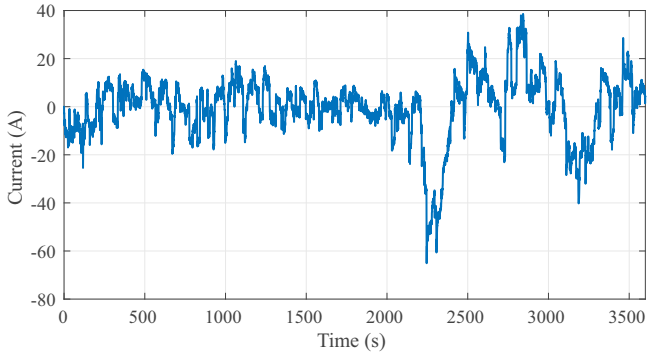

(a)

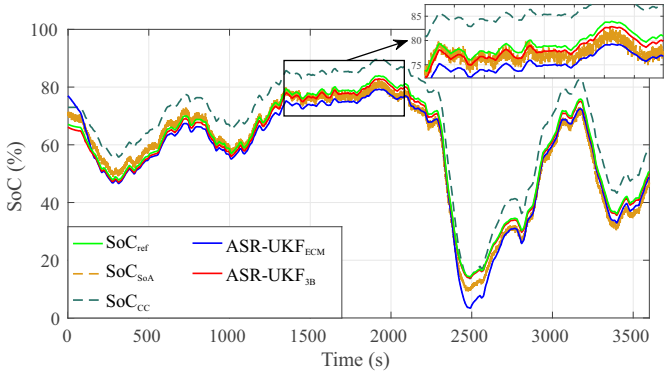

(b)

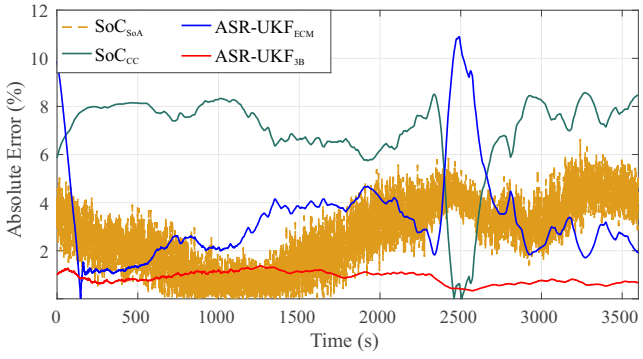

(c)

Figure 6.8: Experimental results for supercapacitor SoC estimation in a HESS: (a) supercapacitor current scaled to its rated range; (b) SoC estimation results; (c) absolute estimation errors compared to the ideal reference.

7 BESS Lifetime Extension using Hybrid Energy Storage Systems

Following the detailed discussion on power management strategies for HESS and the critical role of parameter estimation in ensuring accurate system behavior and control, it is also essential to justify the use of HESS from both technical and economic perspectives. While earlier chapters have focused on the operational benefits and control methods, this chapter takes a step further by addressing the long-term implications of hybridization, particularly in the context of battery aging and cost-effectiveness.

This chapter introduces a novel experimental approach using the PHIL+aging test to realistically assess the impact of hybridization on battery aging. Through PHIL-based experiments, real-time operating scenarios are replicated in a controlled lab environment. The study compares two configurations: a hybrid setup that couples the BESS with a FESS, and a standalone BESS with the same capacity as the HESS. By incorporating a validated PHIL model of the flywheel and conducting accelerated aging tests on Li-ion cells, the investigation captures key degradation factors such as power ramp rates and cycle depth, offering a basis for comparison.

7.1 PHIL-Based Battery Aging Assessment

Battery aging estimation is conducted through a comprehensive methodology combining simulation-based analysis with accelerated aging tests. The testing protocol is informed by the SoC evolution derived from a dynamic simulation model of the energy storage system, which is developed to emulate the real power profiles associated with frequency regulation in the scenario described in Section 5.3.

The methodology enables a comparative lifespan assessment of the battery in two configurations:

- **Case 1:** A HESS composed of a Li-ion BESS and a FESS.
- **Case 2:** A single BESS of equivalent capacity to the HESS, operating independently.

Numerical and experimental activities are combined, targeting an accurate comparative analysis, in terms of battery lifespan assessment under real operating conditions, between Case 1 and Case 2, both contributing to frequency regulation in the investigated micro-grid. In Case 1, the HESS dynamic model is refined, specifically with reference to the flywheel device, through PHIL tests. Once the model is refined, simulations are performed to provide the SoC evolution profile. The methodology globally followed aims to accurately assess battery lifespan according to the specific operating conditions of the application in which the energy storage section is integrated. It consists of three phases:

a) **ESS modeling, sizing, and simulation:** Following the implementation scenario definition (Section 7.3), this phase focuses on developing and tuning the dynamic models of the ESS for both Case 1 and Case 2. In Case 1, PHIL testing is additionally carried out to refine the flywheel representation, particularly with respect to power losses in the HESS model. Furthermore, Case 1 includes the implementation of a real-time stochastic power management algorithm, which performs online power splitting for frequency regulation based on a multi-objective optimization function. The dynamic modeling of both scenarios produces the battery SoC evolution profiles that serve as inputs for the subsequent steps.

b) **Application of Rainflow Cycle Counting (RFC):** The obtained SoC profiles are processed using the RFC algorithm to determine the frequency distribution of charge/discharge cycles categorized by Depth of Discharge (DoD) classes. This distribution forms the statistical basis for designing realistic aging tests.

c) **Design of Experiments (DoE) and Accelerated Aging Tests:** Based on the RFC-derived cycle distribution, a tailored DoE is created for each case to reproduce the actual usage conditions observed in simulation. The DoE outlines the test procedure used to conduct the accelerated aging campaigns, which aim to quantify degradation patterns and estimate battery lifespan under application-specific operating conditions.

The chart of the implemented methodology is illustrated in Figure 7.1.

7.2 Power management strategy

The PHIL platform, previously introduced in Section 3.2, is employed to validate the dynamic performance of the HESS under realistic operating conditions, including grid disturbances and fast power transients. As illustrated in Figure 7.2, the system integrates a real-time simulation environment (Opal-RT OP5700), a power interface (Egston GAMP6, 2×200 kVA), and the

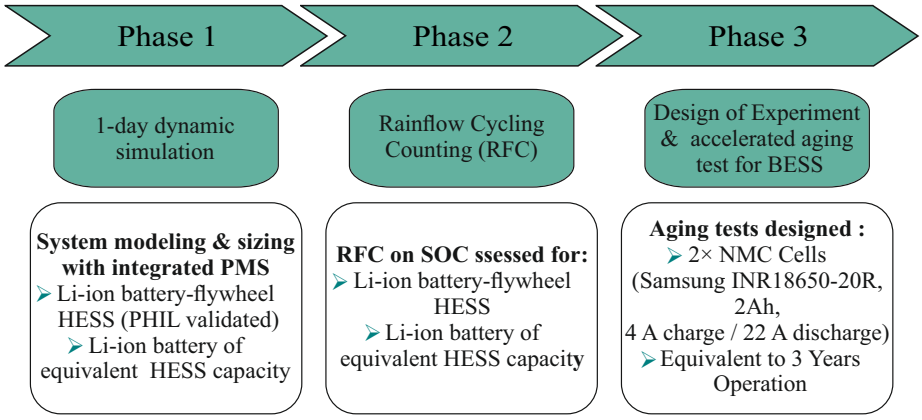

Figure 7.1: Schematic chart of the developed methodology.

physical 120 kW / 8 kWh FESS, whose technical parameters are summarized in Table 3.2 in Subsection 3.2.1.

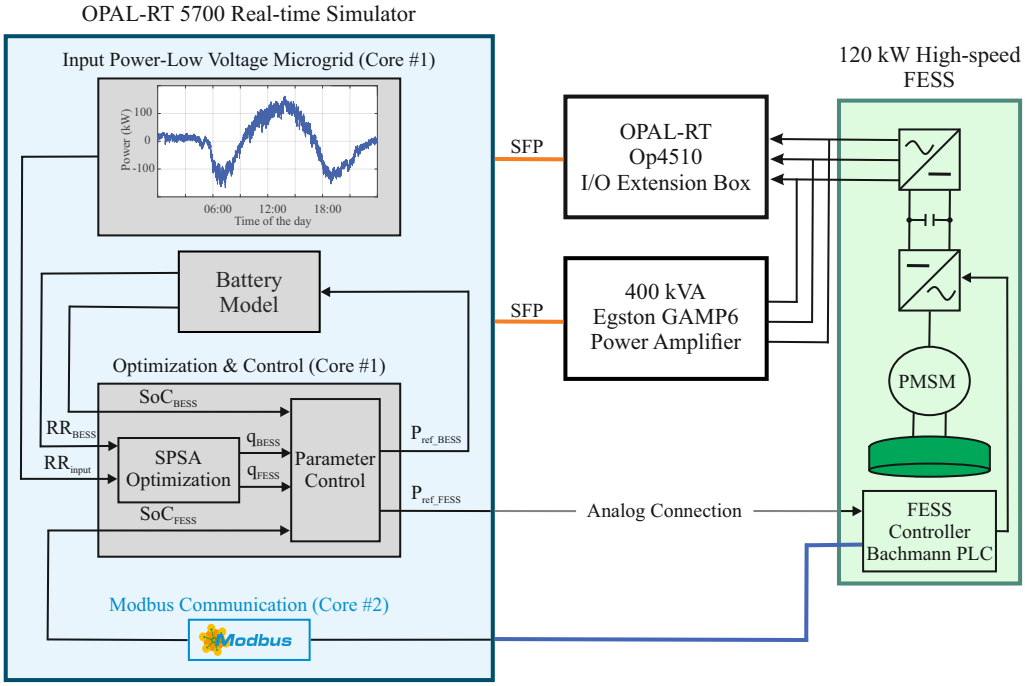

Figure 7.2: Power Hardware in the Loop Setup

As shown in Figure 7.2, the SPSA-based power management strategy explained in Subsection 4.2.2.2 optimizes the power split between the flywheel and battery, prioritizing rapid fluctuations for the flywheel and smoothing battery input power. The SPSA algorithm provides the optimal power share in terms of two coefficients: q_{BESS} and q_{FESS}, representing the proportion of the total input power allocated to the battery and flywheel, respectively. These coefficients are then further adjusted using a control parameter that accounts for the SoC and power constraints of both energy storage systems. Based on this adjustment, the final reference power for each storage unit is determined.

To study the benefits of HESS integration to micro-grids in the view of frequency regulation, a detailed model of the micro-grid including a Li-ion battery and a flywheel as HESS (Case 1) is developed in MATLAB/Simulink environment. A schematic layout of the implemented dynamic model is depicted in Figure 7.3. The real power profile shown in 7.4 provided as input to the model and detailed in Section 5.3 is managed by the power management strategy based on SPSA algorithm. The power management strategy determines the power shares among the HESS components in real-time, considering their specific features in terms of operating C-rates and efficiencies, as well as the defined multi-objective power management function.

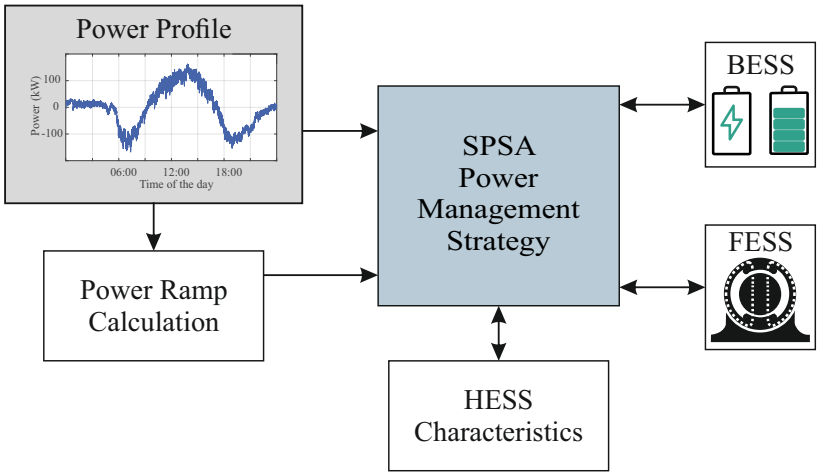

Figure 7.3: Schematic overview of the micro-grid dynamic model integrating HESS Case 1.

Moreover, the current FESS and Li-ion BESS SoCs are taken into account to assess the capabilities of each component in providing/absorbing power at each time step. Furthermore, to assess the benefits of HESS integration in the micro-grid with respect to Case 2, i.e., the sole use of a Li-ion BESS with a capacity equivalent to the sum of capacities of the HESS devices, the model is modified without considering the FESS. This is to compare the different operating conditions of

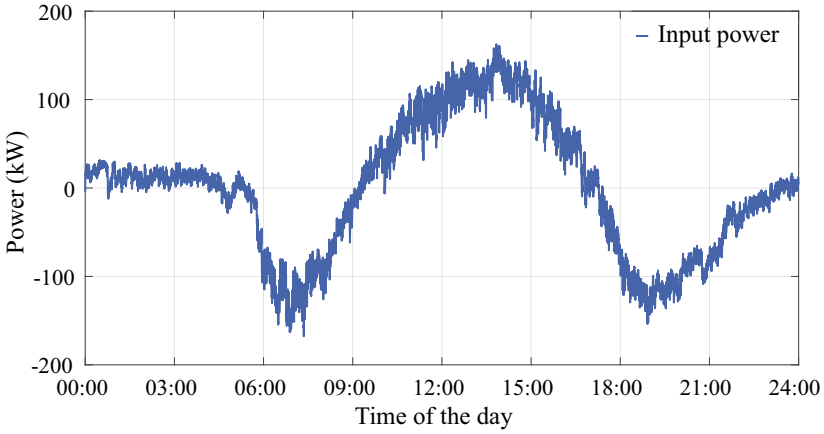

Figure 7.4: The input power profile

the BESS in the hybrid configuration with respect to the non-hybrid case and perform specific aging tests to quantify the lifespan extension of Li-ion BESS when coupled to power-intensive devices as FESS for the specific case study.

In the following, the power management with SPSA for the selected scenario and Li-ion battery and flywheel modeling equations are described in detail.

7.2.1 Simultaneous Perturbation Stochastic Approximation (SPSA) Power Management

Power management strategy is developed based on SPSA algorithm, whose theory is described in Subsection 4.2.2.2. Concerning the problem formulation designed for micro-grid frequency support, the input power to be managed has to be instantaneously split between the FESS and the BESS. Therefore, the vector of unknown parameters (θ) is defined as three dimensionless shares (i.e., Li-ion BESS, FESS, and grid, namely q_{BESS}, q_{FESS}, and q_{GRID}), expressed by (7.1). It is highlighted that q_{GRID} share is included to consider a residual power not managed by the HESS.

$$\theta = \begin{bmatrix} q_{\text{BESS}} \\ q_{\text{FESS}} \\ q_{\text{GRID}} \end{bmatrix} \tag{7.1}$$

Consequently, the split power values are calculated according to (7.2):

$$\begin{cases} P_{\text{BESS}} = q_{\text{BESS}}\,\Delta P \\ P_{\text{FESS}} = q_{\text{FESS}}\,\Delta P \\ P_{\text{GRID}} = q_{\text{GRID}}\,\Delta P \end{cases} \tag{7.2}$$

Where $\Delta P = P^{t}_{\text{freq}} - P^{t-1}_{\text{GRID}}$ (W) is defined as the difference between the required power for frequency regulation at time t and the residual power at the previous instant $(t-1)$. The SPSA parameters, detailed in Section 4.2.2.2, are selected according to [356]. The power shares instantaneously assigned must pursue the following objectives:

I. Maximize micro-grid frequency support, minimizing residual power not managed by HESS over the day within the micro-grid as detailed in:

$$y^{t}_{1}(\theta) = \left(\frac{q_{\text{GRID}} \Delta P}{P^{t-1}_{\text{GRID}}} \right)^{2} \tag{7.3}$$

II. Smooth the Li-ion BESS power profile by means of the ratio between the battery power at timestep t and at the previous instant $(t-1)$, as expressed by:

$$y^{t}_{2}(\theta) = \left(\frac{q_{\text{BESS}} \Delta P}{P^{t-1}_{\text{BESS}}} \right)^{2} \tag{7.4}$$

The multi-objective problem is therefore modeled by means of the weighted sum of the objectives expressed by (7.3) and (7.4), defining the SPSA loss function as (7.5):

$$y^{t}(\theta) = w_1 y^{t}_{1}(\theta) + w_2 y^{t}_{2}(\theta) \tag{7.5}$$

Where the two weights w_1 and w_2 are both set at 0.5. The iterative process starts based on the initial estimate of the vector θ, as specified by (7.6):

$$\theta = \begin{bmatrix} 0.2 \\ 0.78 \\ 0.02 \end{bmatrix} \tag{7.6}$$

7.3 Energy Storage Modeling and Device

The BESS model used in this study is explained in detail in this section. BESS device and experimental setup are also explained while FESS model is explained in Subsection 2.1.3 and the device and experimental setup are explained in Section 3.2.

7.3.1 Battery Energy Storage Modeling

The Li-ion battery model used in this study is based on the work by [357] and has been tuned according to the technical specifications provided by the manufacturer [358]. The battery current I_{BESS} and terminal voltage V_{BESS} are computed in real time from the instantaneous battery power P using the following equations (7.7) and (7.8):

$$I_{\text{BESS}} = \frac{V_{\text{ocv}} - \sqrt{V_{\text{ocv}}^2 - 4R_{\text{BESS}}^{\text{int}} P}}{2R_{\text{BESS}}^{\text{int}}} \tag{7.7}$$

$$V_{\text{BESS}} = V_{\text{ocv}} - R_{\text{BESS}}^{\text{int}} I_{\text{BESS}} \tag{7.8}$$

The open circuit voltage V_{ocv} and internal resistance $R_{\text{BESS}}^{\text{int}}$ depend on the battery state of charge (SoC_{BESS}) and differ between charging and discharging conditions, as described by (7.9) and (7.10):

$$V_{\text{ocv}} = \begin{cases} V_{\text{ocv,c}} = f_1(\text{SoC}_{\text{BESS}}) & \text{(charging)} \\ V_{\text{ocv,d}} = f_2(\text{SoC}_{\text{BESS}}) & \text{(discharging)} \end{cases} \tag{7.9}$$

$$R_{\text{BESS}}^{\text{int}} = \begin{cases} R_{\text{ch}} = f_3(\text{SoC}_{\text{BESS}}) & \text{(charging)} \\ R_{\text{dis}} = f_4(\text{SoC}_{\text{BESS}}) & \text{(discharging)} \end{cases} \tag{7.10}$$

These functions are implemented via look-up tables, derived from experimental characterization of the Li-ion cells to capture the variations in V_{ocv} and $R_{\text{BESS}}^{\text{int}}$ throughout operation. The battery state of charge is computed continuously using (7.11):

$$\text{SoC}_{\text{BESS}} = \text{SoC}_{\text{BESS,ini}} - \int \frac{\eta I_{\text{BESS}}}{Q}\, dt \tag{7.11}$$

The charge/discharge efficiency η is given by (7.12):

$$\eta = \begin{cases} \eta_{\text{ch}} = \frac{V_{\text{ocv}}}{V_{\text{ocv}} - I_{\text{BESS}} R_{\text{ch}}} & \text{(charging)} \\ \eta_{\text{dis}} = \frac{V_{\text{ocv}} - I_{\text{BESS}} R_{\text{dis}}}{V_{\text{ocv}}} & \text{(discharging)} \end{cases} \tag{7.12}$$

Here, $\text{SoC}_{\text{BESS,ini}}$ is the initial battery SoC and Q is the battery capacity in ampere-hours (Ah).

To ensure the battery can support the microgrid frequency regulation requirements over a complete daily cycle, the BESS is sized based on the energy demand profile. In Case 2 (non-hybrid BESS), the battery capacity is determined to be 884 kWh, starting from an initial SoC_{BESS} of 50%. In the HESS configuration (Case 1), the real flywheel installed at the KIT facility has a capacity of 8 kWh (see Subection 3.2.1), reducing the required battery capacity to 876 kWh.

In addition, Case 1 features reduced maximum charge and discharge power limits for the battery compared to Case 2, since the flywheel absorbs high-frequency power fluctuations and alleviates stress on the battery. This results in a lower C-rate requirement for the battery in the HESS, as the flywheel handles the fast dynamics while the battery mainly supplies the smoother, low-frequency power. The technical specifications of the BESS for both configurations are provided in Table 7.1.

Table 7.1: BESS technical features for the considered simulation scenarios.

Parameter	Case 1: HESS Configuration	Case 2: non-hybrid Configuration
Chemestry	Nickel Manganese Cobalt oxide (NMC)	
Nominal Capacity	876 kWh	884 kWh
Max Dis-/charge Rate	0.15C	0.25C
Nominal Voltage	400 V	400 V
Operating voltage	300-420 V	300-420 V
Max DOC	90%	90%

7.3.2 Battery Energy Storage Experimental Setup

The accelerated aging test campaign was carried out on two Samsung INR18650-20R Li-ion cells at the University of Perugia. Cell specifications are deduced from the manufacturer's datasheet [358]. The test was performed by means of a galvanostat/potentiostat BTS4000-5V20A purchased from NEWARE, consisting of 8 channels with a voltage range of 0-5V and $\pm$20 A as maximum current.

Cells were cycled within an operating voltage range of 2.5-4.2 V, with maximum continuous charge and discharge currents of 4 A and 20 A, respectively. This was done while considering the maximum allowable current range of the battery testing system. During the experimental activity, cells were maintained at a fixed temperature of $20 \pm 1°C$. Figure 7.5 illustrates the described experimental test rig and Table 7.2 summarizes the characteristics of the battery.

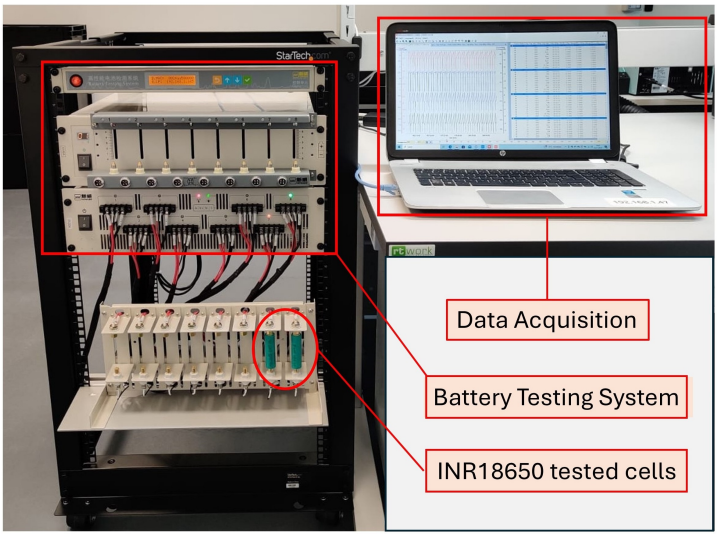

Figure 7.5: Experimental test rig for aging tests on Li-ion cells.

Table 7.2: Key specifications of Samsung INR18650-20R lithium-ion cell (2011 datasheet).

Parameter	Specification	Notes
Cell type	Lithium-ion rechargeable	Cylindrical
Model name	INR18650-20R	18650 format
Nominal capacity	2 Ah	–
Nominal voltage	3.6 V	–
Standard charge	1.0 A CCCV, 4.20 ± 0.05 V, cut-off 100 mA	3 h
Rapid charge	4.0 A CCCV, 4.20 ± 0.05 V, cut-off 100 mA	50 min
Max. continuous discharge	22 A	at $25°C$
Cut-off voltage	2.5 V	Discharge termination
Weight	≤ 45 g	–

7.3.3 Flywheel Energy Storage Modeling

FESS characteristics allow for peak-shaving operations with the aim of extending the Li-ion battery lifetime. To determine the total losses, PHIL simulations are carried out to accurately evaluate the efficiency and power losses of the actual installed flywheel for the studied application. Therefore, the flywheel model explained in Subsection 2.1.3 is tuned according to the specific features and real-time behavior of the installed flywheel system (120 kW, 8 kWh) at the KIT facility, provided by STORNETIC and described in Subsection 3.2.1. The outcomes of PHIL simulations allow for the emulation of the real behavior of the flywheel within the micro-grid under frequency regulation service, in reference to the selected power profile used as input. It is worth noting that Reference [359] provides the detailed flywheel model and its validation using the very same flywheel system installed at the KIT facility.

7.4 Experimental Data Acquisition

The implemented methodology for PHIL testing using the PHIL test facility described in section 3.1 moves from the selection of three windows of the daily input power profile. The length of the three selected patterns is set equal to 30 minutes, to reduce the PHIL test duration. The selection is realized by identifying the most representative and significant patterns depicted in Figure 7.6 of the input power profile, i.e.:

- The window with the maximum mean power.
- The window corresponding to the minimum mean power.
- The window of the power that crosses the zero value.

Simulations are performed with inputs from the selected windows of the input power profile. Simulated power shares between the HESS devices are imposed as input to the PHIL test, including the real FESS. According to the followed methodology, a comparison is carried out between the power trends managed by the modeled FESS and the PHIL FESS, respectively. Power profile measured at the PHIL FESS is therefore used as a feedback parameter to tune modeled flywheel losses. For fine-tuning of the FESS model, it is assumed that the difference between the real and simulated flywheel SoC at the end of the simulations has to be lower than two percentage points.

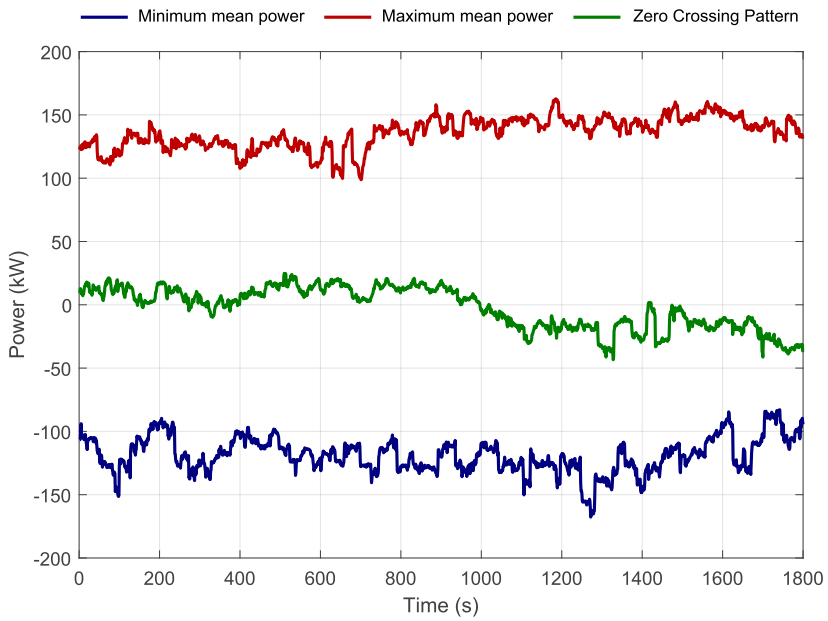

Figure 7.6: Selected patterns of the input power profile. In detail, the profile with the maximum mean power is represented by the red line, while the profile corresponding to the minimum mean power is depicted by the purple line. The green line indicates the selected pattern corresponding to the case of power crossing zero.

7.4.1 Rainflow Cycle Counting (RFC)

Following the procedure summarized in Figure 7.1, Li-ion BESS daily SoCs obtained from one-day simulations in reference to Case 1 and Case 2 are then processed through RFC. In the selected scenarios, RFC is applied to the Li-ion BESS of the Li-ion BESS to determine the daily cycles and the related DoD in reference to the investigated application. Subsequently, it allows us to identify the number of cycles per class of DoD over the day. Cycles with a DoD lower than 0.1% are assumed to be neglected. RFC represents a widely used algorithm for estimating the lifespan of the batteries. Referring to the considered cells, values are properly scaled according to the Samsung SDI INR18650-20R specifications. Theoretical background on RFC is provided in the following.

RFC is a widely used algorithm for assessing fatigue stress on materials. RFC allows cycles counting and quantifying their depths, analyzing damage accumulation in an object subjected to cyclical stress, with the number of cycles leading to a failure of the object dependent on the cycle amplitude [360]. Recently, RFC has also been applied to electrochemical devices, such as batteries, to evaluate their lifespan when subjected to complex charging/discharging cycles [273, 275, 278, 361, 362]. Specifically, RFC finds cycles from local extrema in the load

profile as a function of cycle amplitude. Concerning batteries, the load consists of SoC variation. The SoC-time curves resulting from the simulations are then rotated 90 degrees clockwise, and the time coordinate axis is vertically downward [271, 363]. Firstly, RFC transforms the battery SoC into a sequence of reversals, defined as the local minima and maxima in reference to a load sign changing. Each reversal is seen as a source of water dripping down the roof.

According to American Society for Testing and Materials (ASTM) standard [364], the RFC working procedure is as follows:

I. The number of half-cycles is counted, determining the flow terminations when either:
   - Reaching the time history end.
   - Merging with a flow that started at an earlier reversal.
   - Encountering a greater magnitude trough.

II. A magnitude is assigned to each half-cycle, equal to the difference between its start and termination in terms of stress.

III. To determine the number of full charge-discharge cycles, pair up half-cycles of equal magnitude but in opposite directions. Usually, some incomplete half-cycles remain. For lithium-ion batteries, only cycles with a DoD greater than 2% are important for studying battery degradation [281, 365]. Therefore, cycles with a lower DoD are disregarded.

Figure 7.7 illustrates the operating flow chart of the RFC algorithm according to the ASTM standard. RFC counts cycles by taking into account a moving reference point of the data sequence (Z) and a moving ordered three-point subset with the following features: i) the first and second points are collectively called Y, ii) the second and third points are collectively called X and in both X and Y, the points are sorted from earlier to later in time but not necessarily consecutive, and iii) the range of X, denoted by r(X), represents the absolute value of the difference between the amplitude of the first point and the amplitude of the second point. The definition of r(Y) is analogous.

7.4.2 Design of Experiment (DoE)

Accelerated aging tests are carried out on two Samsung SDI INR18650-20R cells. Initially, the two tested Li-ion cells are characterized to determine their nominal capacities. To perform an accelerated testing procedure, the number of cycles per DoD class over a day is performed by galvanostatic charge and discharge cycles at currents of 4 A and 19.5 A, respectively. The maximum discharge current is limited with respect to what is indicated in the cell specifications (i.e., 22A),

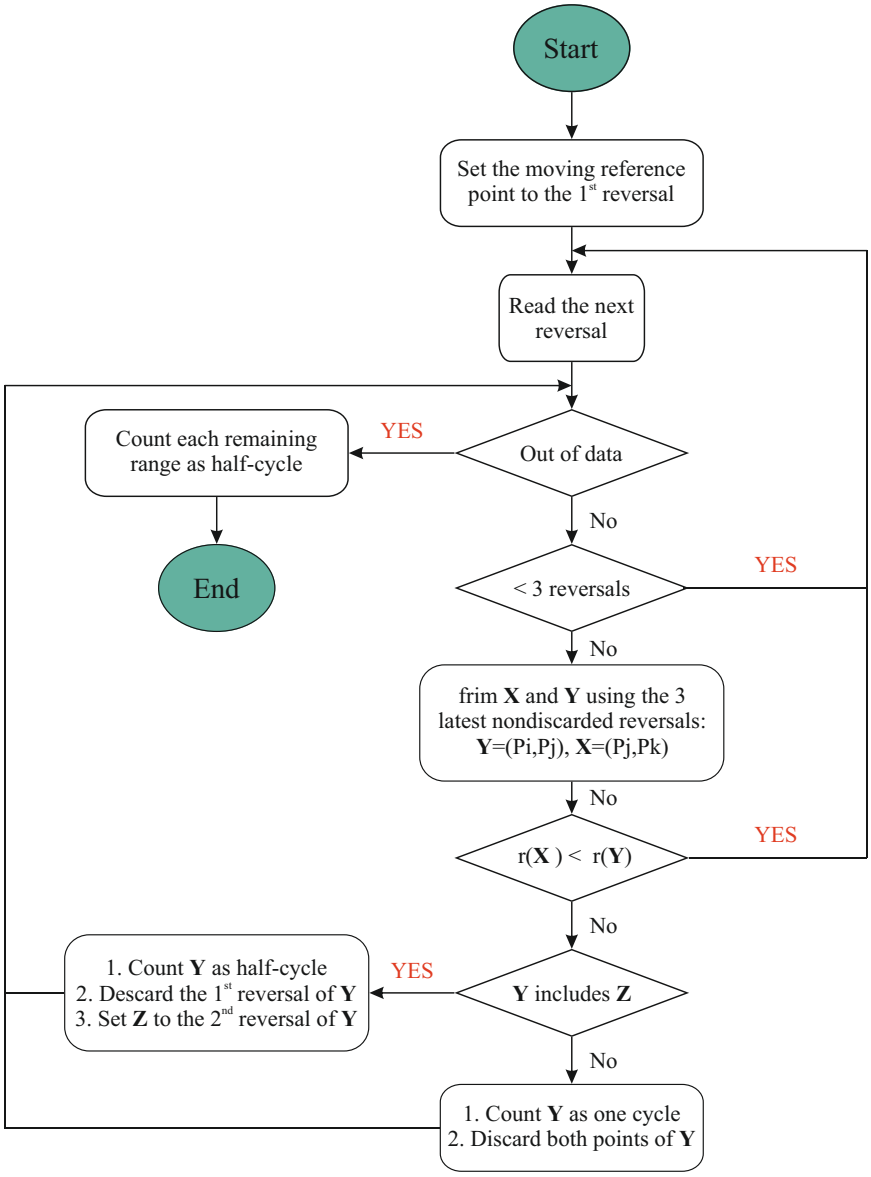

Figure 7.7: Rainflow cycle counting algorithm: schematic view of the flow chart according to ASTM standard.

because of the current limitations of the instrument (the maximum current provided/absorbed equals 20 A).

Moreover, to emulate the different battery stress due to the presence or absence of the flywheel, the average values of the power ramps deduced from the simulations performed for Case 1 and Case 2 are assessed. These result in a power oscillation amplitude of about 0.55 kW/s and 2.3 kW/s for Case 1 and Case 2, respectively. These values are divided by the average of positive values of the input profile and by the average of negative values (respectively 28.2 kW and -28.2 kW). The obtained ratios equal ± 0.02 (Case 1) and ± 0.08 (Case 2). The amplitude of current oscillations to be superimposed to charge and discharge currents is obtained in both cases by multiplying the obtained ratios by the nominal capacity of the tested cells (i.e., 2 Ah). The amplitudes of current oscillations equal ± 0.04 A and ± 0.16 A are obtained.

The overall testing current profile provides accelerated operating conditions relative to 1 day of operation. Therefore, the daily testing procedure is repeated to emulate three equivalent years of battery operation. The capacities of the cells are assessed at each equivalent year of operation through capacity determination performed at 0.5C both in Constant Current-Constant Voltage (CCCV) charge and Constant Current (CC) discharge modes as explained below:

- **CCCV Charge:** During charging, the cells were first subjected to a Constant Current (CC) phase, in which a fixed current (e.g., 1 A for standard charge or 4 A for rapid charge) was applied. The cell voltage increased gradually until reaching the maximum charge voltage of 4.20 V $\pm$ 0.05 V. At this point, the charger switched to the Constant Voltage (CV) phase, maintaining the voltage at 4.20 V while the current naturally decreased. Charging was terminated once the current fell below the cut-off threshold of 100 mA. This approach ensures safe charging while allowing the cell to reach nearly its full capacity without overcharging.
- **CC Discharge:** During discharge, the cells were operated in CC mode, drawing a fixed current (e.g., 20 A) until the cell voltage reached the cut-off voltage of 2.5 V. This mode guarantees reproducible results and prevents over-discharge, which could degrade the cells performance and lifespan.

The State of Health (SoH) of battery cells is assessed at the end of each equivalent year of operation as the ratio between the current measured capacity and the capacity measured before the aging test began.

7.5 Results: State of Health Evaluation

In the following subsections, the experimental validation and results are described in detail.

7.5.1 PHIL-Based Aging Results

In reference to the flow chart depicted in Figure 7.1, the simulation outcomes relating to the two investigated case studies (i.e., HESS configuration and non-hybrid Li-ion BESS of equivalent capacity) are illustrated. In detail, PHIL simulations are carried out aiming at the tuning of flywheel power losses implemented in the developed system dynamic model. Flywheel characteristics, previously presented in Subsection 3.2.1, such as maximum dis-/charge powers, operating speed range, inertia, and a preliminary value of power losses, are implemented in the model to emulate the real flywheel dynamic behavior. Specifically, the three selected patterns of the input power profile, as detailed in Section 7.4, are firstly used to perform dynamic simulations. Simulated trends of power shares between the HESS devices are provided as input to the PHIL test facility, including the real FESS. Then, the power profile at the terminals of the flywheel, installed in the PHIL test rig, is measured. Therefore, flywheel power losses are tuned up to the difference between real and simulated flywheel SoC at the end of the simulations, reducing down to 2 percentage points.

Table 7.3 reports the power loss values obtained from the fine tuning of the FESS model by means of PHIL tests. Specifically, an average flywheel power loss of 2 kW is obtained and consequently implemented in the dynamic model to simulate with greater accuracy the operation of the FESS installed in the PHIL system.

Table 7.3: Assessment of FESS power losses to emulate real FESS behavior.

Case	$P_{loss}(kW)$	$SoC_{r,fin}(\%)$[a]	$SoC_{s,fin}(\%)$[b]
Pattern 1	2.2	50.3	49
Pattern 2	1.5	57.1	55.5
Pattern 3	2.2	51.7	51.45
Average	2		

[a] Final SoC measured from the real flywheel in the PHIL setup.
[b] Final SoC obtained from the simulated flywheel model.

7.5.2 Simulation Results

The FESS primarily operates to mitigate power spikes by continuously performing charge and discharge cycles, thereby protecting the battery from high-frequency variations. This effect can be quantitatively evaluated using the Cumulative Distribution Functions (CDFs) of the FESS and BESS power ramps shown in Figure 7.8. The CDF represents the probability that the power ramp rate remains below a given threshold, providing a statistical measure of how frequently certain ramp magnitudes occur. For instance, at the 90% CDF level, 90% of the observed ramp values are below the corresponding point on the x-axis. As observed, the CDF of the power ramp managed by the BESS is significantly lower compared to the FESS, with values of 0.5 kW/s and 1.8 kW/s at the 90% CDF for the BESS and FESS, respectively, in the HESS mode. This confirms that the FESS takes over the faster transients, while the BESS is exposed only to smoother dynamics, which is beneficial for reducing degradation and extending its operational lifetime. The zoomed-in view (0-7 kW/s, 0.8-1 CDF) further emphasizes this effect in the high-probability region, where the BESS in HESS mode shows markedly lower ramp magnitudes than the standalone BESS.

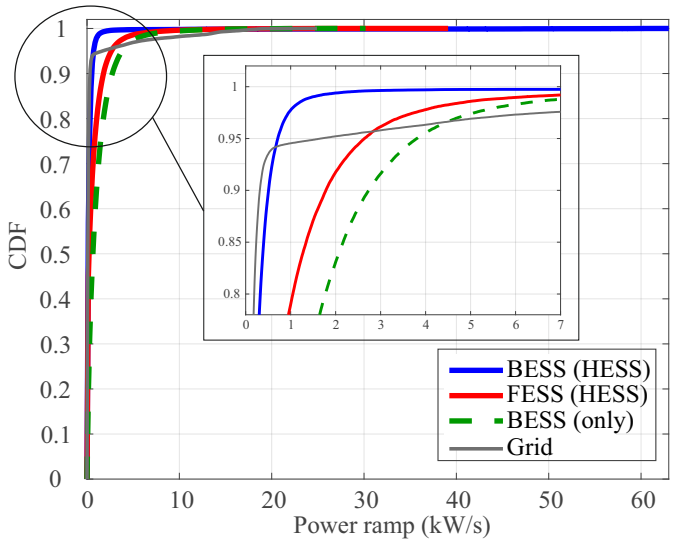

Figure 7.8: cumulative density functions of power ramp rates for BESS (HESS and standalone), FESS, and grid power. The zoomed-in view highlights smoother BESS operation in HESS mode.

Figure 7.8 also illustrates the CDF of the residual power not managed by the HESS due to the power and energy limitations of the integrated devices. For example, as visible in Figure 7.4, around 17h the BESS output power drops to zero once the maximum state of charge is reached. Such outcomes emphasize the efficiency of the SPSA-based power management in both minimizing

the BESS power ramp and reducing the residual portion of the input power that is not absorbed by the HESS, as further detailed in the problem formulation section. The resulting daily residual energy is indeed kept below 6 kWh.

HESS configuration advantages are also reflected in the lower exploitation of the BESS capacity. As a matter of fact, Figure 7.9 reports SoC profiles derived from simulations. RFC algorithm is then applied to these profiles, as described in the following section.

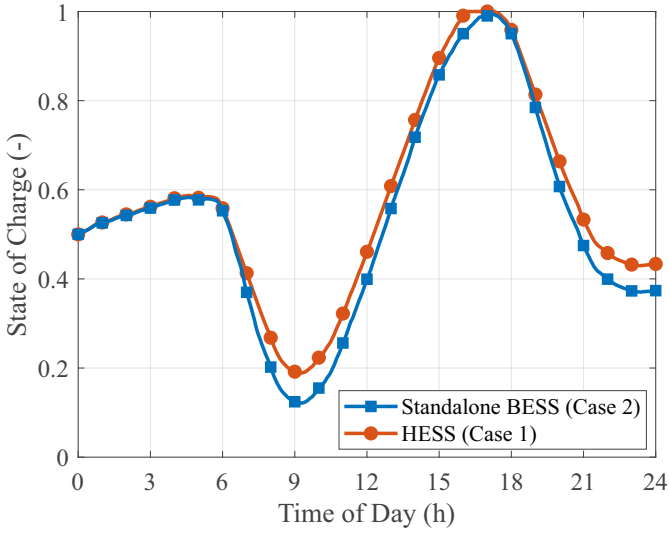

Figure 7.9: BESS SoCs in case of hybrid (orange line) and non-hybrid (blue line) configurations.

7.5.2.1 Rainflow Cycle Counting Results

Simulated profiles of BESS SoC, obtained for Case 1 and Case 2, are processed by applying RFC. Table 7.4 lists the obtained results for both the scenarios taken into account. It is evident that Li-ion BESS is less stressed when coupled with a flywheel (Case 1), with a minimum SoC of 19%, if compared to the minimum SoC registered in the case of Case 2 (i.e., 12.1%). This is also clearly visible from the SoC simulated daily trends reported in Figure 7.9. Seven cycles, listed in Table 7.4, are identified through RFC (according to the procedure detailed in Section 7.4.1, cycles with a DoD lower than 0.1% are neglected). Figure 7.10a shows the zoomed-in SoC figure that depicts cycles 2,3 and 4, and Figure 7.10b shows cycles 5 and 6, respectively. It can be noted that the overall amplitude of the cycles is greater for Case 2 (non-hybrid configuration) with respect to Case 1 (HESS) due to the lack of FESS peak-shaving operation in minimizing the stress towards the BESS.

Table 7.4: Daily cycles obtained by RFC application on Li-ion BESS SoCs for non-hybrid and hybrid cases.

Cycle	Case 1 - HESS Li-ion Battery			Case 2 - Equivalent Li-ion Battery		
	$SoC_{init}(\%)$	$SoC_{fin}(\%)$	$DoD(\%)$	$SoC_{init}(\%)$	$SoC_{fin}(\%)$	$DoD(\%)$
1	50.0	58.7	+8.7	50.0	58.3	+8.3
2	58.7	58.2	-0.5	58.3	57.7	-0.6
3	58.2	58.4	+0.2	57.7	58.0	+0.3
4	58.4	19.0	-39.4	58.0	12.1	-45.9
5	19.0	100	+81.0	12.1	99.3	+87.2
6	100	43.0	-57.0	99.3	37.0	-62.3
7	43.0	43.3	+0.3	37.0	37.3	+0.3

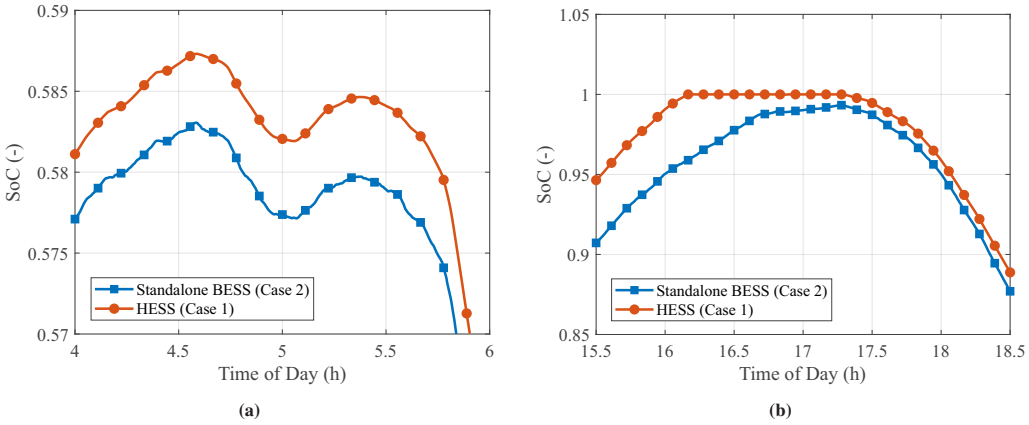

Figure 7.10: Zoomed in BESS SoCs in case of hybrid (orange line) and non-hybrid (blue line) configurations (a) SoC change between 2 and 4 (b) SoC change between 15.5 and 18.5.

7.5.3 Results of experimental aging

Results of RFC application to the daily SoC of BESS operated in both cases are used to design the experimental test campaign on two Samsung SDI INR18650-20R cells. Specifically, the cells are operated, according to the testing conditions detailed in Section 7.4.2, by repeating the cycles of Table 7.4 all over the year. The aging of the two cells is assessed through battery capacity determination after each equivalent year of operation (one equivalent year corresponds to less than 16 and 17 days of test for Case 1 and Case 2, respectively). This can be achieved by increasing the applied current to the cells to their maximum continuous values, aiming to reduce the time required for evaluating cell aging when subjected to complex degradation cycles. Such a procedure is repeated for three consecutive years, each equivalent to the others. The design of the experiment also includes 10-minute resting times to provide relaxation for the cells and

prevent overcharging/overdischarging. All details of the accelerated test campaign are described in Table 7.5.

Table 7.5: Step cycles for the accelerated test campaign on Li-ion cells in relation to Case 1 and Case 2.

Step	Case 1 - HESS Li-ion Battery			Case 2 - Equivalent Li-ion Battery		
	$DoD(\%)$	I_{cell} (A)	Time (s)	$DoD(\%)$	I_{cell} (A)	Time (s)
1	+8.7%	-4 $\pm$0.04	157	+8.3%	-4 $\pm$0.16	149
2	-0.5%	19.5 $\pm$0.04	2	-0.6%	19.5 $\pm$0.16	2
3	+0.2%	-4 $\pm$0.04	4	+0.3%	-4 $\pm$0.16	5
4	-39.4%	19.5 $\pm$0.04	142	-45.9%	19.5 $\pm$0.16	165
5	-	0	600	-	0	600
6	+81.0%	-4 $\pm$0.04	1458	+87.2%	-4 $\pm$0.16	1570
7	-	0	600	-	0	600
8	-57.0%	19.5 $\pm$0.04	205	-62.3%	19.5 $\pm$0.16	224
9	-	0	600	-	0	600
10	+0.3%	-4 $\pm$0.04	5	+0.3%	-4 $\pm$0.16	5

The "Time (s)" column in Table 7.5 indicates the duration of each step in the accelerated test campaign, i.e., how long the battery cell is subjected to a specific combination of current (I_{cell}) and change in DoD. Steps with a dash (-) for DoD correspond to resting periods, where no current is applied, allowing the cell to relax and its voltage to stabilize. The duration of the steps varies depending on the type of energy exchange being replicated: short steps (e.g., 2-5 s) represent fast, small changes in DoD corresponding to rapid power fluctuations in the real system, such as brief power spikes or regenerative events. Long steps (hundreds to thousands of seconds) reproduce slower, larger energy exchanges, where the battery experiences sustained charging or discharging. Resting steps with zero current ensure the cell is not overcharged or over-discharged and allow relaxation between active steps.

Experimental aging results are reported in Table 7.6. It is highlighted that the battery cell capacity in Case 2 exhibits greater degradation, achieving a capacity of 1302.9 mAh compared to 1501.7 mAh measured on the cell tested under the operating conditions of Case 1. This is a clear indication of the benefits of HESS integration for the specific studied application, allowing BESS lifespan extension and leading to fewer device replacements over a long-term horizon.

For the sake of clarity, the reduction of cell aging is also depicted in Figure 7.11. It is evident that in Case 2 the cell SoH dramatically decreases at the end of the third year at 65% of the initial capacity, while in Case 1 it stands at about 75%.

Table 7.6: Registered capacity values for the investigated cases.

Equivalent year	Measured Capacity (mAh)	
	Case 1 - HESS Li-ion Battery	Case 2 - Equivalent Li-ion Battery
0	2008.7	2013.8
1	1838.3	1804.7
2	1668.8	1622.0
3	1501.7	1302.9

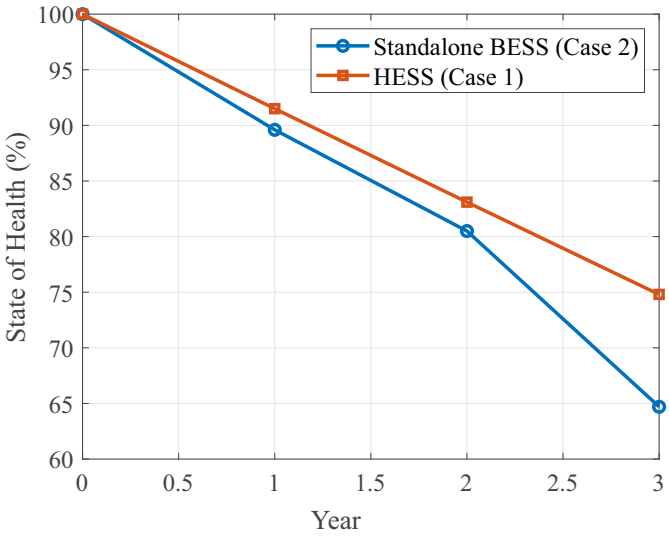

Figure 7.11: BESS SoCs in case of hybrid (blue line) and non-hybrid (red line) configurations.

7.6 Economic Analysis

The experimental results in the previous section confirm that integrating a FESS with a BESS in a HESS configuration significantly improves system performance. The HESS setup reduces high-frequency power fluctuations, leading to smoother battery operation and lower DoD cycles. The RFC analysis revealed that HESS reduces large amplitude charge-discharge cycles, a major contributor to battery degradation. This section provides an overview of the economic analysis of the two cases: HESS and standalone BESS. The Life Cost of Storage (LCOS) and LCOS over a longer period of 20 years, based on the frequency of changes in ESSs, are discussed in this chapter.

7.6.1 Levelized Cost of Storage (LCOS) Framework

Battery degradation has a significant impact on the total cost of energy storage systems over time. This section evaluates the economic impact of integrating a flywheel into a HESS by comparing the battery replacement frequency and LCOS with those of a standalone BESS.

7.6.2 Battery Replacement Frequency Estimation

Based on experimental results, the State of Health (SoH) after three years was observed as 65% for the standalone BESS and 75% for the BESS operating within the HESS configuration. Assuming a linear degradation model and that battery replacement is required when SoH falls below 80%, the annual degradation rates are:

$$\text{Annual degradation (BESS)} = \frac{100\% - 65\%}{3} = 11.67\%/\text{year} \tag{7.13}$$

$$\text{Annual degradation (HESS)} = \frac{100\% - 75\%}{3} = 8.33\%/\text{year} \tag{7.14}$$

From this, the time to reach 80% SoH is described as $T_{\text{End of Life (EoL)}}$:

$$T_{\text{EoL,BESS}} = \frac{100\% - 80\%}{11.67\%} \approx 1.71 \text{ years} \tag{7.15}$$

$$T_{\text{EoL,HESS}} = \frac{100\% - 80\%}{8.33\%} \approx 2.4 \text{ years} \tag{7.16}$$

Over a 20-year service life, this corresponds to:

$$N_{\text{replace,BESS}} = \frac{20}{1.71} \approx 11.67 \tag{7.17}$$

$$N_{\text{replace,HESS}} = \frac{20}{2.4} \approx 8.33 \tag{7.18}$$

This reduction in replacement frequency results in significant long-term cost savings in favor of HESS.

7.6.2.1 LCOS Calculation Methodology

To evaluate cost-effectiveness per unit of energy delivered, we compute the LCOS as:

$$\text{LCOS} = \frac{C_{\text{cap}} \cdot \text{CRF} + C_{\text{O\&M}}}{E_{\text{annual}}} \tag{7.19}$$

where C_{cap} is the total capital expenditure, CRF is the capital recovery factor:

$$\text{CRF} = \frac{r(1+r)^n}{(1+r)^n - 1} \tag{7.20}$$

where:

- C_{cap}: Total capital expenditure,
- CRF: Capital Recovery Factor, defined as

$$\text{CRF} = \frac{r(1+r)^n}{(1+r)^n - 1}, \tag{7.21}$$

  with $r = 7\%$ and $n = 10$ years,
- $C_{\text{O\&M}}$: Annual operation and maintenance costs (2% of C_{cap}),
- E_{annual}: Annual discharged energy,

$$E_{\text{annual}} = E_{\text{usable}} \cdot N_{\text{cycles}} \cdot \eta. \tag{7.22}$$

With $N_{\text{cycles}} = 365$ and round-trip efficiency η (95% for BESS and 90% for FESS), the resulting LCOS values are:

- **Standalone BESS:** \$0.379/kWh,
- **Hybrid Energy Storage System:** \$0.400/kWh.

Although HESS exhibits a slightly higher LCOS due to the high capital cost of the flywheel, the reduction in battery replacements and associated downtime results in long-term economic advantages. These benefits are especially relevant in high-cycling applications where battery longevity is critical.

7.6.3 Long-Term Economic Evaluation over 20 Years

To evaluate the cost-effectiveness of the standalone BESS and the HESS, the Levelized Cost of Storage (LCOS) [366, 367] is computed over a 20-year operational lifetime [368].

The LCOS over 20 years is defined as:

$$\text{LCOS}_{20y} = \frac{\sum_{t=1}^{20} \frac{C_{\text{cap},t} + C_{\text{O\&M},t}}{(1+r)^t}}{\sum_{t=1}^{20} \frac{E_t}{(1+r)^t}} \tag{7.23}$$

where $C_{\text{cap},t}$ is the capital cost in year t (including battery replacements), $C_{\text{O\&M},t}$ is the annual operating cost (assumed to be 2% of initial capital cost, based on the average values reported in the literature [369, 370]), E_t is the discharged energy in year t, and r is the discount rate (7%) which reflects commonly used assumptions and averages from prior studies [160, 371].

The cost parameters for the BESS and FESS, including both energy and power costs, are derived from the latest data provided in the PNNL report [369]. Due to the difficulty of precisely estimating the capital cost, the total project cost is considered for this study. A detailed breakdown of these costs is presented in Table 7.7, and the system specification of each system and the corresponding total calculated cost are presented in Table 7.8. The total cost is calculated based on both the power cost C_P and energy cost C_E of each ESS as (7.24) [369, 372].

$$\text{Total Cost}_{\text{ESS}} = C_P \cdot P_{\text{kW}} + C_E \cdot E_{\text{kWh}} \tag{7.24}$$

Table 7.7: Capital cost parameters for BESS and FESS

Component	Power Cost (C_P) [$/kW]	Energy Cost (C_E) [$/kWh]
BESS	1446	362
FESS	1980	7920

Battery replacement costs are assumed to match the original BESS unit cost. With efficiency of BESS being 90% and efficiency of FESS being 95% [155, 158], the annual discharged energy for BESS is $E_{\text{BESS}} = 884 \cdot 365 \cdot 0.95 = 306{,}181$ kWh/year and for HESS is $E_{\text{HESS}} = (876 \cdot 0.95 + 8 \cdot 0.90) \cdot 365 = 306{,}381$ kWh/year.

The determination of battery end-of-life thresholds in this study is based on the observed SoH degradation trends shown in Figure 7.12b and summarized in Table 7.9. Different SoH thresholds

Table 7.8: Power and Energy Ratings of Storage Systems

Case	System	Power Rating [kW]	Energy Rating [kWh]	Total Cost [$]
Case 1: HESS	BESS	131.4	876	944880
	FESS	120	8	
Case 2: Single BESS	BESS	221	884	639574

Table 7.9: Replacement Intervals for Different SoH Thresholds

SoH Threshold [%]	BESS Interval [years]	BESS (HESS) Interval [years]	FESS Interval [years]
80	1.7	2.4	15
70	2.5	3.6	14
60	3.4	6.8	12
40	5.1	7.2	10

(80%, 70%, 60%, and 40%) were considered to assess the sensitivity of battery replacement intervals on the LCOS [373, 374]. The BESS replacement intervals were derived from experimental SoH degradation rates, while the FESS replacement intervals were assigned based on mechanical fatigue considerations.

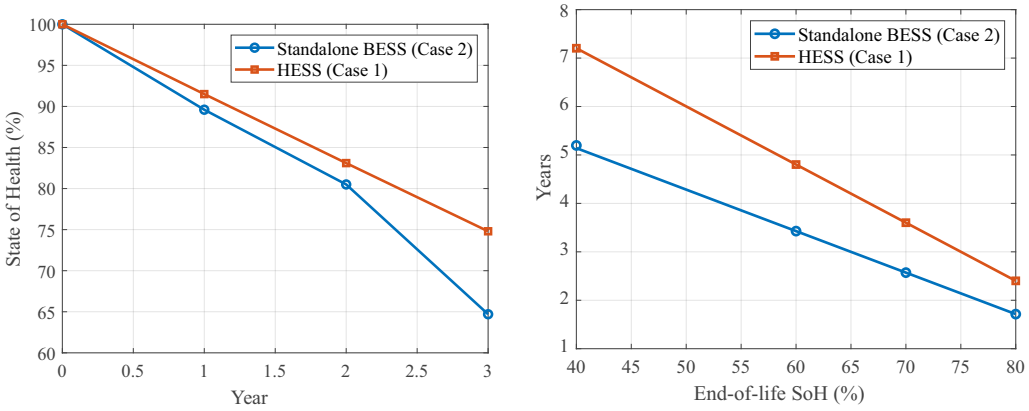

Figure 7.12: (a) Measured state of health for the cells tested according to operating conditions (b) BESS replacement based on end of life on different SoH.

Unlike the battery, whose end-of-life is typically defined by a drop in SoH to a specified threshold, the flywheel's life is governed by mechanical fatigue and bearing wear mechanisms. The fatigue life of composite flywheel rotors is commonly reported between 10^8 to 10^9 equivalent cycles [59, 375, 376], depending on design and operational stresses. Considering the typical operating profiles in energy storage applications and accounting for mechanical stresses induced by deep torque cycles, a variable flywheel replacement schedule was adopted. Specifically, the FESS replacement interval was set to decrease progressively from 15 years to 10 years as cycling severity increased, corresponding to lower SoH thresholds. This approach reflects the increasing mechanical fatigue and bearing stress under more aggressive operational profiles, while maintaining realistic assumptions aligned with industrial practice. The comprehensive comparison across these four cases is illustrated in Figure 7.13, which reports the LCOS evolution over a 20-year horizon.

The results in Figure 7.13 demonstrate that HESS does not universally guarantee lower costs compared to standalone BESS configurations. Instead, the cost competitiveness of HESS strongly depends on the chosen SoH limit for battery end-of-life and the corresponding replacement timing. Specifically, in scenarios with stricter SoH thresholds (e.g., 80% and 70%), the HESS configuration often shows economic advantages due to the reduced battery cycling stress and extended battery lifespan. Conversely, for lower SoH thresholds (e.g., 60% and 40%), where batteries are replaced less frequently, the higher capital cost of integrating a flywheel becomes more pronounced, potentially offsetting the longevity benefits.

7.7 Summary

This chapter presents a comprehensive methodology for evaluating the benefits of hybridizing battery energy storage systems (BESS) with flywheel energy storage systems (FESS) in extending battery lifespan for frequency regulation services in microgrids. Two configurations are assessed: a hybrid energy storage system (HESS) combining a Li-ion battery and a flywheel, and a conventional battery-only system of equivalent energy capacity. The methodology integrates simulation-based modeling, Power Hardware-in-the-Loop (PHIL) experiments, Rainflow Cycle Counting (RFC) analysis, and accelerated aging tests on Li-ion cells.

Dynamic simulations using a detailed MATLAB/Simulink model and an SPSA-based power management algorithm generate battery State of Charge (SoC) profiles under realistic grid conditions. These SoC profiles are analyzed via RFC to extract cycle distributions by depth of discharge (DoD). Subsequently, a tailored Design of Experiments (DoE) defines accelerated degradation tests that reproduce application-specific cycling patterns on real Li-ion cells. PHIL tests refine the

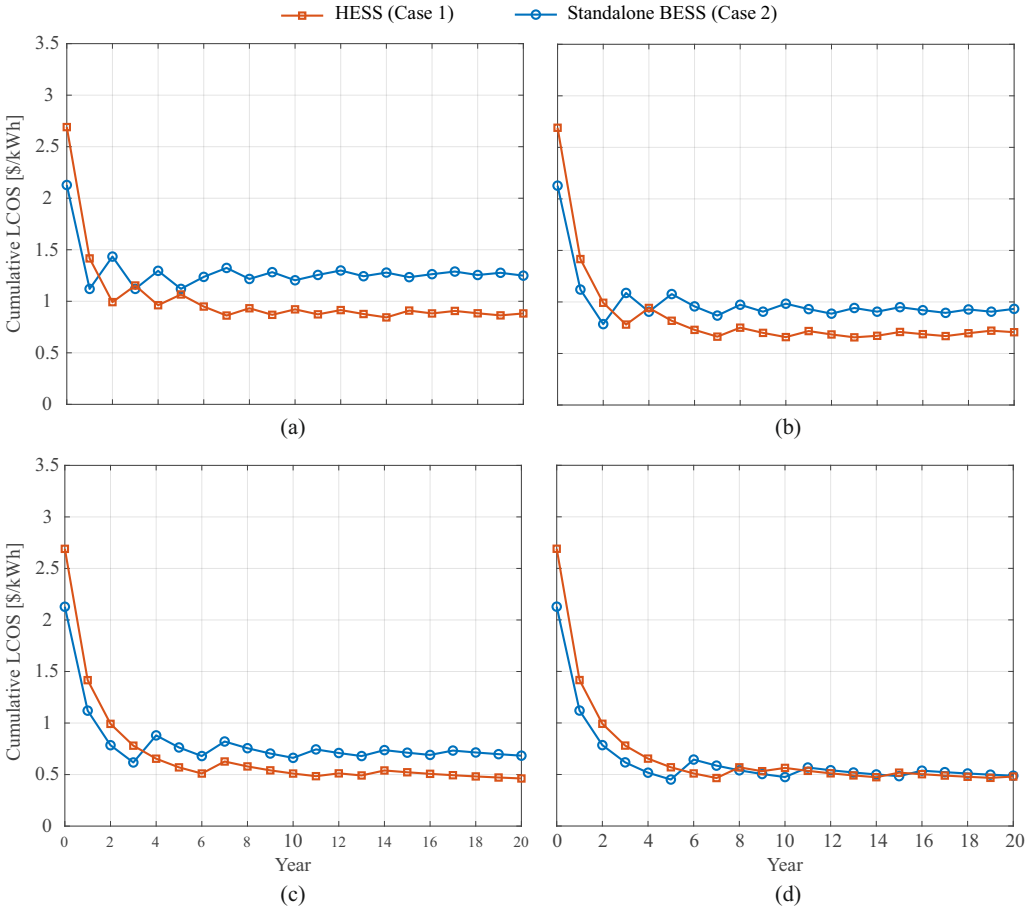

Figure 7.13: Cumulative Levelized Cost of Storage (LCOS) over 20 years (a) replacement of the battery by 80% of SoH (b) replacement of the battery by 70% of SoH (c) replacement of the battery by 60% of SoH (d) replacement of the battery by 40% of SoH.

flywheel model by comparing simulated and measured power losses and SoC evolutions, ensuring accurate emulation of flywheel dynamics.

Results demonstrate that integrating the flywheel substantially reduces battery stress, smoothing power fluctuations, and lowering the frequency and amplitude of deep discharge cycles. Accelerated aging tests reveal that after three equivalent years of operation, the battery in the hybrid configuration retains approximately 75% of its initial capacity, compared to 65% in the battery-only system. This apparent improvement in battery state of health highlights the effectiveness of the hybrid configuration in extending battery life, reducing replacement frequency, and enhancing the sustainability and cost-effectiveness of energy storage solutions for grid support applications. Moreover, a 20-year economic analysis was conducted for both configurations, showing that the HESS case reduces total lifecycle costs by decreasing battery replacement frequency.

8 Summary, Conclusion, and Future Work

8.1 Summary and Conclusion

This work has demonstrated the significant potential of Hybrid Energy Storage Systems (HESS) in improving the performance, longevity, and economic viability of energy storage solutions for modern power systems. By integrating complementary storage technologies, the HESS approach effectively mitigates the inherent limitations of individual devices.

The work began with an in-depth analysis of key energy storage technologies, outlining their characteristics and operational challenges. Flywheels and supercapacitors, with their fast response capabilities and high power densities, are ideal partners for batteries, which provide high energy capacity but suffer from degradation under high cycling stress.

A contribution of this thesis is the experimental validation of HESS performance through Power Hardware-in-the-Loop (PHIL) testing. This methodology enabled realistic emulation of grid conditions while capturing the dynamic behavior and losses of a commercial Flywheel Energy Storage System (FESS) in conjunction with a Battery Energy Storage System (BESS). The results indicate that HESS reduces high-frequency power fluctuations imposed on batteries, leading to smoother operation and lower depth-of-discharge cycles, which are critical factors influencing the degradation of BESS.

Control strategies developed and experimentally validated here, including a power split based on moving average filtering and fuzzy logic, ensure optimal load sharing between the BESS and the FESS. These control methods preserve the FESS State of Charge (SoC) while reducing the Ramp Rate (RR) of BESS. The proposed controller was validated with a commercial 120 kW, 8 kWh high-speed FESS connected to a 400 kVA Egston Power Amplifier.

Further, the thesis introduced a SoC estimation method for supercapacitors based on the Adaptive Square-Root Unscented Kalman Filter (ASR-UKF). This method was successfully adapted and experimentally validated using an Eaton 166F supercapacitor interfaced through a Spitzenberger APS amplifier, and implemented in real-time using Novacor RTDS and Opal-RT simulators. The

results confirmed improved accuracy compared to conventional approaches such as Coulomb Counting and simple capacitive models, confirming improved accuracy over conventional approaches and applicability in HESS contexts.

Accelerated aging experiments further demonstrate the benefits of HESS: batteries integrated within hybrid systems exhibit significantly slower degradation, retaining greater capacity over equivalent operational periods compared to standalone batteries. This translates directly into reduced battery replacement frequency and extended operational lifetimes.

The economic analysis supports these technical gains by showing that, despite higher initial capital costs due to flywheel investment, HESS provides a lower Levelized Cost of Storage (LCOS) over typical 20-year lifespans through fewer battery replacements and reduced downtime. This highlights HESS as a financially attractive option for applications demanding high cycling and reliable energy storage.

In conclusion, this thesis presents a comprehensive and experimentally grounded framework for power management and evaluating HESS. The findings contribute to advancing energy storage technologies that are more durable, efficient, and cost-effective, essential qualities for supporting future resilient and sustainable power grids.

8.2 Outlook

- **Optimal sizing:** While this thesis has demonstrated the benefits of HESS using specific component configurations, the question of optimal sizing remains open. The ratio between high-energy and high-power devices is highly application dependent, and suboptimal sizing can lead to unnecessary investment costs or under-utilization of storage capacity. Future work should focus on optimization frameworks that jointly consider technical constraints, degradation models, economic factors, and grid service requirements to determine the most cost-effective HESS configurations for different use cases, ranging from microgrids to utility-scale storage.
- **Power management considering extended dynamics:** The power management strategies developed in this thesis have successfully reduced battery stress and optimized load sharing, but they primarily focused on SoC, RR, and average power dynamics. In reality, the performance of HESS is also influenced by converter losses, efficiency variations, and thermal dynamics, which were not explicitly included in the control design. Future studies should incorporate these dynamics into the optimization and control framework, ensuring that the HESS not only improves battery lifetime but also minimizes overall system losses and maintains thermal stability during high-demand operation.

- **Exploration of other HESS configurations, such as hydrogen-based systems:** This thesis has concentrated on hybridization of batteries with flywheels and supercapacitors; however, other promising HESS architectures exist. In particular, hydrogen-based HESS (combining batteries with electrolyzers and fuel cells) can provide long-duration energy storage while still supporting fast grid services. Future work should extend the methods developed here, such as PHIL validation, SoC estimation, and aging analysis, to these systems. Such studies would clarify how hybridization with hydrogen can complement high-power-density devices and further enhance the flexibility of renewable-based power systems.
- **Improving high-power-density storage to reduce initial cost:** A key challenge identified in this work is the relatively high capital cost of high-power-density storage technologies such as flywheels and supercapacitors. Although they improve system performance and extend battery lifetime, their cost remains a barrier to large-scale adoption. Future research should therefore investigate technological improvements and material innovations that enhance energy density and reduce production costs of high-power devices.

In summary, while this thesis has established the technical, economic, and experimental foundations for HESS, the future of hybrid storage lies in advancing optimal sizing strategies, integrating extended system dynamics into control frameworks, exploring new architectures such as hydrogen-based hybrids, and reducing the costs of high-power-density devices. Addressing these challenges will not only accelerate the adoption of HESS but also position it as a central enabler of resilient, flexible, and sustainable power systems capable of supporting the global energy transition.

A Appendix

A.1 Kalman Filter (KF)

The standard Kalman Filter is a recursive linear estimator that combines system dynamics with noisy measurements to estimate internal states, such as the supercapacitor SoC. It assumes linear system dynamics and Gaussian noise [334].

System model:

$$x_{k+1} = Ax_k + Bu_k + w_k, \quad w_k \sim \mathcal{N}(0, Q) \tag{A.1}$$

$$y_k = Cx_k + Du_k + v_k, \quad v_k \sim \mathcal{N}(0, R) \tag{A.2}$$

Prediction step:

$$\hat{x}_{k|k-1} = A\hat{x}_{k-1|k-1} + Bu_{k-1} \tag{A.3}$$

$$P_{k|k-1} = AP_{k-1|k-1}A^T + Q \tag{A.4}$$

Update step:

$$K_k = P_{k|k-1}C^T(CP_{k|k-1}C^T + R)^{-1} \tag{A.5}$$

$$\hat{x}_{k|k} = \hat{x}_{k|k-1} + K_k(y_k - C\hat{x}_{k|k-1}) \tag{A.6}$$

$$P_{k|k} = (I - K_kC)P_{k|k-1} \tag{A.7}$$

A.2 Extended Kalman Filter (EKF)

The EKF extends the KF to nonlinear systems by linearizing the system and measurement functions around the current estimate. It is widely used for supercapacitor SoC estimation due to system nonlinearities [335].

Nonlinear system model:

$$x_{k+1} = f(x_k, u_k) + w_k \tag{A.8}$$
$$y_k = h(x_k, u_k) + v_k \tag{A.9}$$

Prediction:

$$\hat{x}_{k|k-1} = f(\hat{x}_{k-1|k-1}, u_{k-1}) \tag{A.10}$$
$$P_{k|k-1} = F_k P_{k-1|k-1} F_k^T + Q \tag{A.11}$$

where $F_k = \frac{\partial f}{\partial x}\big|_{\hat{x}_{k-1|k-1}}$ is the Jacobian of f.

Update:

$$K_k = P_{k|k-1} H_k^T (H_k P_{k|k-1} H_k^T + R)^{-1}, \quad H_k = \frac{\partial h}{\partial x}\big|_{\hat{x}_{k|k-1}} \tag{A.12}$$
$$\hat{x}_{k|k} = \hat{x}_{k|k-1} + K_k(y_k - h(\hat{x}_{k|k-1}, u_k)) \tag{A.13}$$
$$P_{k|k} = (I - K_k H_k) P_{k|k-1} \tag{A.14}$$

A.3 Unscented Kalman Filter (UKF)

The UKF estimates the state of nonlinear systems without linearization. It uses a set of deterministically chosen sigma points to capture the mean and covariance accurately under nonlinear transformations [336].

Sigma point generation and prediction:

$$\chi_{i,k|k-1} = f(\chi_{i,k-1}, u_{k-1}) \tag{A.15}$$
$$\hat{x}_{k|k-1} = \sum_i W_i^m \chi_{i,k|k-1} \tag{A.16}$$
$$P_{k|k-1} = \sum_i W_i^c (\chi_{i,k|k-1} - \hat{x}_{k|k-1})(\chi_{i,k|k-1} - \hat{x}_{k|k-1})^T + Q \tag{A.17}$$

Update: Propagate sigma points through the measurement function $h(\cdot)$ and compute the Kalman gain K_k as in standard KF.

A.4 Square Root UKF (SR-UKF)

The SR-UKF is a numerically stable variant of the UKF that propagates the square root of the covariance matrix, rather than the full covariance. This enhances numerical accuracy and stability, particularly for simulations of long duration [338].

Covariance square root:

$$P = SS^T \tag{A.18}$$

Sigma points are propagated through the nonlinear system, and updates are performed using S via Cholesky or QR decomposition.

A.5 Kalman Filter Particle Filter (KF-PF)

The KF-PF hybrid combines a Kalman Filter for linear parts of the system and a Particle Filter to handle nonlinearities and non-Gaussian noise. Particles are propagated through the nonlinear dynamics, and weights are updated according to measurement likelihood [343].

State estimate:

$$\hat{x}_k = \sum_{i=1}^{N} w_k^{(i)} x_k^{(i)} \tag{A.19}$$

where $x_k^{(i)}$ are particles and $w_k^{(i)}$ their weights, resampled at each step.

A.6 Adaptive Square Root UKF (ASR-UKF)

The ASR-UKF enhances SR-UKF by adapting the process and measurement noise covariances online based on residuals, improving robustness under model uncertainties [339].

Adaptive noise estimation:

$$e_k = y_k - h(\hat{x}_{k|k-1}) \tag{A.20}$$

$$Q_k, R_k \text{ updated using } e_k \tag{A.21}$$

Then the standard SR-UKF prediction and update steps are applied using the adapted Q_k and R_k.

List of Figures

1.1 The table of contents at a glance. 4
2.1 Technical maturity of energy storage systems and their suitability 23
2.2 Diagram of comparison between specific energy, specific power, and discharge time. 24
2.3 Time horizon for power system phenomena and typical discharge times for energy storage systems and the power rating 25
2.4 HESS concept (a) Main power waveform (b) Smoothed waveform (c) High frequency waveform as residual (d) Battery SoH over time, the cases of with and without HESS 27
2.5 HESS connections with Battery Energy Storage System (BESS) and Supercapacitor Energy Storage (SCES) (a) Parallel AC connection, (b) Parallel DC connection, (c) Multi-Port Converter connection, (d) Modular Multi-Level connection. 28
2.6 HESS DC-connections with Battery Energy Storage System (BESS) and Supercapacitor Energy Storage (SCES) (a) Passive connection, (b) Semi-active connection, (c) Multi-Port Converter connection, (d) Active connection. 29
3.1 Power Hardware In the Loop concept 36
3.2 Overview of the 1-MW PHIL setup at KITs EnergyLab. 39
3.3 Five 200 kVA GAMP6 Egston switched-mode power amplifiers (1 MVA in total). 40
3.4 Structure of a high-speed Flywheel Energy Storage System (FESS). 41
3.5 The inside view of the container of the 120 kW high-speed FESS. 42
3.6 Experimental setup for the supercapacitor SoC estimation. 43
3.7 Overview of the internal structure of the power amplifier 44
3.8 EATON XLR-48R6167-R supercapacitor in KIT EnergyLab 45
4.1 Control Strategies with their most common techniques 51
4.2 The basic structure of a fuzzy logic-based controller 53
4.3 Illustration of model predictive control 55
4.4 Flow chart of a typical GA 58
4.5 General HESS management system architecture 63

5.1 Control scheme for HESS including the moving average and fuzzy logic stages . . . 66
5.2 Membership Functions (a) Battery Energy Storage Ramp Rate (b) Flywheel Energy Storage State of Charge (c) Average window of Moving Average . . . 69
5.3 The input power pattern, the filtered signal via moving average, and the resulting difference. . . . 73
5.4 Configuration for prototyping the proposed controller and conducting PHIL simulations using the 120 kW high-speed FESS. . . . 73
5.5 Comparison between reference and hardware-measured power in the flywheel system:(a) Reference and measured power profiles (b) Absolute error between the two signals . . . 75
5.6 Average Window of the moving average . . . 76
5.7 Low-pass filter-based control architecture . . . 76
5.8 Experimental comparison of power in two methods (a) Filter method (b) Fuzzy-Moving average Method . . . 77
5.9 Comparison of the Filter Method and the Fuzzy-Moving average method (a) Flywheel SoC from experimental results (b) Battery ramp rate derived from post-analysis of experimental data . . . 78
5.10 Effect of different membership functions on the ramp rate and the average window (a) Average window between 300 - 900 s (b) Average window between 100 - 1300 s . . . 79
5.11 Comparison of the controller on different power profiles (a) half of the original power profile (b) original power profile (c) twice the original power profile . . . 80
5.12 Comparison of the different cut-off frequency (a) 1.5 mHz (b) 2.5 mHz (c) 3.5 mHZ . . . 81
6.1 Supercapacitor equivalent models: (a) Three-Branch Electric Circuit Model and (b) Generic n-Order Dynamic Equivalent Circuit Model. . . . 90
6.2 Experimental characterization of the supercapacitor: measured current and corresponding terminal voltage during the procedure related to (a) three-branch model and (b) first-order dynamic Equivalent Circuit Model. . . . 94
6.3 Numerical results for SoC estimation: (a) SoC estimation results and (b) errors with respect to the ideal SoC reference. . . . 97
6.4 Experimental setup for the supercapacitor SoC estimation. . . . 98
6.5 Supercapacitor SoC estimation hardware diagram. . . . 99
6.6 Experimental results for real-time SoC estimation: (a) SoC estimation results and (b) errors with respect to the ideal SoC reference. . . . 100

6.7 Experimental results for supercapacitor SoC estimation in a HESS: (a) daily power reference profile in a German MV/LV substation with selected 1-hour window; (b) power profile allocated to the battery; (c) power profile allocated to the supercapacitor. 102
6.8 Experimental results for supercapacitor SoC estimation in a HESS: (a) supercapacitor current scaled to its rated range; (b) SoC estimation results; (c) absolute estimation errors compared to the ideal reference. 103
7.1 Schematic chart of the developed methodology. 107
7.2 Power Hardware in the Loop Setup 107
7.3 Schematic overview of the micro-grid dynamic model integrating HESS Case 1. 108
7.4 The input power profile 109
7.5 Experimental test rig for aging tests on Li-ion cells. 113
7.6 Selected patterns of the input power profile. In detail, the profile with the maximum mean power is represented by the red line, while the profile corresponding to the minimum mean power is depicted by the purple line. The green line indicates the selected pattern corresponding to the case of power crossing zero. 115
7.7 Rainflow cycle counting algorithm: schematic view of the flow chart according to ASTM standard. 117
7.8 cumulative density functions of power ramp rates for BESS (HESS and standalone), FESS, and grid power. The zoomed-in view highlights smoother BESS operation in HESS mode. 120
7.9 BESS SoCs in case of hybrid (orange line) and non-hybrid (blue line) configurations. 121
7.10 Zoomed in BESS SoCs in case of hybrid (orange line) and non-hybrid (blue line) configurations (a) SoC change between 2 and 4 (b) SoC change between 15.5 and 18.5. 122
7.11 BESS SoCs in case of hybrid (blue line) and non-hybrid (red line) configurations. . 124
7.12 (a) Measured state of health for the cells tested according to operating conditions (b) BESS replacement based on end of life on different SoH. 128
7.13 Cumulative Levelized Cost of Storage (LCOS) over 20 years (a) replacement of the battery by 80% of SoH (b) replacement of the battery by 70% of SoH (c) replacement of the battery by 60% of SoH (d) replacement of the battery by 40% of SoH. 130

List of Tables

2.1 Comparison of Battery Energy Storage System (BESS) Types . . . 7
2.2 Comparison of different types of electrical machines used in FESS [62, 75, 76] . . . 14
2.3 Comparison of different bearing technologies used in FESS [76] . . . 15
2.4 Overview of Hydrogen Technologies, Production Pathways, and Fuel Cell/Electrolyzer Types . . . 18
2.5 Characteristics of some Energy Storage Systems [154] . . . 26
2.6 Overview of selected real-world HESS projects . . . 33
3.1 The characteristics of each Egston amplifier at KIT EnergyLab. . . . 40
3.2 Flywheel Energy Storage Parameters . . . 42
3.3 EATON XLR 166F Supercapacitor Specifications . . . 46
4.1 State of the art on hybrid energy storage systems . . . 59
4.2 Key Control Parameters for HESS Management . . . 61
5.1 Fuzzy sets and their linguistic variables . . . 70
5.2 Membership functions sets and their range . . . 70
5.3 Rules of fuzzy logic controller . . . 71
6.1 State of the art on supercapacitor SoC estimation methods . . . 88
6.2 Fitted parameters for the three-branch supercapacitor model . . . 93
6.3 Extracted parameters during **discharge** using PPC procedure for the first-order ECM . . . 95
6.4 Extracted parameters during **charge** using PPC procedure for the first-order ECM . . . 95
7.1 BESS technical features for the considered simulation scenarios. . . . 112
7.2 Key specifications of Samsung INR18650-20R lithium-ion cell (2011 datasheet). . . 113
7.3 Assessment of FESS power losses to emulate real FESS behavior. . . . 119
7.4 Daily cycles obtained by RFC application on Li-ion BESS SoCs for non-hybrid and hybrid cases. . . . 122
7.5 Step cycles for the accelerated test campaign on Li-ion cells in relation to Case 1 and Case 2. . . . 123
7.6 Registered capacity values for the investigated cases. . . . 124
7.7 Capital cost parameters for BESS and FESS . . . 127
7.8 Power and Energy Ratings of Storage Systems . . . 128

7.9 Replacement Intervals for Different SoH Thresholds 128

List of Publications

Journal articles

[J1] D. Fusco, S. Masoome Maroufi, F. Porpora, M. Di Monaco, G. De Carne, and G. Tomasso, "Performance analysis of asr-ukfs for supercapacitor soc estimation in hybrid energy storage systems," *IEEE Journal of Emerging and Selected Topics in Power Electronics*, vol. 12, no. 6, pp. 5602–5612, 2024.

[J2] G. De Carne, S. M. Maroufi, H. Beiranvand, V. De Angelis, S. DArco, V. Gevorgian, S. Waczowicz, B. Mather, M. Liserre, and V. Hagenmeyer, "The role of energy storage systems for a secure energy supply: A comprehensive review of system needs and technology solutions," *Electric Power Systems Research*, vol. 236, p. 110963, 2024. [Online]. Available: https://www.sciencedirect.com/science/article/pii/S0378779624008496

[J3] S. M. Maroufi, S. Karrari, K. Rajashekaraiah, and G. De Carne, "Power management of hybrid flywheel-battery energy storage systems considering the state of charge and power ramp rate," *IEEE Transactions on Power Electronics*, vol. 40, no. 7, pp. 9944–9956, 2025.

[J4] S. M. Maroufi, D. Pelosi, L. Barelli, and G. D. Carne, "Power hardware in the loop-based lifetime assessment of hybrid energy storage systems: A novel realistic approach," *Journal of Energy Storage*, vol. 145, p. 119910, 2026. [Online]. Available: https://www.sciencedirect.com/science/article/pii/S2352152X25046249

Conference contributions

[C1] S. M. Maroufi and G. De Carne, "Optimal design for hybrid energy storage systems considering system aging and costs," in *2023 IEEE 14th International Symposium on Power Electronics for Distributed Generation Systems (PEDG)*, 2023, pp. 496–500.

Book contributions

[B1] G. De Carne, S. M. Maroufi, A. Morandi, and M. Simonazzi, "Power-intensive energy storage systems," in *Hybrid Energy Storage: Case Studies for the Energy Transition*. Springer, 2025, pp. 89–119.

Bibliography

[1] C. Liu and G. Cao, "Fundamentals of rechargeable batteries and electrochemical potentials of electrode materials," in *Nanomaterials for Energy Conversion and Storage*. World Scientific, 2018, pp. 397–451.

[2] X. Tan, Q. Li, and H. Wang, "Advances and trends of energy storage technology in microgrid," *International Journal of Electrical Power and Energy Systems*, vol. 44, p. 179191, 01 2013.

[3] B. C. Melot and J.-M. Tarascon, "Design and preparation of materials for advanced electrochemical storage," *Accounts of chemical research*, vol. 46, no. 5, pp. 1226–1238, 2013.

[4] D. Deng, "Li-ion batteries: basics, progress, and challenges," *Energy Science & Engineering*, vol. 3, no. 5, pp. 385–418, 2015.

[5] Y. Wang, J. Tian, Z. Sun, L. Wang, R. Xu, M. Li, and Z. Chen, "A comprehensive review of battery modeling and state estimation approaches for advanced battery management systems," *Renewable and Sustainable Energy Reviews*, vol. 131, p. 110015, 2020. [Online]. Available: https://www.sciencedirect.com/science/article/pii/S1364032120303063

[6] S. Atcitty, J. Neely, D. Ingersoll, A. Akhil, and K. Waldrip, "Battery energy storage system," in *Power Electronics for Renewable and Distributed Energy Systems: A Sourcebook of Topologies, Control and Integration.* Springer, 2013, pp. 333–366.

[7] Z. Zhao, H. Hu, Z. He, H. H.-C. Iu, P. Davari, and F. Blaabjerg, "Power electronics-based safety enhancement technologies for lithium-ion batteries: An overview from battery management perspective," *IEEE Transactions on Power Electronics*, vol. 38, no. 7, pp. 8922–8955, 2023.

[8] D. Jugović and D. Uskoković, "A review of recent developments in the synthesis procedures of lithium iron phosphate powders," *Journal of Power Sources*, vol. 190, no. 2, pp. 538–544, 2009.

[9] Z. Yang, Y. Dai, S. Wang, and J. Yu, "How to make lithium iron phosphate better: a review exploring classical modification approaches in-depth and proposing future optimization methods," *Journal of Materials Chemistry A*, vol. 4, no. 47, pp. 18 210–18 222, 2016.

[10] A. Nikolian, Y. Firouz, R. Gopalakrishnan, J.-M. Timmermans, N. Omar, P. Van den Bossche, and J. Van Mierlo, "Lithium ion batteriesdevelopment of advanced electrical equivalent circuit models for nickel manganese cobalt lithium-ion," *Energies*, vol. 9, no. 5, p. 360, 2016.

[11] G. Marin-Garcia, G. Vazquez-Guzman, J. Sosa, A. R. Lopez, P. Martinez-Rodriguez, and D. Langarica, "Battery types and electrical models: A review," in *2020 IEEE International Autumn Meeting on Power, Electronics and Computing (ROPEC)*, vol. 4. IEEE, 2020, pp. 1–6.

[12] N. Vangapally, T. R. Penki, Y. Elias, S. Muduli, S. Maddukuri, S. Luski, D. Aurbach, and S. K. Martha, "Lead-acid batteries and lead–carbon hybrid systems: A review," *Journal of Power Sources*, vol. 579, p. 233312, 2023.

[13] A. H. Almarzooqi, M. O. Alhusin, I. P. Nikolakakos, A. Husnain, and H. M. Albeshr, "Improved nas battery state of charge estimation by means of temporal fusion transformer," in *2023 IEEE Texas Power and Energy Conference (TPEC)*. IEEE, 2023, pp. 1–6.

[14] M. Skyllas-Kazacos, M. Chakrabarti, S. Hajimolana, F. Mjalli, and M. Saleem, "Progress in flow battery research and development," *Journal of the electrochemical society*, vol. 158, no. 8, p. R55, 2011.

[15] W. Wang, Q. Luo, B. Li, X. Wei, L. Li, and Z. Yang, "Recent progress in redox flow battery research and development," *Advanced Functional Materials*, vol. 23, no. 8, pp. 970–986, 2013.

[16] F. Lima, J. Ramalho, D. Tavares, J. Duarte, C. Albuquerque, T. Marques, A. Geraldes, A. Casimiro, G. Renkema, J. Been *et al.*, "A novel universal battery charger for nicd, nimh, li-ion and li-polymer," in *ESSCIRC 2004-29th European Solid-State Circuits Conference (IEEE Cat. No. 03EX705)*. IEEE, 2003, pp. 209–212.

[17] J. A. S. Tenório and D. C. R. Espinosa, "Recovery of ni-based alloys from spent nimh batteries," *Journal of Power Sources*, vol. 108, no. 1-2, pp. 70–73, 2002.

[18] Z. Zhou, S. Pugliese, M. Langwasser, and M. Liserre, "Sub-synchronous damping by battery storage system in grid forming control," *IEEE Transactions on Power Electronics (Early Access)*, 2024.

[19] T. Chen, Y. Jin, H. Lv, A. Yang, M. Liu, B. Chen, Y. Xie, and Q. Chen, "Applications of lithium-ion batteries in grid-scale energy storage systems," *Transactions of Tianjin University*, vol. 26, no. 3, pp. 208–217, 2020.

[20] H. C. Hesse, M. Schimpe, D. Kucevic, and A. Jossen, "Lithium-ion battery storage for the grida review of stationary battery storage system design tailored for applications in modern power grids," *Energies*, vol. 10, no. 12, p. 2107, 2017.

[21] S. Agarwal, "Market and technology report: Battery pack for energy storage system," 2023.

[22] S. Wolf and M. Lüken, *Future Battery Market*. Cham: Springer International Publishing, 2024, pp. 103–118.

[23] E. Commission, "Roadmap on advanced materials for batteries," 2021.

[24] A. Poorfakhraei, M. Narimani, and A. Emadi, "A review of multilevel inverter topologies in electric vehicles: Current status and future trends," *IEEE Open Journal of Power Electronics*, vol. 2, pp. 155–170, 2021.

[25] S. Steinhorst, Z. Shao, S. Chakraborty, M. Kauer, S. Li, M. Lukasiewycz, S. Narayanaswamy, M. U. Rafique, and Q. Wang, "Distributed reconfigurable battery system management architectures," in *2016 21st Asia and South Pacific Design Automation Conference (ASP-DAC)*, 2016, pp. 429–434.

[26] T. Pereira, H. Beiranvand, and M. Liserre, "Advanced solid-state-based protection scheme for high-voltage li-ion battery energy storage system," in *PCIM Europe 2023; International Exhibition and Conference for Power Electronics, Intelligent Motion, Renewable Energy and Energy Management*. VDE, 2023, pp. 1–10.

[27] J. Neumann, M. Petranikova, M. Meeus, J. D. Gamarra, R. Younesi, M. Winter, and S. Nowak, "Recycling of lithium-ion batteriescurrent state of the art, circular economy, and next generation recycling," *Advanced energy materials*, vol. 12, no. 17, p. 2102917, 2022.

[28] S. Pelletier, O. Jabali, G. Laporte, and M. Veneroni, "Battery degradation and behaviour for electric vehicles: Review and numerical analyses of several models," *Transportation Research Part B: Methodological*, vol. 103, pp. 158–187, 2017.

[29] X. Han, L. Lu, Y. Zheng, X. Feng, Z. Li, J. Li, and M. Ouyang, "A review on the key issues of the lithium ion battery degradation among the whole life cycle," *ETransportation*, vol. 1, p. 100005, 2019.

[30] J. S. Edge, S. OKane, R. Prosser, N. D. Kirkaldy, A. N. Patel, A. Hales, A. Ghosh, W. Ai, J. Chen, J. Yang *et al.*, "Lithium ion battery degradation: what you need to know," *Physical Chemistry Chemical Physics*, vol. 23, no. 14, pp. 8200–8221, 2021.

[31] K. C. Divya and J. Østergaard, "Battery energy storage technology for power systemsan overview," *Electric power systems research*, vol. 79, no. 4, pp. 511–520, 2009.

[32] S. Nyamathulla and C. Dhanamjayulu, "A review of battery energy storage systems and advanced battery management system for different applications: Challenges and recommendations," *Journal of Energy Storage*, vol. 86, p. 111179, 2024.

[33] J. Weng, Q. Huang, X. Li, G. Zhang, D. Ouyang, M. Chen, A. C. Y. Yuen, A. Li, E. W. M. Lee, W. Yang *et al.*, "Safety issue on pcm-based battery thermal management: material thermal stability and system hazard mitigation," *Energy Storage Materials*, vol. 53, pp. 580–612, 2022.

[34] M. Zhi, R. Fan, X. Yang, L. Zheng, S. Yue, Q. Liu, and Y. He, "Recent research progress on phase change materials for thermal management of lithium-ion batteries," *Journal of Energy Storage*, vol. 45, p. 103694, 2022.

[35] X. Yu and A. Manthiram, "Sustainable battery materials for next-generation electrical energy storage," *Advanced Energy and Sustainability Research*, vol. 2, no. 5, p. 2000102, 2021.

[36] Y. Huang and J. Li, "Key challenges for grid-scale lithium-ion battery energy storage," *Advanced Energy Materials*, vol. 12, no. 48, p. 2202197, 2022.

[37] M. E. Şahin, F. Blaabjerg, and A. Sangwongwanich, "A comprehensive review on supercapacitor applications and developments," *Energies*, vol. 15, no. 3, p. 674, 2022.

[38] V. D. Ivanov, "The helmholtz model," *Journal of Solid State Electrochemistry*, vol. 28, no. 8, pp. 2487–2493, 2024.

[39] H. Wang and L. Pilon, "Accurate simulations of electric double layer capacitance of ultramicroelectrodes," *The Journal of Physical Chemistry C*, vol. 115, no. 33, pp. 16 711–16 719, 2011.

[40] B. K. Kim, S. Sy, A. Yu, and J. Zhang, "Electrochemical supercapacitors for energy storage and conversion," *Handbook of clean energy systems*, pp. 1–25, 2015.

[41] L. Zhang, X. Hu, Z. Wang, F. Sun, and D. G. Dorrell, "A review of supercapacitor modeling, estimation, and applications: A control/management perspective," *Renewable and Sustainable Energy Reviews*, vol. 81, pp. 1868–1878, 2018. [Online]. Available: https://www.sciencedirect.com/science/article/pii/S1364032117309292

[42] W. Zuo, R. Li, C. Zhou, Y. Li, J. Xia, and J. Liu, "Battery-supercapacitor hybrid devices: recent progress and future prospects," *Advanced science*, vol. 4, no. 7, p. 1600539, 2017.

[43] L. Liu, H. Zhao, and Y. Lei, "Review on nanoarchitectured current collectors for pseudocapacitors," *Small Methods*, vol. 3, no. 8, p. 1800341, 2019.

[44] N. R. Chodankar, H. D. Pham, A. K. Nanjundan, J. F. Fernando, K. Jayaramulu, D. Golberg, Y.-K. Han, and D. P. Dubal, "True meaning of pseudocapacitors and their performance metrics: asymmetric versus hybrid supercapacitors," *Small*, vol. 16, no. 37, p. 2002806, 2020.

[45] T. Prasankumar, J. Jose, S. Jose, and S. P. Balakrishnan, "Pseudocapacitors," in *Supercapacitors for the Next Generation*. IntechOpen, 2021.

[46] M. Soltani and S. H. Beheshti, "A comprehensive review of lithium ion capacitor: development, modelling, thermal management and applications," *Journal of Energy Storage*, vol. 34, p. 102019, 2021. [Online]. Available: https://www.sciencedirect.com/science/article/pii/S2352152X20318545

[47] A. Sengupta, T. Pereira, and M. Liserre, "Optimal design of supercapacitor stacks for size-critical applications," in *2024 IEEE Applied Power Electronics Conference and Exposition (APEC)*, 2024, pp. 977–983.

[48] F. Naseri, S. Karimi, E. Farjah, and E. Schaltz, "Supercapacitor management system: A comprehensive review of modeling, estimation, balancing, and protection techniques," *Renewable and Sustainable Energy Reviews*, vol. 155, p. 111913, 2022.

[49] A. Cano, P. Arévalo, D. Benavides, and F. Jurado, "Comparative analysis of hess (battery/supercapacitor) for power smoothing of pv/hkt, simulation and experimental analysis," *Journal of Power Sources*, vol. 549, p. 232137, 2022.

[50] R. Powade and Y. Bhateshvar, "Design of semi-actively controlled battery-supercapacitor hybrid energy storage system," *Materials Today: Proceedings*, vol. 72, pp. 1503–1509, 2023.

[51] C. Abbey and G. Joos, "Supercapacitor energy storage for wind energy applications," *IEEE transactions on Industry applications*, vol. 43, no. 3, pp. 769–776, 2007.

[52] P. Harrop, "Supercapacitor markets, technology roadmap, opportunities 2021-2041," 2021.

[53] M. Xia, J. Nie, Z. Zhang, X. Lu, and Z. L. Wang, "Suppressing self-discharge of supercapacitors via electrorheological effect of liquid crystals," *Nano Energy*, vol. 47, pp. 43–50, 2018.

[54] F. Jiang, Z. Meng, H. Li, H. Liao, Y. Jiao, M. Han, J. Peng, and Z. Huang, "Consensus-based cell balancing of reconfigurable supercapacitors," *IEEE Transactions on Industry Applications*, vol. 56, no. 4, pp. 4146–4154, 2020.

[55] M. E. Amiryar and K. R. Pullen, "A review of flywheel energy storage system technologies and their applications," *Applied Sciences*, vol. 7, no. 3, p. 286, 2017.

[56] S. Karrari, M. Noe, and J. Geisbuesch, "Real-time simulation of high-speed flywheel energy storage system (fess) for distribution networks," in *Proceedings of the Ninth International Conference on Future Energy Systems*, 2018, pp. 388–390.

[57] A. K. Arani, H. Karami, G. Gharehpetian, and M. Hejazi, "Review of flywheel energy storage systems structures and applications in power systems and microgrids," *Renewable and Sustainable Energy Reviews*, vol. 69, pp. 9–18, 2017. [Online]. Available: https://www.sciencedirect.com/science/article/pii/S1364032116309054

[58] L. Barelli, G. Bidini, F. Bonucci, L. Castellini, S. Castellini, A. Ottaviano, D. Pelosi, and A. Zuccari, "Dynamic analysis of a hybrid energy storage system (h-ess) coupled to a photovoltaic (pv) plant," *Energies*, vol. 11, no. 2, 2018. [Online]. Available: https://www.mdpi.com/1996-1073/11/2/396

[59] H. d. Jong and K. Williams, "Development and simulation of a flywheel-based energy storage system on a clamshell dredge," *Westerndredging.Org*, pp. 1401–1414.

[60] [Online]. Available: https://www.siemens-energy.com/global/en/home/stories/killingholme-rotating-grid-stabilizer-conversion.html

[61] [Online]. Available: https://www.stornetic.com/

[62] R. Peña-Alzola, R. Sebastian, J. Quesada, and A. Colmenar, "Review of flywheel based energy storage systems," 05 2011, pp. 1–6.

[63] R. Sebastian and R. Peña-Alzola, "Flywheel energy storage systems: Review and simulation for an isolated wind power system," *Renewable and Sustainable Energy Reviews*, vol. 16, pp. 6803 – 6813, 12 2012.

[64] X. Li, A. Palazzolo, Z. Wang, and H. Toliyat, "A utility scale flywheel energy storage system with a shaftless, hubless, high strength steel rotor," *IEEE Transactions on Industrial Electronics*, vol. 65, pp. 6667 – 6675, 08 2018.

[65] B. Bolund, H. Bernhoff, and M. Leijon, "Flywheel energy and power storage systems," *Renewable and Sustainable Energy Reviews*, vol. 11, no. 2, pp. 235–258, 2007. [Online]. Available: https://www.sciencedirect.com/science/article/pii/S1364032105000146

[66] J. Zhang, Y. Wang, G. Liu, and G. Tian, "A review of control strategies for flywheel energy storage system and a case study with matrix converter," *Energy Reports*, vol. 8, pp. 3948–3963, 2022. [Online]. Available: https://www.sciencedirect.com/science/article/pii/S2352484722005649

[67] R. H. Richman, "Flywheel energy storage," Palo Alto, California, Tech. Rep., 1997.

[68] (2020) The next frontier in energy storage | amber kinetics. [Accessed: 20-Nov-2020]. [Online]. Available: https://www.amberkinetics.com/product/

[69] L. Jiang and C. W. Wu, "Shape optimization of energy storage flywheel rotor," *Structural and Multidisciplinary Optimization*, vol. 55, pp. 739–750, 2016.

[70] P. C. Krause, O. Wasynczuk, S. D. Sudhoff, and S. Pekarek, *Analysis of Electric Machinery and Drive Systems*, 3rd ed. Hoboken, New Jersey: Wiley-IEEE Press, 2010.

[71] L. Uri and M. Nemec, "Permanent magnet synchronous machine demagnetisation prevention and torque estimation control considering rotor temperature," *IET Power Electronics*, vol. 12, no. 9, pp. 2161–2169, 2019.

[72] C. Y. Ho, J. C. Wang, K. W. Hu, and C. M. Liaw, "Development and operation control of a switched-reluctance motor driven flywheel," *IEEE Transactions on Power Electronics*, vol. 34, no. 1, pp. 526–537, 2019.

[73] S. J. Amodeo, H. G. Chiacchiarini, J. A. Solsona, and C. A. Busada, "High-performance sensorless nonlinear power control of a flywheel energy storage system," *Energy Conversion and Management*, vol. 50, no. 7, pp. 1722–1729, 2009.

[74] S. Nagaya, N. Hirano, T. Katagiri, T. Tamada, K. Shikimachi, Y. Iwatani, F. Saito, and Y. Ishii, "The state of the art of the development of smes for bridging instantaneous voltage dips in japan," *Cryogenics*, vol. 52, no. 12, pp. 708–712, 2012, special Issue: ACASC 2011.

[75] S. Koohi-Kamali, V. Tyagi, N. Rahim, N. Panwar, and H. Mokhlis, "Emergence of energy storage technologies as the solution for reliable operation of smart power systems: A review," *Renewable and Sustainable Energy Reviews*, vol. 25, pp. 135–165, 2013. [Online]. Available: https://www.sciencedirect.com/science/article/pii/S1364032113002153

[76] S. Karrari, *A Flywheel Energy Storage System (FESS) for Low Voltage Distribution Grids: Modeling, Simulation and Power Hardware-in-the-Loop Testing*. Karlsruhe: KIT Scientific Publishing, 2023, collection: AG Universitätsverlage. Classification: Electrical engineering. [Online]. Available: https://library.oapen.org/handle/20.500.12657/60864

[77] A. K. Arani, H. Karami, G. Gharehpetian, and M. Hejazi, "Review of Flywheel Energy Storage Systems structures and applications in power systems and microgrids," *Renewable and Sustainable Energy Reviews*, vol. 69, no. C, pp. 9–18, 2017. [Online]. Available: https://ideas.repec.org/a/eee/rensus/v69y2017icp9-18.html

[78] G. Suvire, M. Molina, and P. Mercado, "Improving the integration of wind power generation into ac microgrids using flywheel energy storage," *Smart Grid, IEEE Transactions on*, vol. 3, pp. 1945–1954, 12 2012.

[79] B. Wang and G. Venkataramanan, "Dynamic voltage restorer utilizing a matrix converter and flywheel energy storage," *IEEE Transactions on Industry Applications*, vol. 45, pp. 222–231, 01 2009.

[80] S. J. Amodeo, H. G. Chiacchiarini, and A. R. Oliva, "High-performance control of a dcdc z-source converter used for an excitation field driver," *IEEE Transactions on Power Electronics*, vol. 27, no. 6, pp. 2947–2957, 2012.

[81] W. Santiago, "Inverter output filter effect on pwm motor drives of a flywheel energy storage system," 10 2004.

[82] A. De Bernardinis, R. Lallemand, and A. Kolli, "Highly efficient three-phase bi-directional sic dcac inverter for electric vehicle flywheel emulator," *Energies*, vol. 16, no. 12, 2023. [Online]. Available: https://www.mdpi.com/1996-1073/16/12/4644

[83] K. Mongird, V. Viswanathan, P. Balducci, J. Alam, V. Fotedar, V. Koritarov, and B. Hadjerioua, "An evaluation of energy storage cost and performance characteristics," *Energies*, vol. 13, p. 3307, 06 2020.

[84] M. Strasik, P. E. Johnson, A. C. Day, J. Mittleider, M. D. Higgins, J. Edwards, J. R. Schindler, K. E. McCrary, C. R. McIver, D. Carlson, J. F. Gonder, and J. R. Hull, "Design, fabrication, and test of a 5-kwh/100-kw flywheel energy storage utilizing a high-temperature superconducting bearing," *IEEE Transactions on Applied Superconductivity*, vol. 17, no. 2, pp. 2133–2137, 2007.

[85] M. Komori and N. Akinaga, "A prototype of flywheel energy storage system suppressed by hybrid magnetic bearings with h/sup /spl infin// controller," *IEEE Transactions on Applied Superconductivity*, vol. 11, no. 1, pp. 1733–1736, 2001.

[86] T. Mulcahy, J. Hull, K. Uherka, R. Abboud, and J. Juna, "Test results of 2-kwh flywheel using passive pm and hts bearings," *IEEE Transactions on Applied Superconductivity*, vol. 11, no. 1, pp. 1729–1732, 2001.

[87] F. Werfel, U. Floegel-Delor, T. Riedel, R. Rothfeld, D. Wippich, and B. Goebel, "Encapsulated hts bearings: technical and cost considerations," *IEEE Transactions on Applied Superconductivity*, vol. 15, no. 2, pp. 2306–2311, 2005.

[88] A. D. Sapowith and W. E. Handy, "Composite-flywheel burst-containment study," Lawrence Livermore National Laboratory, Livermore, CA, Tech. Rep., 1982.

[89] M. S. Mahdavi, G. B. Gharehpetian, and H. A. Moghaddam, "Enhanced frequency control method for microgrid-connected flywheel energy storage system," *IEEE Systems Journal*, vol. 15, no. 3, pp. 4503–4513, 2021.

[90] H. García-Pereira, M. Blanco, G. Martínez-Lucas, J. I. Pérez-Díaz, and J.-I. Sarasúa, "Comparison and influence of flywheels energy storage system control schemes in the frequency regulation of isolated power systems," *IEEE Access*, vol. 10, pp. 37 892–37 911, 2022.

[91] H. H. Abdeltawab and Y. A.-R. I. Mohamed, "Robust energy management of a hybrid wind and flywheel energy storage system considering flywheel power losses minimization and grid-code constraints," *IEEE Transactions on Industrial Electronics*, vol. 63, no. 7, pp. 4242–4254, 2016.

[92] N. S. Gayathri, N. Senroy, and I. N. Kar, "Smoothing of wind power using flywheel energy storage system," *IET Renewable Power Generation*, vol. 11, no. 3, pp. 289–298, 2017.

[93] G. Wang, M. Ciobotaru, and V. G. Agelidis, "Power smoothing of large solar pv plant using hybrid energy storage," *IEEE Transactions on Sustainable Energy*, vol. 5, no. 3, pp. 834–842, 2014.

[94] A. Awad, I. Tumar, M. Hussein, W. Ghanem *et al.*, "Pv output power smoothing using flywheel storage system," in *2017 IEEE International Conference on Environment and Electrical Engineering and 2017 IEEE Industrial and Commercial Power Systems Europe (EEEIC/I&CPS Europe)*. IEEE, 2017, pp. 1–6.

[95] P. Mouratidis, B. Schüler, and S. Rinderknecht, "Hybrid energy storage system consisting of a flywheel and a lithium-ion battery for the provision of primary control reserve," in *2019 8th International Conference on Renewable Energy Research and Applications (ICRERA)*, 2019, pp. 94–99.

[96] F. Goris and E. L. Severson, "A review of flywheel energy storage systems for grid application," in *IECON 2018 - 44th Annual Conference of the IEEE Industrial Electronics Society*, 2018, pp. 1633–1639.

[97] M. E. Amiryar and K. R. Pullen, "A review of flywheel energy storage system technologies and their applications," *Applied Sciences*, vol. 7, no. 3, 2017. [Online]. Available: https://www.mdpi.com/2076-3417/7/3/286

[98] S. Wicki and E. G. Hansen, "Clean energy storage technology in the making: An innovation systems perspective on flywheel energy storage," *Journal of cleaner production*, vol. 162, pp. 1118–1134, 2017.

[99] F. Goris and E. L. Severson, "A review of flywheel energy storage systems for grid application," in *IECON 2018-44th Annual Conference of the IEEE Industrial Electronics Society*. IEEE, 2018, pp. 1633–1639.

[100] X. Li and A. Palazzolo, "A review of flywheel energy storage systems: state of the art and opportunities," *Journal of Energy Storage*, vol. 46, p. 103576, 2022. [Online]. Available: https://www.sciencedirect.com/science/article/pii/S2352152X2101255X

[101] S. Choudhury, "Flywheel energy storage systems: A critical review on technologies, applications, and future prospects," *International transactions on electrical energy systems*, vol. 31, no. 9, p. e13024, 2021.

[102] E. Wolf, "Large-scale hydrogen energy storage," in *Electrochemical energy storage for renewable sources and grid balancing*. Elsevier, 2015, pp. 129–142.

[103] K. Ham, S. Bae, and J. Lee, "Classification and technical target of water electrolysis hydrogen production," *Journal of Energy Chemistry*, 2024.

[104] T. B. Nkwanyana, M. W. Siti, Z. Wang, I. Toudjeu, N. T. Mbungu, and W. Mulumba, "An assessment of hybrid-energy storage systems in the renewable environments," *Journal of Energy Storage*, vol. 72, p. 108307, 2023.

[105] R. Taccani, S. Malabotti, C. DallArmi, and D. Micheli, "High energy density storage of gaseous marine fuels: An innovative concept and its application to a hydrogen powered ferry," *International Shipbuilding Progress*, vol. 67, no. 1, pp. 33–56, 2020.

[106] N. P. Brandon and Z. Kurban, "Clean energy and the hydrogen economy," *Philosophical Transactions of the Royal Society A: Mathematical, Physical and Engineering Sciences*, vol. 375, no. 2098, p. 20160400, 2017.

[107] M. El-Shafie, S. Kambara, and Y. Hayakawa, "Hydrogen production technologies overview," 2019.

[108] S. Banerjee, M. N. Musa, and A. B. Jaafar, "Economic assessment and prospect of hydrogen generated by otec as future fuel," *international journal of hydrogen energy*, vol. 42, no. 1, pp. 26–37, 2017.

[109] G. Maggio, A. Nicita, and G. Squadrito, "How the hydrogen production from res could change energy and fuel markets: A review of recent literature," *International journal of hydrogen energy*, vol. 44, no. 23, pp. 11 371–11 384, 2019.

[110] H. Lee, B. Lee, M. Byun, and H. Lim, "Comparative techno-economic analysis for steam methane reforming in a sorption-enhanced membrane reactor: Simultaneous h2 production and co2 capture," *Chemical Engineering Research and Design*, vol. 171, pp. 383–394, 2021.

[111] L. Valverde-Isorna, D. Ali, D. Hogg, and M. Abdel-Wahab, "Modelling the performance of wind–hydrogen energy systems: Case study the hydrogen office in scotland/uk," *Renewable and sustainable energy reviews*, vol. 53, pp. 1313–1332, 2016.

[112] D. Parra, G. S. Walker, and M. Gillott, "Modeling of pv generation, battery and hydrogen storage to investigate the benefits of energy storage for single dwelling," *Sustainable Cities and Society*, vol. 10, pp. 1–10, 2014.

[113] J. Garcia-Navarro, M. A. Isaacs, M. Favaro, D. Ren, W.-J. Ong, M. Grätzel, and P. Jiménez-Calvo, "Updates on hydrogen value chain: A strategic roadmap," *Global Challenges*, p. 2300073, 2023.

[114] L. Jesus, R. Castro, and A. S. Lopes, "Hydrogen-based solutions to help the electrical grid management: Application to the terceira island case," *International Journal of Hydrogen Energy*, vol. 48, no. 4, pp. 1514–1532, 2023.

[115] R. Cozzolino and G. Bella, "A review of electrolyzer-based systems providing grid ancillary services: current status, market, challenges and future directions," *Frontiers in Energy Research*, vol. 12, p. 1358333, 2024.

[116] M. Rasul, M. Hazrat, M. Sattar, M. Jahirul, and M. Shearer, "The future of hydrogen: Challenges on production, storage and applications," *Energy Conversion and Management*, vol. 272, p. 116326, 2022.

[117] E. Ghirardi, G. Brumana, G. Franchini, and A. Perdichizzi, "H2 contribution to power grid stability in high renewable penetration scenarios," *International Journal of Hydrogen Energy*, vol. 48, no. 32, pp. 11 956–11 969, 2023.

[118] A. Wang, J. Jens, D. Mavins, M. Moultak, M. Schimmel, K. van der Leun, D. Peters, M. Buseman *et al.*, "Analysing future demand, supply, and transport of hydrogen," 2021.

[119] I. Rolo, V. A. Costa, and F. P. Brito, "Hydrogen-based energy systems: current technology development status, opportunities and challenges," *Energies*, vol. 17, no. 1, p. 180, 2023.

[120] S. M. Mahmoudi, A. Maleki, and D. R. Ochbelagh, "Techno-economic assessment of hydrogen-based energy storage systems in determining the optimal configuration of the nuclear-renewable hybrid energy system," *Energy Reports*, vol. 11, pp. 4713–4725, 2024.

[121] M. Shatnawi, N. Al Qaydi, N. Aljaberi, and M. Aljaberi, "Hydrogen-based energy storage systems: A review," in *2018 7th International Conference on Renewable Energy Research and Applications (ICRERA)*. IEEE, 2018, pp. 697–700.

[122] V. S. Vulusala G and S. Madichetty, "Application of superconducting magnetic energy storage in electrical power and energy systems: a review," *International Journal of Energy Research*, vol. 42, no. 2, pp. 358–368, 2018.

[123] X. Luo, J. Wang, M. Dooner, and J. Clarke, "Overview of current development in electrical energy storage technologies and the application potential in power system operation," *Applied Energy*, vol. 137, pp. 511–536, 2015. [Online]. Available: https://www.sciencedirect.com/science/article/pii/S0306261914010290

[124] N. Koshizuka, F. Ishikawa, H. Nasu, M. Murakami, K. Matsunaga, S. Saito, O. Saito, Y. Nakamura, H. Yamamoto, R. Takahata, Y. Itoh, H. Ikezawa, and M. Tomita, "Progress of superconducting bearing technologies for flywheel energy storage systems," *Physica C: Superconductivity*, vol. 386, pp. 444–450, 2003, proceedings of the topical conference of the International Cryogenic Materials Conference (ICMC 2002). Superconductors for Practical Applications. [Online]. Available: https://www.sciencedirect.com/science/article/pii/S0921453402022062

[125] A. Morandi, B. Gholizad, and M. Fabbri, "Design and performance of a 1 mw-5 s high temperature superconductor magnetic energy storage system," *Superconductor Science and Technology*, vol. 29, no. 1, p. 015014, 2015.

[126] S. Schoenung, W. Meier, R. Fagaly, M. Heiberger, R. Stephens, J. Leuer, and R. Guzman, "Design, performance, and cost characteristics of high temperature superconducting magnetic energy storage," *IEEE Transactions on Energy Conversion*, vol. 8, no. 1, pp. 33–39, 1993.

[127] S. Suzuki, J. Baba, K. Shutoh, and E. Masada, "Effective application of superconducting magnetic energy storage (smes) to load leveling for high speed transportation system," *IEEE Transactions on Applied Superconductivity*, vol. 14, no. 2, pp. 713–716, 2004.

[128] C.-S. Hsu and W.-J. Lee, "Superconducting magnetic energy storage for power system applications," *IEEE Transactions on industry applications*, vol. 29, no. 5, pp. 990–996, 1993.

[129] X. Xue, K. W. E. Cheng, and D. Sutanto, "Power system applications of superconducting magnetic energy storage systems," in *Fourtieth IAS Annual Meeting. Conference Record of the 2005 Industry Applications Conference, 2005.*, vol. 2. IEEE, 2005, pp. 1524–1529.

[130] S. Nagaya, N. Hirano, T. Katagiri, T. Tamada, K. Shikimachi, Y. Iwatani, F. Saito, and Y. Ishii, "The state of the art of the development of smes for bridging instantaneous voltage dips in japan," *Cryogenics*, vol. 52, no. 12, pp. 708–712, 2012, special Issue: ACASC 2011. [Online]. Available: https://www.sciencedirect.com/science/article/pii/S0011227512000859

[131] V. J. Lyons, G. A. Gonzalez, M. G. Houts, C. J. Iannello, J. H. Scott, and S. Surampudi, "Space power and energy storage roadmap," *NASA, Tech. Rep.*, 2012.

[132] M. Bortolotti, "European energy storage technology development roadmap 2017 update," *EASE and EERA*, 2017.

[133] B. G. Marchionini, Y. Yamada, L. Martini, and H. Ohsaki, "High-temperature superconductivity: a roadmap for electric power sector applications, 2015–2030," *IEEE Transactions on Applied Superconductivity*, vol. 27, no. 4, pp. 1–7, 2017.

[134] B. B. Adetokun, O. Oghorada, and S. J. Abubakar, "Superconducting magnetic energy storage systems: Prospects and challenges for renewable energy applications," *Journal of Energy Storage*, vol. 55, p. 105663, 2022. [Online]. Available: https://www.sciencedirect.com/science/article/pii/S2352152X22016516

[135] U. Bhunia, S. Saha, and A. Chakrabarti, "Design optimization of superconducting magnetic energy storage coil," *Physica C: Superconductivity*, vol. 500, pp. 25–32, 2014. [Online]. Available: https://www.sciencedirect.com/science/article/pii/S0921453414000483

[136] A. Colmenar-Santos, E.-L. Molina-Ibáñez, E. Rosales-Asensio, and J.-J. Blanes-Peiró, "Legislative and economic aspects for the inclusion of energy reserve by a superconducting magnetic energy storage: Application to the case of the spanish electrical system," *Renewable and Sustainable Energy Reviews*, vol. 82, pp. 2455–2470, 2018.

[137] S. Nomura, T. Shintomi, S. Akita, T. Nitta, R. Shimada, and S. Meguro, "Technical and cost evaluation on smes for electric power compensation," *IEEE Transactions on Applied Superconductivity*, vol. 20, no. 3, pp. 1373–1378, 2010.

[138] A. Blakers, M. Stocks, B. Lu, and C. Cheng, "A review of pumped hydro energy storage," *Progress in Energy*, vol. 3, no. 2, p. 022003, 2021.

[139] E. Barbour, I. G. Wilson, J. Radcliffe, Y. Ding, and Y. Li, "A review of pumped hydro energy storage development in significant international electricity markets," *Renewable and sustainable energy reviews*, vol. 61, pp. 421–432, 2016.

[140] C.-J. Yang and R. B. Jackson, "Opportunities and barriers to pumped-hydro energy storage in the united states," *Renewable and Sustainable Energy Reviews*, vol. 15, no. 1, pp. 839–844, 2011. [Online]. Available: https://www.sciencedirect.com/science/article/pii/S1364032110003072

[141] J. Menéndez, J. Loredo, J. M. Fernandez, and M. Galdo, "Underground pumped-storage hydro power plants with mine water in abandoned coal mines," in *Proceedings of the IMWA 13th international congress*, vol. 1. Lappeenranta, Finland, 2017, pp. 6–13.

[142] F. Winde, F. Kaiser, and E. Erasmus, "Exploring the use of deep level gold mines in south africa for underground pumped hydroelectric energy storage schemes," *Renewable and Sustainable Energy Reviews*, vol. 78, pp. 668–682, 2017.

[143] M. Gimeno-Gutierrez and R. Lacal-Arantegui, "Assessment of the european potential for pumped hydropower energy storage based on two existing reservoirs," *Renewable Energy*, vol. 75, pp. 856–868, 2015. [Online]. Available: https://www.sciencedirect.com/science/article/pii/S096014811400706X

[144] T. Hino and A. Lejeune, "Pumped storage hydropower developments," 2012.

[145] A. Mitteregger and G. Penninger, "Austrian pumped storage power stations supply peak demands," *World Pumps*, vol. 2008, no. 500, pp. 16–21, 2008.

[146] M. Nazari, M. Ardehali, and S. Jafari, "Pumped-storage unit commitment with considerations for energy demand, economics, and environmental constraints," *Energy*, vol. 35, no. 10, pp. 4092–4101, 2010.

[147] M. R. N. Vilanova, A. T. Flores, and J. A. P. Balestieri, "Pumped hydro storage plants: a review," *Journal of the Brazilian Society of Mechanical Sciences and Engineering*, vol. 42, no. 8, p. 415, 2020.

[148] M. S. Javed, T. Ma, J. Jurasz, and M. Y. Amin, "Solar and wind power generation systems with pumped hydro storage: Review and future perspectives," *Renewable Energy*, vol. 148, pp. 176–192, 2020. [Online]. Available: https://www.sciencedirect.com/science/article/pii/S0960148119318592

[149] H. L. Ferreira, R. Garde, G. Fulli, W. Kling, and J. P. Lopes, "Characterisation of electrical energy storage technologies," *Energy*, vol. 53, pp. 288–298, 2013.

[150] K. Kumaraswamy and J. Cotrone, "Evaluating the regulation market maturity for energy storage devices," *The Electricity Journal*, vol. 26, no. 10, pp. 75–83, 2013.

[151] H. Chen, T. N. Cong, W. Yang, C. Tan, Y. Li, and Y. Ding, "Progress in electrical energy storage system: A critical review," *Progress in Natural Science*, vol. 19, no. 3, pp. 291–312, 2009. [Online]. Available: https://www.sciencedirect.com/science/article/pii/S100200710800381X

[152] S. Sahoo and P. Timmann, "Energy storage technologies for modern power systems: A detailed analysis of functionalities, potentials, and impacts," *IEEE Access*, vol. 11, pp. 49 689–49 729, 2023.

[153] P. Munuera-Mínguez, R. Rocca, K. N. Malamaki, M. Zafeiropulou, N. Apostolidou, and D. Martínez-López, "Maturity assessment of grid-scale flexibility and energy storage services towards a decarbonized europe," *Open Research Europe*, vol. 4, no. 196, p. 196, 2024.

[154] G. De Carne, S. M. Maroufi, H. Beiranvand, V. De Angelis, S. DArco, V. Gevorgian, S. Waczowicz, B. Mather, M. Liserre, and V. Hagenmeyer, "The role of energy storage systems for a secure energy supply: A comprehensive review of system needs and technology solutions," *Electric Power Systems Research*, vol. 236, p. 110963, 2024.

[155] X. Hu, C. Zou, C. Zhang, and Y. Li, "Technological developments in batteries: A survey of principal roles, types, and management needs," *IEEE Power and Energy Magazine*, vol. 15, no. 5, pp. 20–31, 2017.

[156] F. Milano and Á. O. Manjavacas, *Converter-interfaced Energy Storage Systems: Need for energy storage; 2. Technical and economic aspects; 3. Energy storage technologies; Part II. Modelling: 4. Power system model; 5. Voltage-sourced converter model; 6. Energy storage system models; Part III. Dynamic Analysis: 7. Comparison of dynamic models; 8. Control techniques; 9. Stability analysis; Part IV. Appendices*. Cambridge University Press, 2019.

[157] I. Hadjipaschalis, A. Poullikkas, and V. Efthimiou, "Overview of current and future energy storage technologies for electric power applications," *Renewable and Sustainable Energy Reviews*, vol. 13, no. 6, pp. 1513–1522, 2009. [Online]. Available: https://www.sciencedirect.com/science/article/pii/S1364032108001664

[158] M. E. Amiryar, K. R. Pullen, and D. Nankoo, "Development of a high-fidelity model for an electrically driven energy storage flywheel suitable for small scale residential applications," *Applied Sciences*, vol. 8, no. 3, p. 453, 2018. [Online]. Available: https://www.mdpi.com/2076-3417/8/3/453

[159] K. Xu, Y. Guo, G. Lei, and J. Zhu, "A review of flywheel energy storage system technologies," *Energies*, vol. 16, no. 18, 2023. [Online]. Available: https://www.mdpi.com/1996-1073/16/18/6462

[160] B. Zakeri and S. Syri, "Electrical energy storage systems: A comparative life cycle cost analysis," *Renewable and Sustainable Energy Reviews*, vol. 42, pp. 569–596, 2015. [Online]. Available: https://www.sciencedirect.com/science/article/pii/S1364032114008284

[161] H. Behabtu, M. Messagie, T. Coosemans, M. Berecibar, K. Fante, A. Alem, and J. Van Mierlo, "A review of energy storage technologies' application potentials in renewable energy sources grid integration," *Sustainability*, vol. 12, p. 10511, 12 2020.

[162] A. Khaligh and Z. Li, "Battery, ultracapacitor, fuel cell, and hybrid energy storage systems for electric, hybrid electric, fuel cell, and plug-in hybrid electric vehicles: State of the art," *IEEE Transactions on Vehicular Technology*, vol. 59, no. 6, pp. 2806–2814, 2010.

[163] P. Mukherjee and V. Rao, "Design and development of high temperature superconducting magnetic energy storage for power applications - a review," *Physica C: Superconductivity and its Applications*, vol. 563, pp. 67–73, 2019. [Online]. Available: https://www.sciencedirect.com/science/article/pii/S0921453419301066

[164] F. A. Diawuo, E. O. Antwi, and R. T. Amanor, "Chapter 3 - characteristic features of pumped hydro energy storage systems," in *Pumped Hydro Energy Storage for Hybrid Systems*, A. T. Kabo-Bah, F. A. Diawuo, and E. O. Antwi, Eds. Academic Press, 2023, pp. 43–59. [Online]. Available: https://www.sciencedirect.com/science/article/pii/B9780128188538000066

[165] G. G. Farivar, W. Manalastas, H. D. Tafti, S. Ceballos, A. Sanchez-Ruiz, E. C. Lovell, G. Konstantinou, C. D. Townsend, M. Srinivasan, and J. Pou, "Grid-connected energy storage systems: State-of-the-art and emerging technologies," *Proceedings of the IEEE*, vol. 111, no. 4, pp. 397–420, 2023.

[166] Y. Liu, X. Han, Z. Xing, P. Li, H. Liu, and Z. Jiang, "Research on control strategy of hybrid superconducting energy storage based on reinforcement learning algorithm," *IEEE Transactions on Applied Superconductivity*, vol. 34, no. 8, pp. 1–4, 2024.

[167] J. Zhu, M. Qiu, B. Wei, H. Zhang, X. Lai, and W. Yuan, "Design, dynamic simulation and construction of a hybrid hts smes for chinese power grid," *Energy, Available online*, vol. 10, 2012.

[168] T. S. Babu, K. R. Vasudevan, V. K. Ramachandaramurthy, S. B. Sani, S. Chemud, and R. M. Lajim, "A comprehensive review of hybrid energy storage systems: Converter topologies, control strategies and future prospects," *IEEE Access*, vol. 8, pp. 148 702–148 721, 2020.

[169] C. Jia, J. Cui, W. Qiao, and L. Qu, "Real-time model predictive control for battery-supercapacitor hybrid energy storage systems using linear parameter-varying models," *IEEE Journal of Emerging and Selected Topics in Power Electronics*, vol. 11, no. 1, pp. 251–263, 2023.

[170] L. Sun, K. Feng, C. Chapman, and N. Zhang, "An adaptive power-split strategy for batterysupercapacitor powertraindesign, simulation, and experiment," *IEEE Transactions on Power Electronics*, vol. 32, no. 12, pp. 9364–9375, 2017.

[171] X. Li, R. Ma, N. Yan, S. Wang, and D. Hui, "Research on optimal scheduling method of hybrid energy storage system considering health state of echelon-use lithium-ion battery," *IEEE Transactions on Applied Superconductivity*, vol. 31, no. 8, pp. 1–4, 2021.

[172] S. Bobba, F. Mathieux, F. Ardente, G. A. Blengini, M. A. Cusenza, A. Podias, and A. Pfrang, "Life cycle assessment of repurposed electric vehicle batteries: an adapted method based on modelling energy flows," *Journal of Energy Storage*, vol. 19, pp. 213–225, 2018.

[173] L. Ahmadi, A. Yip, M. Fowler, S. B. Young, and R. A. Fraser, "Environmental feasibility of re-use of electric vehicle batteries," *Sustainable Energy Technologies and Assessments*, vol. 6, pp. 64–74, 2014.

[174] R. Li, L. Bao, L. Chen, C. Zha, J. Dong, N. Qi, R. Tang, Y. Lu, M. Wang, R. Huang, K. Yan, Y. Su, and F. Wu, "Accelerated aging of lithium-ion batteries: bridging battery aging analysis and operational lifetime prediction," *Science Bulletin*, vol. 68, no. 23, pp. 3055–3079, 2023. [Online]. Available: https://www.sciencedirect.com/science/article/pii/S2095927323007296

[175] W. Vermeer, G. R. Chandra Mouli, and P. Bauer, "A comprehensive review on the characteristics and modeling of lithium-ion battery aging," *IEEE Transactions on Transportation Electrification*, vol. 8, no. 2, pp. 2205–2232, 2022.

[176] V. Muenzel, J. de Hoog, M. Brazil, A. Vishwanath, and S. Kalyanaraman, "A multi-factor battery cycle life prediction methodology for optimal battery management," 07 2015.

[177] H. Ruan, J. Barreras, T. Engstrom, Y. Merla, R. Millar, and B. Wu, "Lithium-ion battery lifetime extension: A review of derating methods," *Journal of Power Sources*, vol. 563, 02 2023.

[178] R. Sarrias-Mena, L. M. Fernández-Ramírez, C. A. García-Vázquez, and F. Jurado, "Fuzzy logic based power management strategy of a multi-mw doubly-fed induction generator wind turbine with battery and ultracapacitor," *Energy*, vol. 70, pp. 561–576, 2014.

[179] A. M. Gee, F. V. Robinson, and R. W. Dunn, "Analysis of battery lifetime extension in a small-scale wind-energy system using supercapacitors," *IEEE transactions on energy conversion*, vol. 28, no. 1, pp. 24–33, 2013.

[180] T. Guan, P. Zuo, S. Sun, C. Du, L. Zhang, Y. Cui, L. Yang, Y. Gao, G. Yin, and F. Wang, "Degradation mechanism of licoo2/mesocarbon microbeads battery based on accelerated aging tests," *Journal of Power Sources*, vol. 268, pp. 816–823, 2014.

[181] J. Li, A. M. Gee, M. Zhang, and W. Yuan, "Analysis of battery lifetime extension in a smes-battery hybrid energy storage system using a novel battery

lifetime model," *Energy*, vol. 86, pp. 175–185, 2015. [Online]. Available: https://www.sciencedirect.com/science/article/pii/S0360544215004843

[182] S. Hajiaghasi, A. Salemnia, and M. Hamzeh, "Hybrid energy storage system for microgrids applications: A review," *Journal of Energy Storage*, vol. 21, pp. 543–570, 2019.

[183] T. Sutikno, W. Arsadiando, A. Wangsupphaphol, A. Yudhana, and M. Facta, "A review of recent advances on hybrid energy storage system for solar photovoltaics power generation," *Ieee Access*, vol. 10, pp. 42 346–42 364, 2022.

[184] S. Kumar, "Comparative analysis of ac coupled and dc coupled microgrids: analyzing electrical performances and economics," Master's Thesis, Cal Poly Humboldt, 2024. [Online]. Available: https://digitalcommons.humboldt.edu/etd/788

[185] M. J. Lencwe, T. O. Olwal, S. D. Chowdhury, and M. Sibanyoni, "Nonsolitary two-way dc-to-dc converters for hybrid battery and supercapacitor energy storage systems: A comprehensive survey," *Energy Reports*, vol. 11, pp. 2737–2767, 2024. [Online]. Available: https://www.sciencedirect.com/science/article/pii/S2352484724001057

[186] B. L.-H. Nguyen, H. Cha, T. Vu, and T.-T. Nguyen, "Integrated multiport bidirectional dc-dc converter for hev/fcv applications," 2022. [Online]. Available: https://arxiv.org/abs/2209.05969

[187] Y. Tong, I. Salhi, Q. Wang, G. Lu, and S. Wu, "Bidirectional dc-dc converter topologies for hybrid energy storage systems in electric vehicles: A comprehensive review," *Energies*, vol. 18, no. 9, 2025. [Online]. Available: https://www.mdpi.com/1996-1073/18/9/2312

[188] R. Hemmati and H. Saboori, "Emergence of hybrid energy storage systems in renewable energy and transport applications–a review," *Renewable and Sustainable Energy Reviews*, vol. 65, pp. 11–23, 2016.

[189] W. Jing, C. Hung Lai, S. H. W. Wong, and M. L. D. Wong, "Battery-supercapacitor hybrid energy storage system in standalone dc microgrids: areview," *IET Renewable Power Generation*, vol. 11, no. 4, pp. 461–469, 2017.

[190] A. Etxeberria, I. Vechiu, H. Camblong, and J. Vinassa, "Hybrid energy storage systems for renewable energy sources integration in microgrids: A review," in *2010 Conference Proceedings IPEC*, 2010, pp. 532–537.

[191] S. Athikkal, G. G. Kumar, K. Sundaramoorthy, and A. Sankar, "A non-isolated bridge-type dc–dc converter for hybrid energy source integration," *IEEE Transactions on industry applications*, vol. 55, no. 4, pp. 4033–4043, 2019.

[192] H. Tao, J. L. Duarte, and M. A. Hendrix, "Multiport converters for hybrid power sources," in *2008 IEEE Power Electronics Specialists Conference*. IEEE, 2008, pp. 3412–3418.

[193] T. Pereira, F. Hoffmann, R. Zhu, and M. Liserre, "A comprehensive assessment of multiwinding transformer-based dc–dc converters," *IEEE Transactions on Power Electronics*, vol. 36, no. 9, pp. 10 020–10 036, 2021.

[194] M. Vasiladiotis and A. Rufer, "Analysis and control of modular multilevel converters with integrated battery energy storage," *IEEE Transactions on Power Electronics*, vol. 30, no. 1, pp. 163–175, 2014.

[195] W. Jiang, C. Zhu, C. Yang, L. Zhang, S. Xue, and W. Chen, "The active power control of cascaded multilevel converter based hybrid energy storage system," *IEEE Transactions on Power Electronics*, vol. 34, no. 8, pp. 8241–8253, 2018.

[196] W. Jiang, K. Ren, S. Xue, C. Yang, and Z. Xu, "Research on the asymmetrical multilevel hybrid energy storage system based on hybrid carrier modulation," *IEEE Transactions on Industrial Electronics*, vol. 68, no. 2, pp. 1241–1251, 2020.

[197] L. Deguenon, D. Yamegueu, A. Gomna *et al.*, "Overcoming the challenges of integrating variable renewable energy to the grid: A comprehensive review of electrochemical battery storage systems," *Journal of Power Sources*, vol. 580, p. 233343, 2023.

[198] M. Khalid, "Smart grids and renewable energy systems: Perspectives and grid integration challenges," *Energy Strategy Reviews*, vol. 51, p. 101299, 2024.

[199] A. A. Kebede, T. Kalogiannis, J. Van Mierlo, and M. Berecibar, "A comprehensive review of stationary energy storage devices for large scale renewable energy sources grid integration," *Renewable and Sustainable Energy Reviews*, vol. 159, p. 112213, 2022.

[200] A. M. Adeyinka, O. C. Esan, A. O. Ijaola, and P. K. Farayibi, "Advancements in hybrid energy storage systems for enhancing renewable energy-to-grid integration," *Sustainable Energy Research*, vol. 11, no. 1, p. 26, July 2024. [Online]. Available: https://doi.org/10.1186/s40807-024-00120-4

[201] H. Rezaei, S. E. Abdollahi, S. Abdollahi, and S. Filizadeh, "Energy management strategies of battery-ultracapacitor hybrid storage systems for electric vehicles: Review, challenges, and future trends," *Journal of Energy Storage*, vol. 53, p. 105045, 2022. [Online]. Available: https://www.sciencedirect.com/science/article/pii/S2352152X22010477

[202] A. M. Bazzi, Y. Liu, and D. S. Fay, "Electric machines and energy storage: Over a century of technologies in electric and hybrid electric vehicles," *IEEE Electrification Magazine*, vol. 6, no. 3, pp. 49–53, 2018.

[203] A. González-Gil, R. Palacin, and P. Batty, "Sustainable urban rail systems: Strategies and technologies for optimal management of regenerative braking energy," *Energy conversion and management*, vol. 75, pp. 374–388, 2013.

[204] T. Ise, M. Kita, and A. Taguchi, "A hybrid energy storage with a smes and secondary battery," *IEEE Transactions on Applied Superconductivity*, vol. 15, no. 2, pp. 1915–1918, 2005.

[205] S. Vazquez, S. M. Lukic, E. Galvan, L. G. Franquelo, and J. M. Carrasco, "Energy storage systems for transport and grid applications," *IEEE Transactions on industrial electronics*, vol. 57, no. 12, pp. 3881–3895, 2010.

[206] M. Banaei, M. Rafiei, J. Boudjadar, and M.-H. Khooban, "A comparative analysis of optimal operation scenarios in hybrid emission-free ferry ships," *IEEE Transactions on Transportation Electrification*, vol. 6, no. 1, pp. 318–333, 2020.

[207] X. He, B. Luo, X. Deng, G. Zhu, G. Zhang, and Q. Wang, "Research on energy management strategy of hybrid energy storage system for electric ship," in *2021 IEEE 5th Conference on Energy Internet and Energy System Integration (EI2)*, 2021, pp. 4272–4277.

[208] Duke Energy, "Duke energy to put new battery and ultracapacitor system to the test in n.c." https://news.duke-energy.com/releases/duke-energy-to-put-new-battery-and-ultracapacitor-system-to-the-test-in-n-c, 2016, [Online; accessed 2024-08-19].

[209] Skeleton Technologies, "Superbattery," https://www.skeletontech.com/superbattery, n.d., [Online; accessed 2024-08-19].

[210] Beyonder, "Beyonder and abb to collaborate on battery technology of the future," https://www.beyonder.no/latest-news/beyonder-and-abb-to-collaborate-on-battery-technology-of-the-future-myecs, 2024, [Online; accessed 2024-08-19].

[211] VAccess Consortium, "Review of the storage technologies," VAccess Project (EU), Technical Report, D11, 2025, accessed: 2025-07-23. [Online]. Available: https://v-access.eu/reports/d11-review-of-the-storage-technologies/

[212] Green Hydrogen Coalition. (2024) Construction begins on long-duration energy storage and green hydrogen microgrid project in california. Green Hydrogen for Climate. Accessed: 2025-08-01. [Online]. Available: https://gh2forclimate.org/construction-begins-on-long-duration-energy-storage-and-green-hydrogen-microgrid-project-in-california/

[213] Blathnaid O'Dea. (2025, Mar. 3) Hybrid pumped hydrobess project in finland doubles battery capacity. Energy StorageNews. Accessed: 20250801. [Online].

Available: https://www.ess-news.com/2025/03/03/sens-finland-increases-capacity-hybrid-pumped-hydro-bess-project/

[214] F. Ashrafidehkordi, D. Kottonau, and G. De Carne, "Multi-rate discrete domain modeling of power hardware-in-the-loop setups," *IEEE Open Journal of Power Electronics*, vol. 4, pp. 539–548, 2023.

[215] F. Ashrafidehkordi and G. De Carne, "Investigating the impact of sensor placement on the stability of power hardware-in-the-loop with a grid-following inverter as hardware-of-interest," in *2024 IEEE 10th International Power Electronics and Motion Control Conference (IPEMC2024-ECCE Asia)*, 2024, pp. 4611–4616.

[216] J. Bélanger, P. Venne, and J.-N. Paquin, "The what, where, and why of real-time simulation," *Planet RT*, pp. 37–49, 01 2010.

[217] M. O. Faruque, T. Strasser, G. Lauss, V. Jalili-Marandi, P. Forsyth, C. Dufour, V. Dinavahi, A. Monti, P. Kotsampopoulos, J. A. Martinez, K. Strunz, M. Saeedifard, X. Wang, D. Shearer, and M. Paolone, "Real-time simulation technologies for power systems design, testing, and analysis," 2015, attribution-NonCommercial-NoDerivatives 4.0 International license. [Online]. Available: https://doi.org/10.7939/r3-8gs5-ve92

[218] K. Rajashekaraiah, C. Iurlaro, S. Bruno, and G. De Carne, "Modelling of 3-phase p-q theory-based dynamic load for real-time simulation," *IEEE Open Access Journal of Power and Energy*, vol. 10, pp. 654–664, 2023.

[219] G. F. Lauss, M. O. Faruque, K. Schoder, C. Dufour, A. Viehweider, and J. Langston, "Characteristics and design of power hardware-in-the-loop simulations for electrical power systems," *IEEE Transactions on Industrial Electronics*, vol. 63, no. 1, pp. 406–417, 2016.

[220] A. Yamane, S. Abourida, Y. Bouzid, and F. Tempez, "Real-time simulation of distributed energy systems and microgrids," *IFAC-PapersOnLine*, vol. 49, no. 27, pp. 183–187, 2016, iFAC Workshop on Control of Transmission and Distribution Smart Grids CTDSG 2016. [Online]. Available: https://www.sciencedirect.com/science/article/pii/S2405896316322984

[221] W. Li, G. Joós, and J. Bélanger, "Real-time simulation of a wind turbine generator coupled with a battery supercapacitor energy storage system," *IEEE transactions on industrial electronics*, vol. 57, no. 4, pp. 1137–1145, 2009.

[222] G. F. Lauss, M. O. Faruque, K. Schoder, C. Dufour, A. Viehweider, and J. Langston, "Characteristics and design of power hardware-in-the-loop simulations for electrical power systems," *IEEE Transactions on Industrial Electronics*, vol. 63, no. 1, pp. 406–417, 2015.

[223] E. Guillo-Sansano, M. H. Syed, A. J. Roscoe, G. M. Burt, and F. Coffele, "Characterization of time delay in power hardware in the loop setups," *IEEE Transactions on Industrial Electronics*, vol. 68, no. 3, pp. 2703–2713, 2020.

[224] M. R. I. Sheikh, Ed., *Energy Storage*. Rijeka, Croatia: Sciyo / InTech, Sep. 2010, open-access edition.

[225] M. Andoni, W. Tang, V. Robu, and D. Flynn, "Real-time simulation of large distribution networks with distributed energy storage systems," *CIRED Open Access Proceedings Journal*, vol. 2017, no. 1, pp. 96–99, Oct. 2017, 24th International Conference and Exhibition on Electricity Distribution (CIRED 2017).

[226] Spitzenberger & Spies GmbH & Co. KG, *APS Serie Leistungsverstärker: 4-Quadranten Spannungs-/Stromverstärker*, 2021, technisches Datenblatt, Dokument-Nr. SPS-TD-APS-Overview-1108-d-0008. [Online]. Available: https://www.spitzenberger.de/weblink/1108

[227] Eaton Electronics, Power and Energy Management Products, *XLR48 Supercapacitor Module Data Sheet (48 V, 166 F Rugged Module)*, Eaton Corporation, Jul. 2023, effective July 2023, supersedes July 2019. [Online]. Available: https://www.eaton.com/content/dam/eaton/products/electronic-components/resources/data-sheet/eatonxlr48supercapacitormoduledatasheet.pdf

[228] T. Bocklisch, "Hybrid energy storage systems for renewable energy applications," *Energy Procedia*, vol. 73, pp. 103–111, 2015.

[229] E. Wikner and T. Thiringer, "Extending battery lifetime by avoiding high soc," *Applied Sciences*, vol. 8, no. 10, 2018. [Online]. Available: https://www.mdpi.com/2076-3417/8/10/1825

[230] B. Wang, C. Wang, Z. Wang, H. Xue, and S. Ni, "Adaptive energy estimation for supercapacitor based on a real-time voltage state observer in electric vehicle applications," *IEEE Transactions on Power Electronics*, vol. 36, no. 7, pp. 7337–7341, 2021.

[231] H. Yang, "Estimation of supercapacitor charge capacity bounds considering charge redistribution," *IEEE Transactions on Power Electronics*, vol. 33, no. 8, pp. 6980–6993, 2018.

[232] A. El Mejdoubi, H. Chaoui, H. Gualous, and J. Sabor, "Online parameter identification for supercapacitor state-of-health diagnosis for vehicular applications," *IEEE Transactions on Power Electronics*, vol. 32, no. 12, pp. 9355–9363, 2017.

[233] A. Bharatee, P. K. Ray, B. Subudhi, and A. Ghosh, "Power management strategies in a hybrid energy storage system integrated ac/dc microgrid: A review," *Energies*, vol. 15, no. 19, 2022. [Online]. Available: https://www.mdpi.com/1996-1073/15/19/7176

[234] Y. Cho and H. A. Gabbar, "Review of energy storage technologies in harsh environment," *Safety in Extreme Environments*, vol. 1, no. 1, pp. 11–25, 2019.

[235] T. S. Babu, K. R. Vasudevan, V. K. Ramachandaramurthy, S. B. Sani, S. Chemud, and R. M. Lajim, "A comprehensive review of hybrid energy storage systems: Converter topologies, control strategies and future prospects," *IEEE Access*, vol. 8, pp. 148 702–148 721, 2020.

[236] I. A. Galkin, A. Blinov, M. Vorobyov, A. Bubovich, R. Saltanovs, and D. Peftitsis, "Interface converters for residential battery energy storage systems: Practices, difficulties and prospects," *Energies*, vol. 14, no. 12, 2021. [Online]. Available: https://www.mdpi.com/1996-1073/14/12/3365

[237] A. Khan, M. Bressel, A. Davigny, D. Abbes, and B. Ould Bouamama, "Comprehensive review of hybrid energy systems: Challenges, applications, and optimization strategies," *Energies*, vol. 18, no. 10, 2025. [Online]. Available: https://www.mdpi.com/1996-1073/18/10/2612

[238] W. Yanzi, X. Changle, and W. Wang, "Energy management strategy based on fuzzy logic for a new hybrid battery-ultracapacitor energy storage system," *IEEE Transportation Electrification Conference and Expo, ITEC Asia-Pacific 2014 - Conference Proceedings*, pp. 1–5, 2014.

[239] B. Wang, H. Fan, Z. Li, G. Feng, and Y. Han, "An Ultra-Local Model based Control Method with the Bus Voltage Supervisor for Hybrid Energy Storage System in Electric Vehicles," *IEEE Journal of Emerging and Selected Topics in Power Electronics*, vol. PP, pp. 1–1, 2023.

[240] A. Clemente, P. Arias, L. Gevorkov, L. Trilla, S. Obrador Rey, X. S. Roger, J. L. Dominguez-Garcia, and A. Filba Martinez, "Optimizing performance of hybrid electrochemical energy storage systems through effective control: A comprehensive review," *Electronics*, vol. 13, no. 7, 2024. [Online]. Available: https://www.mdpi.com/2079-9292/13/7/1258

[241] T. Hofman, M. Steinbuch, R. Van Druten, and A. Serrarens, "Rule-based energy management strategies for hybrid vehicles," *International Journal of Electric and Hybrid Vehicles*, vol. 1, no. 1, pp. 71–94, 2007.

[242] B. Moulik and D. Söffker, "Optimal rule-based power management for online, real-time applications in hevs with multiple sources and objectives: a review," *Energies*, vol. 8, no. 9, pp. 9049–9063, 2015.

[243] Y. Wang, S. G. Advani, and A. K. Prasad, "A comparison of rule-based and model predictive controller-based power management strategies for fuel cell/battery hybrid vehicles considering

degradation," *International Journal of Hydrogen Energy*, vol. 45, no. 58, pp. 33 948–33 956, 2020.

[244] H. Mohammadi and M. Mohammadi, "A multi-criteria logical based approach for optimal planning and assessment of rule-based hybrid load following micro combined heat and power systems," *Energy Conversion and Management*, vol. 243, p. 114338, 2021. [Online]. Available: https://www.sciencedirect.com/science/article/pii/S0196890421005148

[245] U. Manandhar, A. Ukil, H. B. Gooi, N. R. Tummuru, S. K. Kollimalla, B. Wang, and K. Chaudhari, "Energy management and control for grid connected hybrid energy storage system under different operating modes," *IEEE Transactions on Smart Grid*, vol. 10, no. 2, pp. 1626–1636, 2017.

[246] S. M. Lukic, S. G. Wirasingha, F. Rodriguez, J. Cao, and A. Emadi, "Power management of an ultracapacitor/battery hybrid energy storage system in an hev," in *2006 IEEE Vehicle Power and Propulsion Conference*, 2006, pp. 1–6.

[247] K. Ding, F. Li, and X. Zhang, *Power Smoothing Control of DC Microgrid Hybrid Energy Storage System Based on Fuzzy Control*, 7 2019.

[248] M. Ali, M. I. Hossain, and M. Shafiullah, "Fuzzy logic for energy management in hybrid energy storage systems integrated dc microgrid," in *2022 International Conference on Power Energy Systems and Applications (ICoPESA)*. IEEE, 2022, pp. 424–429.

[249] V. K. SadolaluBoregowda, R. Shree, Ranjana, VineetSaxena, Sheetal, and S. Kumar, "Enhancing dc microgrid performance with fuzzy logic control for hybrid energy storage system," *Signal, Image and Video Processing*, vol. 18, no. 5, pp. 4505–4514, 2024.

[250] T. Yamakawa, "A fuzzy logic controller," *Journal of Biotechnology*, vol. 24, no. 1, pp. 1–32, 1992.

[251] Y. Wang, W. Wang, Y. Zhao, L. Yang, and W. Chen, "A fuzzy-logic power management strategy based on markov random prediction for hybrid energy storage systems," *Energies*, vol. 9, no. 1, p. 25, 2016.

[252] L. Zadeh, "Fuzzy logic," *Computer*, vol. 21, no. 4, pp. 83–93, 1988.

[253] L. A. Zadeh, "On fuzzy algorithms," in *fuzzy sets, fuzzy logic, and fuzzy systems: selected papers By Lotfi A Zadeh*. World Scientific, 1996, pp. 127–147.

[254] M. Usta, Ö. Akyazi, and A. Akpinar, "Aircraft roll control system using lqr and fuzzy logic controller," 06 2011.

[255] H. Maghfiroh, O. Wahyunggoro, and A. I. Cahyadi, "Energy management in hybrid electric and hybrid energy storage system vehicles: A fuzzy logic controller review," *IEEE Access*, vol. 12, pp. 56 097–56 109, 2024.

[256] A. G. Abo-Khalil, A. Sobhy, M. A. Abdelkareem, and A. Olabi, "Advancements and challenges in hybrid energy storage systems: Components, control strategies, and future directions," *International Journal of Thermofluids*, vol. 20, p. 100477, 2023.

[257] M. M. Rana, M. Uddin, M. R. Sarkar, G. Shafiullah, H. Mo, and M. Atef, "A review on hybrid photovoltaic–battery energy storage system: Current status, challenges, and future directions," *Journal of Energy Storage*, vol. 51, p. 104597, 2022.

[258] A. Kumar, A. Yazdanbakhsh, M. Hashemi, K. Swersky, and S. Levine, "Data-driven offline optimization for architecting hardware accelerators," *arXiv preprint arXiv:2110.11346*, 2021.

[259] M. Li, L. Wang, Y. Wang, and Z. Chen, "Sizing optimization and energy management strategy for hybrid energy storage system using multiobjective optimization and random forests," *IEEE Transactions on Power Electronics*, vol. 36, no. 10, pp. 11 421–11 430, 2021.

[260] A. Chasse and A. Sciarretta, "Supervisory control of hybrid powertrains: An experimental benchmark of offline optimization and online energy management," *Control engineering practice*, vol. 19, no. 11, pp. 1253–1265, 2011.

[261] H. M. Amine, B. Aissa, B. Ibrahim, L. Abdallah, H. Oussama, Z. Seddik, T. Fadila, and H. Messaoud, "Investigating fitness functions using bonobo optimizer for optimal control of pv-hess systems: A comparative analysis," in *2023 Second International Conference on Energy Transition and Security (ICETS)*, 2023, pp. 1–8.

[262] M. Ghanaatian and S. Lotfifard, "Control of Flywheel Energy Storage Systems in the Presence of Uncertainties," *IEEE Transactions on Sustainable Energy*, vol. 10, no. 1, pp. 36–45, 2019.

[263] S. Karrari, G. De Carne, and M. Noe, "Adaptive droop control strategy for flywheel energy storage systems: A power hardware-in-the-loop validation," *Electric Power Systems Research*, vol. 212, p. 108300, 2022. [Online]. Available: https://www.sciencedirect.com/science/article/pii/S0378779622004874

[264] S. Chen, Q. Yang, J. Zhou, and X. Chen, "A model predictive control method for hybrid energy storage systems," *CSEE Journal of Power and Energy Systems*, vol. 7, no. 2, pp. 329–338, 2020.

[265] S. A. G. K. Abadi, S. I. Habibi, T. Khalili, and A. Bidram, "A model predictive control strategy for performance improvement of hybrid energy storage systems in dc microgrids," *IEEE Access*, vol. 10, pp. 25 400–25 421, 2022.

[266] L. Wang, Y. Wang, C. Liu, D. Yang, and Z. Chen, "A power distribution strategy for hybrid energy storage system using adaptive model predictive control," *IEEE Transactions on Power Electronics*, vol. 35, no. 6, pp. 5897–5906, 2019.

[267] S. Maroufi, R. V. Monteiro, A. Bretas, and S. C. Dhulipala, "Smart grids volt-var frequency control: A smart building distributed model predictive control based approach," in *2020 52nd North American Power Symposium (NAPS)*, 2021, pp. 1–6.

[268] M. Arnold, R. Negenborn, G. Andersson, and B. De Schutter, "Multi-area predictive control for combined electricity and natural gas systems," *2009 European Control Conference, ECC 2009*, 03 2015.

[269] D. Pelosi and L. Barelli, "A multi-objective stochastic power management strategy for vehicle-to-building and building-to-vehicle integration into residential microgrids," in *2023 AEIT International Annual Conference (AEIT)*, 2023, pp. 1–6.

[270] L. Barelli, G. Bidini, D. Ciupageanu, A. Micangeli, P. Ottaviano, and D. Pelosi, "Real time power management strategy for hybrid energy storage systems coupled with variable energy sources in power smoothing applications," *Energy Reports*, vol. 7, pp. 2872–2882, 2021. [Online]. Available: https://www.sciencedirect.com/science/article/pii/S2352484721002961

[271] D. Pelosi, F. Gallorini, G. Alessandri, and L. Barelli, "A hybrid energy storage system integrated with a wave energy converter: Data-driven stochastic power management for output power smoothing," *Energies*, vol. 17, no. 5, 2024. [Online]. Available: https://www.mdpi.com/1996-1073/17/5/1167

[272] A. Neffati, M. Guemri, S. Caux, and M. Fadel, "Energy management strategies for multi source systems," *Electric Power Systems Research*, vol. 102, pp. 42–49, 2013. [Online]. Available: https://www.sciencedirect.com/science/article/pii/S0378779613000795

[273] R. H. Byrne, T. A. Nguyen, D. A. Copp, B. R. Chalamala, and I. Gyuk, "Energy management and optimization methods for grid energy storage systems," *IEEE Access*, pp. 1–1, 2017.

[274] L. Barelli, G. Bidini, D. A. Ciupageanu, A. Ottaviano, D. Pelosi, F. Gallorini, G. Alessandri, and M. Atcheson Cruz, "An effective solution to boost generation from waves: Benefits of a hybrid energy storage system integration to wave energy converter in grid-connected systems," *Open Research Europe*, vol. 2, p. 40, 2022.

[275] J. Spall, "Multivariate stochastic approximation using a simultaneous perturbation gradient approximation," *IEEE Transactions on Automatic Control*, vol. 37, no. 3, pp. 332–341, 1992.

[276] P. Sadegh and J. Spall, "Optimal random perturbations for stochastic approximation using a simultaneous perturbation gradient approximation," *IEEE Transactions on Automatic Control*, vol. 43, no. 10, pp. 1480–1484, 1998.

[277] J. Spall, "Overview of the simultaneous perturbation method for efficient optimization. hopkins apl technical digest 19, 482–492 (1998)."

[278] J. C. Spall, "A one-measurement form of simultaneous perturbation stochastic approximation," *Automatica*, vol. 33, no. 1, pp. 109–112, 1997. [Online]. Available: https://www.sciencedirect.com/science/article/pii/S0005109896001495

[279] M. Ho, J. Lim, C. Y. Chong, K. K. Chua, and A. Siah, "High dimensional origin destination calibration using metamodel assisted simultaneous perturbation stochastic approximation," *IEEE Transactions on Intelligent Transportation Systems*, vol. PP, pp. 1–10, 04 2023.

[280] O. Granichin, V. Erofeeva, Y. Ivanskiy, and Y. Jiang, "Simultaneous perturbation stochastic approximation-based consensus for tracking under unknown-but-bounded disturbances," *IEEE Transactions on Automatic Control*, vol. 66, no. 8, pp. 3710–3717, 2021.

[281] K.-H. Chang and G. Lin, "Optimal design of hybrid renewable energy systems using simulation optimization," *Simulation Modelling Practice and Theory*, vol. 52, 03 2015.

[282] S. M. Maroufi and G. De Carne, "Optimal design for hybrid energy storage systems considering system aging and costs," in *2023 IEEE 14th International Symposium on Power Electronics for Distributed Generation Systems (PEDG)*, 2023, pp. 496–500.

[283] D. Pelosi, E. Ciotti, M. Tritoni, and L. Barelli, "Genetic algorithm optimization of fuel cell electric bus fleet operation for carbon-neutral districts," in *2024 International Conference on Electrical, Computer and Energy Technologies (ICECET*, 2024, pp. 1–6.

[284] S. B. Wali, M. A. Hannan, P. J. Ker, and T. S. Kiong, "Optimal sizing of pv-battery based hybrid renewable system using particle swarm optimization for economic sustainability," in *2023 IEEE International Conference on Energy Technologies for Future Grids (ETFG)*, 2023, pp. 1–6.

[285] S. Liqun, L. Pengwei, and Z. Weiwei, "Capacity optimization of hybrid energy storage in wind/pv complementary power generation system based on improved particle swarm optimization," in *2018 China International Conference on Electricity Distribution (CICED)*, 2018, pp. 2295–2300.

[286] T. Mesbahi, N. Rizoug, P. Bartholomeüs, R. Sadoun, F. Khenfri, and P. Le Moigne, "Optimal energy management for a li-ion battery/supercapacitor hybrid energy storage system based on a particle swarm optimization incorporating neldermead simplex approach," *IEEE Transactions on Intelligent Vehicles*, vol. 2, no. 2, pp. 99–110, 2017.

[287] M. Albadr, S. Tiun, M. Ayob, and F. Al-Dhief, "Genetic algorithm based on natural selection theory for optimization problems," *Symmetry*, vol. 12, pp. 1–31, 10 2020.

[288] A. Lambora, K. Gupta, and K. Chopra, "Genetic algorithm-a literature review," in *2019 international conference on machine learning, big data, cloud and parallel computing (COMITCon)*. IEEE, 2019, pp. 380–384.

[289] J. Hou, Z. Song, H. F. Hofmann, and J. Sun, "Control Strategy for Battery/Flywheel Hybrid Energy Storage in Electric Shipboard Microgrids," *IEEE Transactions on Industrial Informatics*, vol. 17, no. 2, pp. 1089–1099, 2021.

[290] S. T. Sisakat and S. M. Barakati, "Fuzzy energy management in electrical vehicles with different hybrid energy storage topologies," *4th Iranian Joint Congress on Fuzzy and Intelligent Systems, CFIS 2015*, pp. 10–15, 2016.

[291] O. Erdinc, B. Vural, and M. Uzunoglu, "A wavelet-fuzzy logic based energy management strategy for a fuel cell/battery/ultra-capacitor hybrid vehicular power system," *Journal of Power Sources*, vol. 194, no. 1, pp. 369–380, 2009.

[292] C. Balasundar, C. K. Sundarabalan, N. S. Srinath, J. Sharma, and J. M. Guerrero, "Interval Type2 Fuzzy Logic-Based Power Sharing Strategy for Hybrid Energy Storage System in Solar Powered Charging Station," *IEEE Transactions on Vehicular Technology*, vol. 70, no. 12, pp. 12 450–12 461, 2021.

[293] D. Xu and H. Cen, "A hybrid energy storage strategy based on multivariable fuzzy coordinated control of photovoltaic grid-connected power fluctuations," *IET Renewable Power Generation*, vol. 15, no. 8, pp. 1826–1835, 2021.

[294] S. Sinha and P. Bajpai, "Power management of hybrid energy storage system in a standalone DC microgrid," *Journal of Energy Storage*, vol. 30, no. May, 2020.

[295] H. Chen, R. Xiong, C. Lin, and W. Shen, "Model predictive control based real-time energy management for hybrid energy storage system," *CSEE Journal of Power and Energy Systems*, vol. 7, no. 4, pp. 862–874, 2021.

[296] C. Zheng, W. Li, and Q. Liang, "An energy management strategy of hybrid energy storage systems for electric vehicle applications," *IEEE Transactions on Sustainable Energy*, vol. 9, no. 4, pp. 1880–1888, 2018.

[297] C. Romaus, K. Gathmann, and J. Böcker, "Optimal energy management for a hybrid energy storage system for electric vehicles based on stochastic dynamic programming," in *2010 IEEE Vehicle Power and Propulsion Conference*, 2010, pp. 1–6.

[298] D. R. Conover, A. J. Crawford, V. V. Viswanathan, S. Ferreira, and D. Schoenwald, "Protocol for uniformly measuring and expressing the performance of energy storage systems," Pacific Northwest National Laboratory, Richland, WA, USA, Tech. Rep. PNNL-22010 Rev 2/SAND2016-3078 R, 2014.

[299] S. Zhou, Z. Chen, D. Huang, and T. Lin, "Model prediction and rule based energy management strategy for a plug-in hybrid electric vehicle with hybrid energy storage system," *IEEE Transactions on Power Electronics*, vol. 36, no. 5, pp. 5926–5940, 2021.

[300] N. Omar, M. A. Monem, Y. Firouz, J. Salminen, J. Smekens, O. Hegazy, H. Gaulous, G. Mulder, P. Van den Bossche, T. Coosemans, and J. Van Mierlo, "Lithium iron phosphate based battery assessment of the aging parameters and development of cycle life model," *Applied Energy*, vol. 113, pp. 1575–1585, 2014. [Online]. Available: https://www.sciencedirect.com/science/article/pii/S0306261913007393

[301] E. Chemali, P. J. Kollmeyer, M. Preindl, and A. Emadi, "State-of-charge estimation of li-ion batteries using deep neural networks: A machine learning approach," *Journal of Power Sources*, vol. 400, pp. 242–255, 2018.

[302] A. Karnama, F. Resende, and J. A. Lopes, "Optimal management of battery charging of electric vehicles: A new microgrid feature," *Conf. Rec. IEEE PowerTech*, 06 2011.

[303] F. Garcia-Torres, D. Vilaplana, C. Bordons, P. Roncero-Sánchez, and M. Ridao, "Optimal management of microgrids with external agents including battery/fuel cell electric vehicles," *IEEE Transactions on Smart Grid*, vol. PP, pp. 1–1, 07 2018.

[304] M. T. Lawder, B. Suthar, P. W. Northrop, S. De, C. M. Hoff, O. Leitermann, M. L. Crow, S. Santhanagopalan, and V. R. Subramanian, "Battery energy storage system (bess) and battery management system (bms) for grid-scale applications," *Proceedings of the IEEE*, vol. 102, no. 6, pp. 1014–1030, 2014.

[305] K. W. E. Cheng, B. Divakar, H. Wu, K. Ding, and H. F. Ho, "Battery-management system (bms) and soc development for electrical vehicles," *IEEE transactions on vehicular technology*, vol. 60, no. 1, pp. 76–88, 2010.

[306] J. Garche and A. Jossen, "Battery management systems (bms) for increasing battery life time," in *TELESCON 2000. Third International Telecommunications Energy Special Conference (IEEE Cat. No. 00EX424)*. IEEE, 2000, pp. 81–88.

[307] L. Tziovani, L. Hadjidemetriou, C. Charalampous, M. Tziakouri, S. Timotheou, and E. Kyriakides, "Energy management and control of a flywheel storage system for peak shaving applications," *IEEE Transactions on Smart Grid*, vol. 12, no. 5, pp. 4195–4207, 2021.

[308] G. Boukettaya and L. Krichen, "A dynamic power management strategy of a grid connected hybrid generation system using wind, photovoltaic and flywheel energy storage system in residential applications," *Energy*, vol. 71, pp. 148–159, 2014.

[309] R. J. Hyndman, "Moving averages," Tech. Rep., 2009.

[310] A. C. Szakmary, Q. Shen, and S. C. Sharma, "Trend-following trading strategies in commodity futures: A re-examination," *Journal of Banking and Finance*, vol. 34, no. 2, pp. 409–426, 2010. [Online]. Available: http://dx.doi.org/10.1016/j.jbankfin.2009.08.004

[311] X. Liu, H. An, L. Wang, and Q. Guan, "Quantified moving average strategy of crude oil futures market based on fuzzy logic rules and genetic algorithms," *Physica A: Statistical Mechanics and its Applications*, vol. 482, pp. 444–457, 2017. [Online]. Available: http://dx.doi.org/10.1016/j.physa.2017.04.082

[312] C. Lee, "Fuzzy logic in control systems: fuzzy logic controller. i," *IEEE Transactions on Systems, Man, and Cybernetics*, vol. 20, no. 2, pp. 404–418, 1990.

[313] S. M. Maroufi, S. Karrari, K. Rajashekaraiah, and G. De Carne, "Power management of hybrid flywheel-battery energy storage systems considering the state of charge and power ramp rate," *IEEE Transactions on Power Electronics*, vol. 40, no. 7, pp. 9944–9956, 2025.

[314] W. KICKERT and E. MAMDANI, "Analysis of a fuzzy logic controller," in *Readings in Fuzzy Sets for Intelligent Systems*, D. Dubois, H. Prade, and R. R. Yager, Eds. Morgan Kaufmann, 1993, pp. 290–297. [Online]. Available: https://www.sciencedirect.com/science/article/pii/B978148321450450033X

[315] H. R. Berenji, "Fuzzy logic controllers," in *An introduction to fuzzy logic applications in intelligent systems*. Springer, 1992, pp. 69–96.

[316] E. H. Mamdani and S. Assilian, "An experiment in linguistic synthesis with a fuzzy logic controller," *International Journal of Man-Machine Studies*, vol. 7, no. 1, pp. 1–13, 1975.

[317] Z. Song, H. Hofmann, J. Li, J. Hou, X. Han, and M. Ouyang, "Energy management strategies comparison for electric vehicles with hybrid energy storage system," *Applied Energy*, vol. 134, pp. 321–331, 2014. [Online]. Available: https://www.sciencedirect.com/science/article/pii/S0306261914008381

[318] S. Karrari, N. Ludwig, G. De Carne, and M. Noe, "Sizing of Hybrid Energy Storage Systems Using Recurring Daily Patterns," *IEEE Transactions on Smart Grid*, vol. 13, no. 4, pp. 3290–3300, 2022.

[319] S. Karrari, M. Vollmer, G. D. Carne, M. Noe, K. Böhm, and J. Geisbüsch, "A data-driven approach for estimating relative voltage sensitivity," in *2020 IEEE Power & Energy Society General Meeting (PESGM)*, 2020, pp. 1–5.

[320] A. Eberle GmbH & Co. KG, "Power quality-interface and disturbance recorder pqi-da smart," https://www.aeberle.de/en/product-groups/pq-fix-installed/devices/pqi-da-smart, [Online; accessed 2021-06-02].

[321] J. P. L. Keil, "Linear and Nonlinear Aging of Lithium-Ion Cells," 2021.

[322] N. B. Lai, A. Tarraso, G. N. Baltas, L. V. Marin Arevalo, and P. Rodriguez, "External Inertia Emulation Controller for Grid-Following Power Converter," *IEEE Transactions on Industry Applications*, vol. 57, no. 6, pp. 6568–6576, 2021.

[323] H. H. Abdeltawab and Y. A. R. I. Mohamed, "Robust Energy Management of a Hybrid Wind and Flywheel Energy Storage System Considering Flywheel Power Losses Minimization and Grid-Code Constraints," *IEEE Transactions on Industrial Electronics*, vol. 63, no. 7, pp. 4242–4254, 2016.

[324] J. Xiao, P. Wang, and L. Setyawan, "Hierarchical Control of Hybrid Energy Storage System in DC Microgrids," *IEEE Transactions on Industrial Electronics*, vol. 62, no. 8, pp. 4915–4924, 2015.

[325] T. Wu, W. Yu, and L. Guo, "A Study on Use of Hybrid Energy Storage System along with Variable Filter Time Constant to Smooth DC Power Fluctuation in Microgrid," *IEEE Access*, vol. 7, pp. 175 377–175 385, 2019.

[326] A. S. Gardouh, S. Abulanwar, F. Deng, E. Gouda, and A. Ghanem, "Novel fuzzy-based open-switch fault detection scheme of voltage source inverter induction motor drive," *IEEE Transactions on Power Electronics*, vol. 39, no. 11, pp. 14 961–14 973, 2024.

[327] V. Gurugubelli, A. Ghosh, A. K. Panda, and B. P. Behera, "Fuzzy-based adaptive voc methods for parallel inverters," *IEEE Transactions on Power Electronics*, vol. 39, no. 4, pp. 3956–3961, 2024.

[328] Y. Shen, J. Xie, T. He, L. Yao, and Y. Xiao, "Ceemd-fuzzy control energy management of hybrid energy storage systems in electric vehicles," *IEEE Transactions on Energy Conversion*, vol. 39, no. 1, pp. 555–566, 2024.

[329] A. Nadeau, M. Hassanalieragh, G. Sharma, and T. Soyata, "Energy awareness for supercapacitors using kalman filter state-of-charge tracking," *Journal of Power Sources*, vol. 296, pp. 383–391, 2015.

[330] M. Ceraolo, G. Lutzemberger, and D. Poli, "State-of-charge evaluation of supercapacitors," *Journal of Energy Storage*, vol. 11, pp. 211–218, 2017.

[331] H. Yang, "Estimation of supercapacitor charge capacity bounds considering charge redistribution," *IEEE Transactions on Power Electronics*, vol. 33, no. 8, pp. 6980–6993, 2018.

[332] G. Welch, G. Bishop *et al.*, "An introduction to the kalman filter," 1995.

[333] M. Khodarahmi and V. Maihami, "A review on kalman filter models," *Archives of Computational Methods in Engineering*, vol. 30, no. 1, pp. 727–747, 2023.

[334] R. E. Kalman, "A New Approach to Linear Filtering and Prediction Problems," *Journal of Basic Engineering*, vol. 82, no. 1, pp. 35–45, 03 1960.

[335] G. L. Plett, "Kalman-filter soc estimation for lipb hev cells," 2002.

[336] E. A. Wan and R. Van Der Merwe, "The unscented kalman filter for nonlinear estimation," in *Proceedings of the IEEE 2000 Adaptive Systems for Signal Processing, Communications, and Control Symposium (Cat. No.00EX373)*, 2000, pp. 153–158.

[337] P. Saha, S. Dey, and M. Khanra, "Modeling and state-of-charge estimation of supercapacitor considering leakage effect," *IEEE Transactions on Industrial Electronics*, vol. 67, no. 1, pp. 350–357, 2020.

[338] R. Van der Merwe and E. A. Wan, "The square-root unscented kalman filter for state and parameter-estimation," in *2001 IEEE International Conference on Acoustics, Speech, and Signal Processing. Proceedings (Cat. No.01CH37221)*, vol. 6, 2001, pp. 3461–3464 vol.6.

[339] M. Partovibakhsh and G. Liu, "An adaptive unscented kalman filtering approach for online estimation of model parameters and state-of-charge of lithium-ion batteries for autonomous mobile robots," *IEEE Transactions on Control Systems Technology*, vol. 23, no. 1, pp. 357–363, 2015.

[340] M. Luzi, M. Paschero, A. Rossini, A. Rizzi, and F. M. F. Mascioli, "Comparison between two nonlinear kalman filters for reliable soc estimation on a prototypal bms," in *IECON 2016 - 42nd Annual Conference of the IEEE Industrial Electronics Society*, 2016, pp. 5501–5506.

[341] R. Mohammadi Asl, Y. Shabbouei Hagh, S. Simani, and H. Handroos, "Adaptive square-root unscented kalman filter: An experimental study of hydraulic actuator state

estimation," *Mechanical Systems and Signal Processing*, vol. 132, pp. 670–691, 2019. [Online]. Available: https://www.sciencedirect.com/science/article/pii/S0888327019304510

[342] D. Fusco, M. Di Monaco, F. Porpora, and G. Tomasso, "A novel adaptive square-root unscented kalman filter for battery soc estimation," in *PCIM Europe digital days 2021; International Exhibition and Conference for Power Electronics, Intelligent Motion, Renewable Energy and Energy Management*, 2021, pp. 1–8.

[343] J. Wang, L. Zhang, J. Mao, J. Zhou, and D. Xu, "Fractional order equivalent circuit model and soc estimation of supercapacitors for use in hess," *IEEE Access*, vol. 7, pp. 52 565–52 572, 2019.

[344] S. Dey, S. Mohon, B. Ayalew, H. Arunachalam, and S. Onori, "A novel model-based estimation scheme for battery-double-layer capacitor hybrid energy storage systems," *IEEE Transactions on Control Systems Technology*, vol. 27, no. 2, pp. 689–702, 2019.

[345] L. Zhang, Z. Wang, H. Xiaosong, and D. Dorrell, "Residual capacity estimation for ultracapacitors in electric vehicles using artificial neural network," 08 2014.

[346] L. Zhang, X. Hu, Z. Wang, F. Sun, and D. G. Dorrell, "A review of supercapacitor modeling, estimation, and applications: A control/management perspective," *Renewable and Sustainable Energy Reviews*, vol. 81, pp. 1868–1878, 2018.

[347] D. Fusco, M. Di Monaco, F. Porpora, and G. Tomasso, "A novel adaptive square-root unscented kalman filter for battery soc estimation," in *PCIM Europe digital days 2021; International Exhibition and Conference for Power Electronics, Intelligent Motion, Renewable Energy and Energy Management*, 2021, pp. 1–8.

[348] G. De Carne, A. Morandi, and S. Karrari, "Supercapacitor modeling for real-time simulation applications," *IEEE Journal of Emerging and Selected Topics in Industrial Electronics*, vol. 3, no. 3, pp. 509–518, 2022.

[349] A. Morandi, A. Lampasi, A. Cocchi, F. Gherdovich, U. Melaccio, P. L. Ribani, C. Rossi, and F. Soavi, "Characterization and model parameters of large commercial supercapacitor cells," *IEEE Access*, vol. 9, pp. 20 376–20 390, 2021.

[350] D. Fusco, S. Masoome Maroufi, F. Porpora, M. Di Monaco, G. De Carne, and G. Tomasso, "Performance analysis of asr-ukfs for supercapacitor soc estimation in hybrid energy storage systems," *IEEE Journal of Emerging and Selected Topics in Power Electronics*, vol. 12, no. 6, pp. 5602–5612, 2024.

[351] Y. Parvini, J. B. Siegel, A. G. Stefanopoulou, and A. Vahidi, "Supercapacitor electrical and thermal modeling, identification, and validation for a wide range of temperature and power

applications," *IEEE Transactions on Industrial Electronics*, vol. 63, no. 3, pp. 1574–1585, 2016.

[352] L. Zubieta and R. Bonert, "Characterization of double-layer capacitors for power electronics applications," *IEEE Transactions on Industry Applications*, vol. 36, no. 1, pp. 199–205, 2000.

[353] V. Sedlakova, J. Sikula, J. Majzner, P. Sedlak, T. Kuparowitz, B. Buergler, and P. Vasina, "Supercapacitor equivalent electrical circuit model based on charges redistribution by diffusion," *Journal of Power Sources*, vol. 286, pp. 58–65, 2015.

[354] J. P. Christophersen, "Battery test manual for electric vehicles, revision 3," 6 2015.

[355] X. Huang, Y. Li, A. Acharya, X. Sui, J. Meng, R. Teodorescu, and D.-I. Stroe, "A review of pulsed current technique for lithium-ion batteries," *Energies*, vol. 13, p. 2458, 05 2020.

[356] L. Barelli, D.-A. Ciupageanu, A. Ottaviano, D. Pelosi, and G. Lazaroiu, "Stochastic power management strategy for hybrid energy storage systems to enhance large scale wind energy integration," *Journal of energy storage*, vol. 31, p. 101650, 2020.

[357] L. Barelli, G. Bidini, P. Ottaviano, F. Gallorini, and D. Pelosi, "Coupling hybrid energy storage system to regenerative actuators in a more electric aircraft: Dynamic performance analysis and co2 emissions assessment concerning the italian regional aviation scenario," *Journal of Energy Storage*, vol. 45, p. 103776, 2022. [Online]. Available: https://www.sciencedirect.com/science/article/pii/S2352152X21014493

[358] SAMSUNG SDI, "Lithium-ion rechargeable cell for power tools model name: Inr18650-20r," 2011, technical datasheet.

[359] S. Karrari, G. De Carne, and M. Noe, "Model validation of a high-speed flywheel energy storage system using power hardware-in-the-loop testing," *Journal of Energy Storage*, vol. 43, p. 103177, 2021.

[360] D.-A. Ciupageanu, L. Barelli, A. Ottaviano, D. Pelosi, and G. Lazaroiu, "Innovative power management of hybrid energy storage systems coupled to res plants: The simultaneous perturbation stochastic approximation approach," in *2019 IEEE PES Innovative Smart Grid Technologies Europe (ISGT-Europe)*, 2019, pp. 1–5.

[361] J. Spall, "Implementation of the simultaneous perturbation algorithm for stochastic optimization," *IEEE Transactions on Aerospace and Electronic Systems*, vol. 34, no. 3, pp. 817–823, 1998.

[362] R. Siddaiah and R. Saini, "A review on planning, configurations, modeling and optimization techniques of hybrid renewable energy systems for off grid applications,"

Renewable and Sustainable Energy Reviews, vol. 58, pp. 376–396, 2016. [Online]. Available: https://www.sciencedirect.com/science/article/pii/S1364032115016640

[363] D. Pelosi and L. Barelli, "A multi-objective stochastic power management strategy for vehicle-to-building and building-to-vehicle integration into residential microgrids," 10 2023, pp. 1–6.

[364] ASTM, "E1049-85: Standard practices for cycle counting in fatigue analysis," 2011, e1049 - 85, 1–10.

[365] L. Barelli, D.-A. Ciupageanu, A. Ottaviano, D. Pelosi, and L. Gheorghe, "Stochastic power management strategy for hybrid energy storage systems to enhance large scale wind energy integration," *Journal of Energy Storage*, vol. 31, p. 101650, 10 2020.

[366] P. G. Anselma, P. J. Kollmeyer, S. Feraco, A. Bonfitto, G. Belingardi, A. Emadi, N. Amati, and A. Tonoli, "Economic payback time of battery pack replacement for hybrid and plug-in hybrid electric vehicles," *IEEE Transactions on Transportation Electrification*, vol. 9, no. 1, pp. 1021–1033, 2023.

[367] S. Atalay, M. Sheikh, A. Mariani, Y. Merla, E. Bower, and W. D. Widanage, "Theory of battery ageing in a lithium-ion battery: Capacity fade, nonlinear ageing and lifetime prediction," *Journal of Power Sources*, vol. 478, p. 229026, 2020. [Online]. Available: https://www.sciencedirect.com/science/article/pii/S0378775320313239

[368] O. Schmidt, S. Melchior, A. Hawkes, and I. Staffell, "Projecting the future levelized cost of electricity storage technologies," *Joule*, vol. 3, no. 1, pp. 81–100, 2019. [Online]. Available: https://www.cell.com/joule/fulltext/S2542-4351(18)30583-X

[369] K. Mongird, V. V. Viswanathan, P. J. Balducci, M. J. E. Alam, V. Fotedar, V. S. Koritarov *et al.*, "Energy storage technology and cost characterization report," Pacific Northwest National Laboratory (PNNL), Richland, WA, United States, Tech. Rep., 2020, accessed: 2020-05-16. [Online]. Available: https://energystorage.pnnl.gov/pdf/PNNL-28866.pdf

[370] V. Jülch, "Comparison of electricity storage options using levelized cost of storage (lcos) method," *Applied Energy*, vol. 183, pp. 1594–1606, 2016. [Online]. Available: https://www.sciencedirect.com/science/article/pii/S0306261916312740

[371] J. M. Eyer, "Benefits from flywheel energy storage for area regulation in california-demonstration results: a study for the doe energy storage systems program." Sandia National Laboratories (SNL), Albuquerque, NM, and Livermore, CA , Tech. Rep., 2009.

[372] O. o. E. U.S. Department of Energy and E. Reliability, "Energy storage technology and cost characterization report," Pacific Northwest National Laboratory (PNNL), Technical

Report PNNL-29766, Jul. 2019, accessed: 2025-06-20. [Online]. Available: https://www.pnnl.gov/publications/energy-storage-technology-and-cost-characterization-report

[373] E. Martinez-Laserna, E. Sarasketa-Zabala, I. Villarreal Sarria, D.-I. Stroe, M. Swierczynski, A. Warnecke, J.-M. Timmermans, S. Goutam, N. Omar, and P. Rodriguez, "Technical viability of battery second life: A study from the ageing perspective," *IEEE Transactions on Industry Applications*, vol. 54, no. 3, pp. 2703–2713, 2018.

[374] M. Shahjalal, P. K. Roy, T. Shams, A. Fly, J. I. Chowdhury, M. R. Ahmed, and K. Liu, "A review on second-life of li-ion batteries: prospects, challenges, and issues," *Energy*, vol. 241, p. 122881, 2022. [Online]. Available: https://www.sciencedirect.com/science/article/pii/S0360544221031303

[375] R. Sebastián and R. Peña Alzola, "Flywheel energy storage systems: Review and simulation for an isolated wind power system," *Renewable and Sustainable Energy Reviews*, vol. 16, no. 9, pp. 6803–6813, 2012. [Online]. Available: https://www.sciencedirect.com/science/article/pii/S1364032112004777

[376] C. Mc Nelis, S. Dunleavy, D. Stenzel, and S. Cummins, "Design and development of a large scale flywheel energy storage system," Ph.D. dissertation, 02 2022.